

TOYOHASHI UNIVERSITY OF TECHNOLOGY

DOCTORAL THESIS

**Nonlinear Friction Modeling and
Adaptive Compensation for
Precision Contouring Control of
Industrial Machines**

Author:
Bùi Đình Bá

Supervisor:
Prof. Naoki Uchiyama

*A thesis submitted in fulfillment of the requirements
for the degree of Doctor of Engineering
in the*

Systems Engineering Laboratory
Department of Mechanical Engineering



January 2017

Declaration of Authorship

I, Bùi Đình Bá, declare that this thesis titled, “Nonlinear Friction Modeling and Adaptive Compensation for Precision Contouring Control of Industrial Machines” and the work presented in it are my own. I confirm that:

- This work was done wholly or mainly while in candidature for a research degree at this University.
- Where any part of this thesis has previously been submitted for a degree or any other qualification at this University or any other institution, this has been clearly stated.
- Where I have consulted the published work of others, this is always clearly attributed.
- Where I have quoted from the work of others, the source is always given. With the exception of such quotations, this thesis is entirely my own work.
- I have acknowledged all main sources of help.
- Where the thesis is based on work done by myself jointly with others, I have made clear exactly what was done by others and what I have contributed myself.

Signed:

Date:

Nonlinear Friction Modeling and Adaptive Compensation for Precision Contouring Control of Industrial Machines

Author:

Bùi Đình Bá

Student ID:

D125112

Submitted to the Department of Mechanical Engineering of Toyohashi University of Technology as partial fulfillment of requirements to achieve degree of Doctor of Engineering

At

Department of Mechanical Engineering

Toyohashi University of Technology

Committee members:

Prof. Hideki Yanada

Assoc. Prof. Shigenori Sano

Prof. Naoki Uchiyama

TOYOHASHI UNIVERSITY OF TECHNOLOGY

Abstract

Systems Engineering Laboratory
Department of Mechanical Engineering

Doctor of Engineering

**Nonlinear Friction Modeling and Adaptive Compensation for
Precision Contouring Control of Industrial Machines**

by Bùi Đình Bá

Industrial machines have contributed significantly to the development of manufacturing and productivity. There are numerous types of industrial machine, ranging from low-precision agriculture machines to highly complex industrial robots with nanometer precision. Above all, machine tools are essential industrial machines because they facilitate the manufacture of more productive high-precision machines in other industries. In addition, machine tools have the ability to reproduce themselves. Machine tools have developed notably over time in order to adapt to the increasing requirements for speed, precision, and productivity. Such development requires highly intense research in fields such as structural design, sensors, materials, and controller methods. This thesis focuses mainly on precision motion control in the feed-drive systems of machine tools by modeling nonlinear friction behavior. An adaptive friction-compensation model is constructed, and a robust sliding-mode contouring controller is designed.

Friction is the main hindrance in mechanical systems, especially in computerized numerical control (CNC) machine tools for which high precision, high speed, and performance are critical. The body of research into friction compensation in machine tools has shown that a controller with friction compensation provides better performance than one without. For instance, conventional friction models such as the Coulomb-viscous-Stribeck friction model, the LuGre model, and the Generalized Maxwell Slip (GMS) model have been proposed to compensate for frictional effects, reduce the contour error, and improve the surface quality. Such research focus mainly on nonlinear friction properties in the pre-sliding and low-speed regimes, whereas the friction properties in the high-speed regime are simplified by the use of a viscous coefficient. However, there are numerous sources of friction in experimental feed-drive systems, such as the lubrication conditions, eccentricity properties, thermal deformations, and uneven contact surfaces that cause nonlinear friction properties in the low-speed regime and especially in the high-speed regime. Therefore, the conventional static friction model that is based on modeling friction between two sliding surfaces is insufficient to cover all possible friction behavior in a feed-drive system. In chapter 2 of this thesis, two mathematical models are proposed of the nonlinear friction properties of various feed-drive systems based on experimentally obtained friction data. One friction model uses Gaussian functions to reinforce the conventional static friction model. This Gaussian-augmented friction model includes a nominal conventional static friction model and a number of Gaussian functions that represent sensitive nonlinear-friction sources in a ball-screw feed-drive system. The other model uses a sinusoidal component combined with the conventional static friction model to describe the friction behavior in systems with eccentric motion, such as a lead-screw feed-drive system. This eccentric friction model can better describe the friction properties of a feed drive system that have eccentric properties. Derivation of the conventional static friction model and the two proposed friction models are presented in chapter 2. In chapter 3 and chapter 4 of this thesis, the proposed friction models are used to design a tracking controller, a contouring controller, and a sliding-mode contouring controller to improve the accuracy of motion in a uniaxial ball-screw feed drive, a biaxial table and a triaxial machine tool.

Acknowledgements

I would like to express my sincere gratitude to Prof. Dr. Naoki Uchiyama for his willingness to take me into his research group and for his valuable instruction, guidance, and support which he has provided throughout my graduate studies at the Systems Engineering Laboratory. His enthusiasm and interest for science are contagious, and motivate me to overcome difficult problems in scientific research. I have learned not only scientific techniques from him, but also more importantly, the method of scientific thinking, how to identify a research problem, how to form and carry out a research plan and how to get results. I hope to continue keep contact with him and receive precious advise from him.

I am grateful thank to my committee members, Prof. Dr. Hideki Yanada and Prof. Dr. Shigenori Sano for their great support and constructive comments. In addition, I would like to thank to all members of the Systems Engineering Laboratory for their assistance and friendship during my graduate study.

Furthermore, I would like to thank Toyohashi University of Technology - 豊橋技術科学大学 and The Hori Sciences and Arts Foundation for their financial support and thanks for all Toyohashi University of Technology staff members for their assistance and friendship.

I extend most heartfelt thanks to my parents for their endless support, sacrifice, and unconditional love. I also thank my sisters, sisters-in-law, and brothers-in-law, and for their constant understanding and encouragement. The warm love of my family motivates me to go on.

Finally, and not the last, I want to thank The Vietnamese Students Association at Toyohashi University of Technology and all my friends I made in Japan and Toyohashi city...

Bùi Đình Bá

Contents

Declaration of Authorship	iii
Committes	v
Abstract	viii
Acknowledgements	ix
Contents	xi
1 Introduction and Literature Review	1
1.1 Industrial Machines and Research Motivation	1
1.2 Feed Drive System in Industrial Machines	4
1.3 Control of Uniaxial Feed Drive Systems	7
1.4 Control of Multi-Axis Feed Drive System	9
1.4.1 Introduction	9
1.4.2 Tracking Controller	9
1.4.3 Contouring Controller	9
1.4.4 Sliding Mode Contouring Controller	10
1.5 Friction Modeling and Compensation Methods	12
1.6 Contributions	13
1.7 Outlines	14
2 Mathematical Modeling of Feed Drive Systems with Friction and Identification	17
2.1 Introduction	17
2.2 Feed Drive Dynamics with Friction	18
2.3 Conventional Friction Model and Identification	23
2.3.1 Conventional Friction Model	23
2.3.2 Identification Method by Unbiased Least Squares Scheme and Kalman Filter	24
2.3.3 Identification Method by Velocity Control and Disturbance Observer	29
2.4 Gaussian Augmented Friction Model and Identification Method	30
2.4.1 Tracking Controller with Disturbance Observer	30
2.4.2 Gaussian Augmented Friction Model	32
2.4.3 Identification Method with Continuous Velocity-Friction Map	32
2.5 Eccentric Consideration Friction Model and Identification Method	34
2.5.1 Triaxial Machine Tool and Frictional Properties	34
2.5.2 Friction Model Considering Eccentric Property	35
2.5.3 Identification Method with Velocity-Friction Map and Position-Friction Map	38
2.6 Verification Experiment	39

2.7	Conclusions	41
3	Uniaxial Feed Drive and Biaxial Table Control	45
3.1	Uniaxial Feed Drive Control	45
3.1.1	Introduction	45
3.1.2	Uniaxial Feed Drive Dynamics and Identification . . .	45
3.1.3	Tracking Controller Design	46
3.1.4	Simulation Results	46
3.1.5	Experimental Results	46
3.1.6	Conclusions	49
3.2	Bi-Axial Table Control	51
3.2.1	Introduction	51
3.2.2	Identification of Bi-Axial Table Dynamics	53
3.2.3	Contouring Control of Bi-axial Table	54
3.2.3.1	Estimation of Two-Dimensional Contour . . .	54
3.2.3.2	Contouring Controller Design for Bi-axial Ta- ble	55
3.2.3.3	Experimental Results	56
3.2.4	Conclusions	61
4	Triaxial Machine Tool Control	67
4.1	Introduction	67
4.2	Identification of Triaxial Machine Tool	69
4.3	Tool Position Contour Error Estimation	69
4.4	Contouring Control Design with Eccentric Configuration Fric- tion Model	71
4.4.1	Identification of Conventional Friction Model	71
4.4.2	Identification of Eccentric Configuration Friction Model	72
4.4.3	Contouring Controller Design	73
4.4.4	Experimental Results	74
4.4.4.1	Experimental Results of Circular Contouring	75
4.4.4.2	Experimental Results of Non-Circular Con- touring	77
4.5	Sliding Mode Contouring Controller Design with Adaptive Friction Compensation	81
4.5.1	Sliding Mode Contouring Controller Design	81
4.5.2	Friction Model Design for Adaptive Control	83
4.5.3	Experimental Results	84
4.6	Conclusions	87
5	Conclusions and Future Research	91
5.1	Conclusions	91
5.2	Future Research	93
A	Publications	109

List of Figures

1.1	Industrial machines	1
1.2	Machine tool in production circle	2
1.3	Friction sources in machine tool	3
1.4	Friction definition and friction effects	3
1.5	Ball-screw feed drive system	4
1.6	Direct drive - linear motor	4
1.7	Feed drive system structure	5
1.8	Triaxial machine tool	6
1.9	Feedback controller for a uniaxial feed drive systems	7
1.10	Feed-forward and feed-back controller for a uniaxial feed drive system	8
1.11	State trajectory during reaching phase and sliding phase in sliding mode control	11
2.1	Bi-axial table system	19
2.2	Bi-axial table RmechCNC controller user interface	20
2.3	General feed drive dynamics	20
2.4	Feed drive dynamics with various friction sources	21
2.5	Modeling of DC motor in feed drive systems Control tutorials for MATLAB and Simulink (CTMS)	22
2.6	Feed drive dynamics with unified friction	22
2.7	Combined friction sources in feed drive dynamics	23
2.8	Coulomb-viscous-Stribeck friction model	24
2.9	Input signal used in identification tests	26
2.10	Input signal used in identification tests	26
2.11	X and Y axes parameters - Use simple least squares and unbiased least squares identification techniques	27
2.12	Input signal used in identification tests	28
2.13	Observed and original modeled friction of the X axis	28
2.14	Observed and original modeled friction of the X axis use velocity control method	29
2.15	Simplified Feed drive dynamics with unified friction	30
2.16	Controller design with disturbance observer for feed drive systems	31
2.17	Reference and measured position	33
2.18	Driving force	33
2.19	PD Controller with disturbance observer for feed drive systems	34
2.20	Measured and estimated non linear static friction model	35
2.21	Triaxial machine tool	36
2.22	Reference for y-axis motion	37
2.23	Observed friction on y-axis	37
2.24	Eccentric friction in feed drive system	38
2.25	Modeling of eccentric phenomenon between lead screw and nut	38

2.26	Reference for y-axis motion	40
2.27	Observed friction on y-axis	40
2.28	Observed eccentric friction	41
2.29	Comparison with conventional friction model	42
2.30	Real velocity and Velocity prediction from model A, B and C for ball-screw in x axis of bi-axial table	42
2.31	Real velocity and Velocity prediction from model A, B and D for lead-screw in y axis of triaxial machine tool	43
3.1	Ball-screw feed drive system	45
3.2	Simulation results, $\omega = 30$	46
3.3	Simulation results, $\omega = 30$	47
3.4	Simulation results, $\omega = 40$	48
3.5	Simulation results, $\omega = 40$	48
3.6	Simulation results, $\omega = 40$	49
3.7	Simulation results, $\omega = 60$	49
3.8	Simulation results, $\omega = 60$	50
3.9	Simulation results, $\omega = 60$	50
3.10	Biaxial feed drive system	52
3.11	Original friction model and observed friction X axis	53
3.12	The Gaussian augmented friction model and observed friction X axis	53
3.13	Definition of Contour Error	54
3.14	Identified conventional friction model, x axis	55
3.15	Identified nonlinear friction model, x axis	55
3.16	Reference and real circular contour	56
3.17	Tangential error profile	57
3.18	Normal error profile	57
3.19	Contour error profile	58
3.20	Maximum contour error	58
3.21	Mean of contour error in 10 times experiment	59
3.22	Reference and real circular contour	59
3.23	Tangential error profile	60
3.24	Normal error profile	60
3.25	Contour error profile	61
3.26	Maximum contour error	61
3.27	Mean of contour error in 10 times experiment	62
3.28	Contour error profile-Experiment results with eight curve	62
3.29	Reference contour -Experiment results with eight curve	63
3.30	Max contour error in 10 times experiment -Experiment results with eight curve	63
3.31	Contour error profile-Experiment results with trifolium curve	64
3.32	Reference contour -Experiment results with trifolium curve	64
3.33	Max contour error in 10 times experiment -Experiment results with trifolium curve	65
3.34	Measured position and contour error at 9.5mm/s for controller (a), (b), and (c)	65
3.35	Measured position and contour error at 9.5mm/s for con- trollers (d), (e), and (f)	65
3.36	Measured position and contour error at 9.5mm/s for controller (a), (b), and (c)	66

3.37 Measured position and contour error at 9.5mm/s for controllers (d), (e), and (f)	66
4.1 Triaxial machine tool	67
4.2 Linear dynamics of a feed drive	70
4.3 Definition of contour error	71
4.4 Observed friction and approximation by a conventional friction model	72
4.5 Reference for y-axis motion	73
4.6 Conventional friction model and observed friction on y-axis	73
4.7 Eccentric configuration friction model and observed friction	74
4.8 Graphical user interface for experiment	75
4.9 Circular contour tracking results for controller (a)	76
4.10 Circular contour tracking results for controller (b)	76
4.11 Circular contour tracking results for controller (c)	77
4.12 Maximum contour error results in circular reference	77
4.13 Mean contour error results in circular reference	78
4.14 Non-circular contour tracking results for controller (a)	78
4.15 Non-circular contour tracking results for controller (b)	79
4.16 Non-circular contour tracking results for controller (c)	79
4.17 Maximum contour error results in non-circular reference	80
4.18 Mean contour error results in non-circular reference	80
4.19 Circular contour tracking results for controller (a)	85
4.20 Circular contour tracking results for controller (b)	86
4.21 Mean contour error results	87
4.22 Power consumption results	87
4.23 Non-circular contour tracking results for controller (a)	88
4.24 Non-circular contour tracking results for controller (b)	89
4.25 Mean contour error results	89
4.26 Power consumption results	90

List of Tables

2.1	Estimated feed drive dynamics with conventional friction . . .	27
2.2	Estimated feed drive dynamics with conventional friction . . .	30
2.3	Estimated Gaussian augmented friction model parameters . . .	34
2.4	Estimated nonlinear friction model parameters	39
3.1	Contour error in different friction compensation strategies at 3mm/s	62
3.2	Contour error in different friction compensation strategies at 9.5mm/s	62
4.1	Triaxial machine tool parameters	70
4.2	Estimated conventional friction model parameters	72
4.3	Estimated eccentric configuration friction model parameters . .	74
4.4	Machine tool parameters	84
4.5	Controller gains	84

List of Abbreviations

CAD Computer-Aided Design

CAM Computer-Aided Manufacturing

MPC model predictive control

UAV Unmanned Aerial Vehicle

UGV Unmanned Ground Vehicle

CV Computer Vision

AI Artificial Intelligent

CNC Computer Numerical Controlled

DOF Degree of Freedom

FRF Frequency Response Function

LES Least Squares Estimation

PID Proportional-Integral-Derivative

PD Proportional-Derivative

PI Proportional-Integral

ZPETC Zero Phase Tracking Error Control

DOB Disturbance Observer

SMC Sliding Mode Control

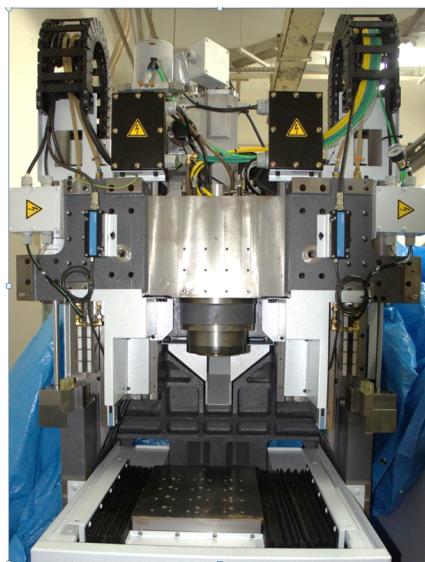
Chapter 1

Introduction and Literature Review

1.1 Industrial Machines and Research Motivation



(A) Industrial robots
www.wsj.com - Bloomberg News



(B) Commercial 3 axis machine tool

FIGURE 1.1: Industrial machines

Industrial machines such as industrial robots and machine tools (Fig. 1.1) play crucial roles in different industries. In manufacturing industries, they have greatly increased productivity, accuracy, robustness, and cost efficiency. Among industrial machines, machine tools are some of the most importance machines when they are powered to manufacture products or parts (usually metallic but not necessarily so), thereby enabling the production of all other machines including themselves. Although Unmanned Aerial Vehicle (UAV), Unmanned Ground Vehicle (UGV), Computer Vision (CV), Artificial Intelligent (AI), robotics, machine learning, and deep learning might be considered "trendier" topics at the moment, the continuously rising demands for faster and more accurate machine tools still requires elementary research on machine tools, such as mechanical structural design and machine-tool controllers [1]–[3], components, and sensors. Figure 1.2 shows the manufacturing production cycle and the important role of machine tools in the machining process. The cycle begins with the design of molds or metal parts, aided by Computer-Aided Design (CAD) and Computer-Aided

Manufacturing (CAM) software. Once the design is ready, these software packages generate a machining program (Gcode) that is passed to the machine tools in the machining center in order to execute the machining process. The machine-tool controller moves the cutting tool according to this Gcode program to form the designed part from the work-piece. Finally, different parts are combined to form the final product.

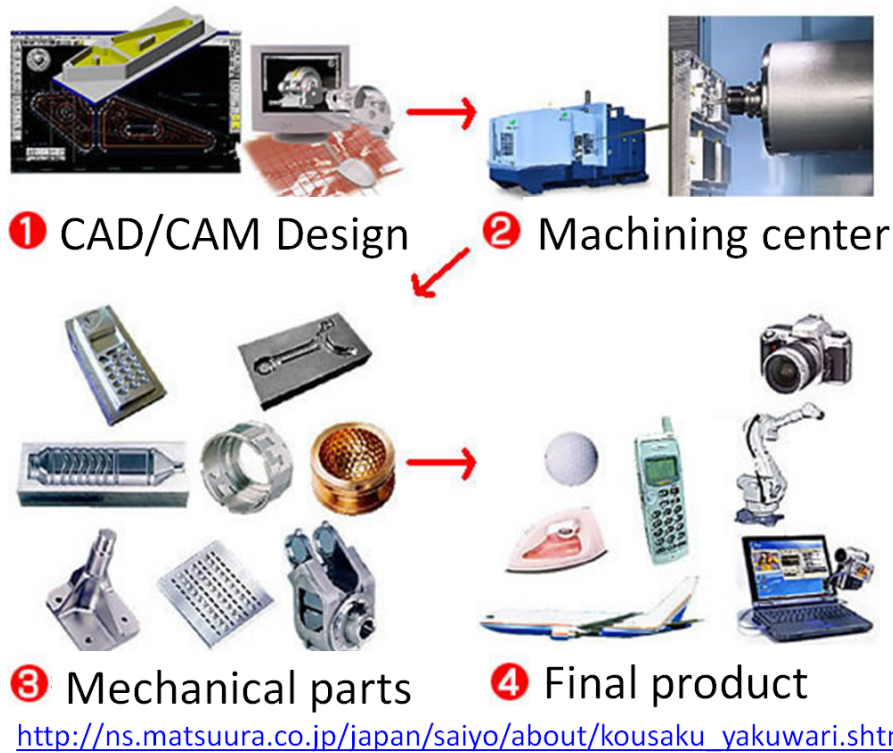


FIGURE 1.2: Machine tool in production circle

This thesis focuses on the controllers of the machine tools in the machining center in the production cycle, especially the design of a contouring controller for a machine-tool system. Nowadays, most machine tools have an integrated computer to improve flexibility and accelerate the machining progress. These are known as Computer Numerical Controlled (CNC) machines. The advances in computers have boosted all manner of technological fields, including computing, materials, motor manufacturing, and especially the highly accurate sensors that contribute to the precision and speed of machine tools. The same advances have also improved the computational speed of machine-tool controllers, resulting in more complicated controller methods to improve machine-tool accuracy. Such methods include contouring controllers, sliding-mode contouring controls, and adaptive compensation.

As we know, CNC machine tools run both day and night for years on end in manufacturing factories in order to increase productivity and efficiency. Hence, wear and friction are among the main concerns in maintaining machining performance and stability. Figure 1.3 shows some sources of friction in a machine-tool system and their undesired effects. In general, these require maintenance effort (e.g., lubrication, replacing parts, sensor calibration) to

keep the system working well. However, we can also improve the machining performance and decrease the frictional effects from a control perspective. This motivated my PhD research into control approaches to compensating the frictional effects and reducing chattering and energy consumption by modeling the nonlinear friction properties.

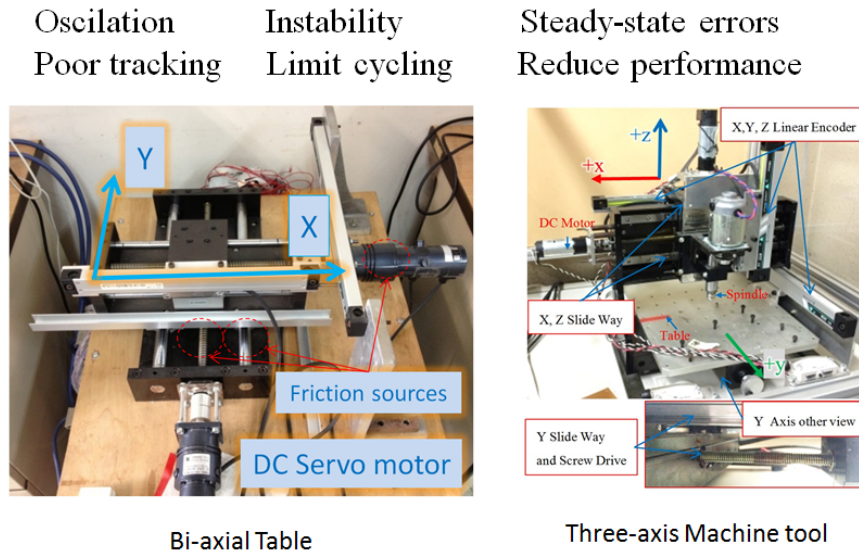


FIGURE 1.3: Friction sources in machine tool

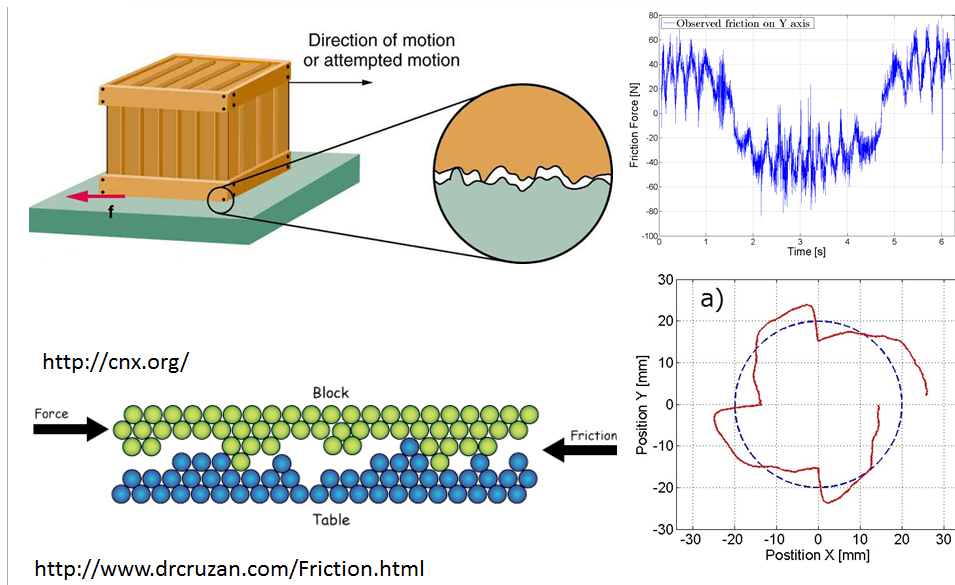


FIGURE 1.4: Friction definition and friction effects

In the present context, a frictional force is a nonlinear phenomenon that originates from the motor, guide ways, gear system, and support bearings of servo drive systems[4]. In many ordinary cases, friction is a beneficial

phenomenon that facilitates everyday tasks such as holding a book, walking, or applying the brakes in a vehicle. However, in mechanical systems, friction often causes undesired effects as energy loss, vibration, and wear. Therefore, friction compensation plays an essential role in applications that involve precise motion control. However, friction is difficult to model because of its nonlinear properties, and the conventional method is often to reduce the complexity by modeling friction as being between two sliding surfaces as in Fig.1.4 [5], [6]. The present thesis focuses on nonlinear friction models in feed-drive systems of machine tools, and on control techniques to actively compensate the influence of friction at high speeds. The novel aspects of this thesis concern the effect of all the friction sources in a machine tool system, and the development of an analysis method to filter disturbances and noise in order to precisely measure the total nonlinear friction effect. Friction feed-forward compensation based on the nonlinear friction models is added to a conventional controller to reduce the tracking errors of single feed-drive systems and the contouring errors of multi-axis feed-drive systems. In addition, a robust sliding-mode controller and adaptive friction compensation are presented in order to reduce contour errors and energy consumption in a triaxial machine tool. The following sections review some of the research on the modeling of feed-drive dynamics and the control of ball-screw feed-drive systems.

1.2 Feed Drive System in Industrial Machines



FIGURE 1.5: Ball-screw feed drive system



FIGURE 1.6: Direct drive - linear motor

The feed-drive system is an importance part in industrial machines such as biaxial tables, multi-axis machines, and machine tools because it directs,

guides, and conducts the motion of the cutting tool to make the machine work. Two types of feed drive are often used in machine tools: a ball-screw drive (Fig. 1.5) and a direct drive (e.g., linear motor; Fig. 1.6). Ball-screw feed drives such as shown in Fig. 1.5 are often used in machine tools because of their advantages in relation to low cost, high stiffness against cutting-forces, being robust to disturbances, and table load variations due to their high gear ratio [7]. Nevertheless, because of their contact-type design and high gear ratio, ball-screw drives are subject to high friction and are limited by lower accelerations and speeds in comparison to direct drives, which are being used increasingly in high-speed machine tools. Shortcomings of linear motors are that they are significantly more expensive and their control is still a challenge, because of the direct conversion of motor current to driving force without a motion transmission ratio. This enables the disturbances or load variations to directly affect the tool or part motion, thereby raising serious robustness issues. So, for particular control purposes, ball-screw feed drives are still widely used in machine tools and other types of industrial machine. In addition, certain machining tasks require high cutting forces, consistency, and stability, and for these a machine tool with a ball-screw feed drive is the best solution.

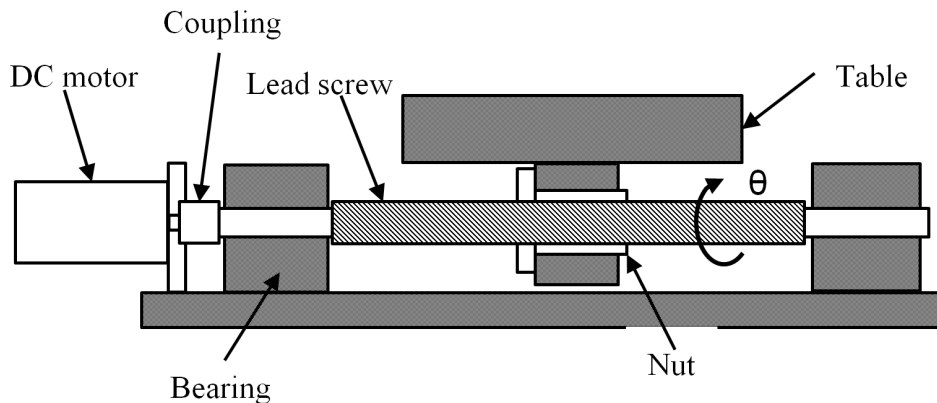


FIGURE 1.7: Feed drive system structure

Generally, ball-screw feed-drive systems are modeled as in Fig. 1.7 [8]–[10]. The driving system provides thrust and linear motion of the feed drive through a ball-screw mechanism. In a ball-screw feed-drive system, the motor torque is transmitted to the ball-screw shaft through a transmission-mechanism such as a coupling or gears. The screw-nut mechanism transforms the motor’s rotational motion into the linear motion of the table that holds the work-piece or the spindle that holds the cutting tool (Fig. 1.8). There are two smooth guide ways that support the screw-nut motion, enhance stability, and allow smooth linear movement [11], [12].

In machine tools, the feed-drives are required to provide fast and accuracy motion while maintaining stability. This encourages research into the accurate modeling of feed-drive dynamics with emphasis on electrical dynamics, bearing and guide-way friction, and high-order vibration. Throughout the years, a lot of research effort has gone into modeling ball-screw feed drives,

including their friction behavior. Rigid-body modeling is one of the common approaches, which captures the fundamental behavior that dominates the low-frequency range. This essentially consists of the effects of inertia as well as viscous and Coulomb-type friction. Other advanced models that considers axial coupling effect, torsional, and possibly bending vibrations [13]–[15], the dynamics and kinematics that affect the motion loss in the pre-loaded nut [16]–[18], motor torque ripples [19]–[21], vibration mode analysis [22]–[25] and the velocity dependent nonlinear friction [26]–[28], that enables more accurate prediction of the feed-drive's response.

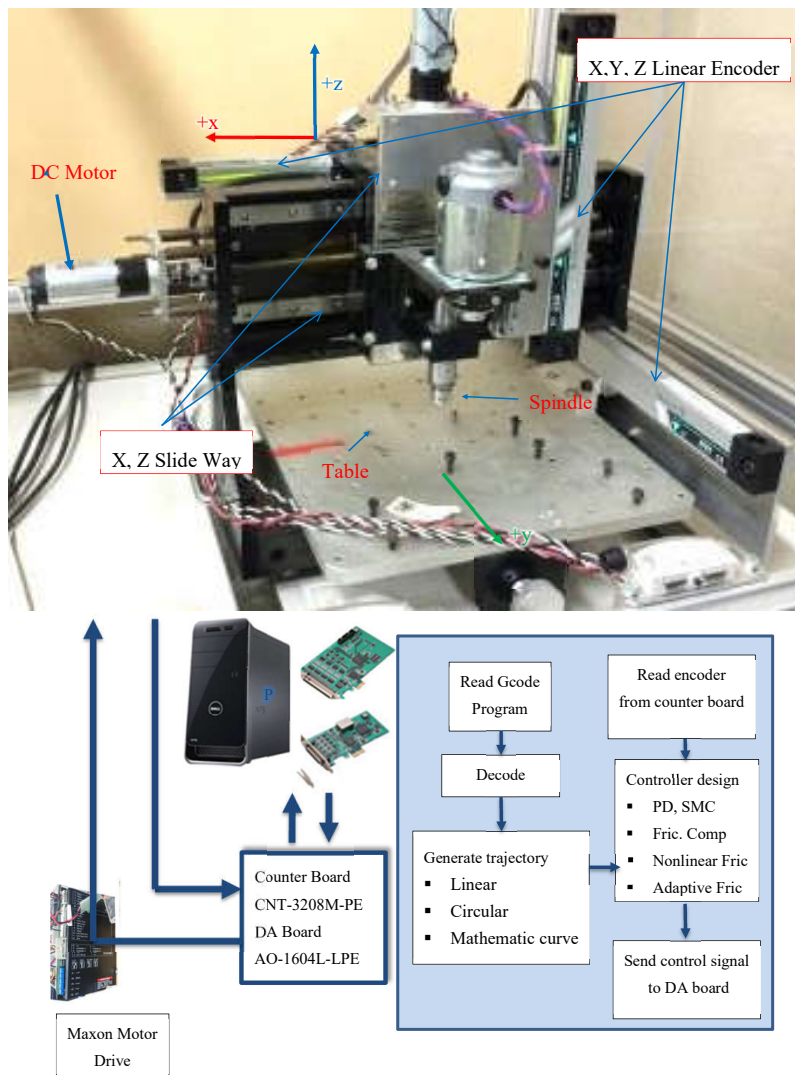


FIGURE 1.8: Triaxial machine tool

Some experimental measurements and optimization methods have been proposed to obtain parameters for the feed-drive model. Kamalzadeh and

Erkorkmaz [29] identified the mass, damping, and stiffness matrices of a two Degree of Freedom (DOF) ball-screw feed-drive model by matching the Frequency Response Function (FRF) acquired from the model to the FRF measured from the feed drive. However, their method was not concerned with identifying off-diagonal terms in the mass matrix of the feed drive which are very important for precise control of flexible ball-screw feed drives, which are very important for precise control of flexible ball-screw feed drives. Okwudire[30] presented a simple but effective least-squares (LS) method for identifying the mass, damping, and stiffness matrices of a 2-DOF model of ball-screw drives (including the off-diagonal terms in the drive's mass matrix) based on FRF data. He also presented Flexible ball-screw feed drive that focus on modeling all mechanical parts of a ball-screw feed drive as ball Rigid body modeling. It is usually used in the controller of a machine-tool feed drive as feed-forward compensation. In order to obtain the parameters of a feed-drive system with a rigid-body model, Erkorkmaz and Altintas (2000) [27] proposed the Least Squares Estimation (LES) method for the identification process. They took into account the Coulomb friction of the system as an extra parameter, enabling the parameters of the linear model to be estimated without bias. Consequently, the friction model is refined by jogging the machine tool axes under closed-loop control at various velocities by using a disturbance observer (DOB) based on a Kalman filter [31]. Some other feed-drive models have been proposed and analyzed [22]–[25]. Khalick et al. [32] have proposed a controller method to reduce energy consumption in feed drive system by using nonlinear sliding-mode control with a nonlinear sliding surface.

This thesis considers the rigid-body modeling of a feed-drive system that concerns the effects of inertia and friction. In addition, we propose friction models that include viscous, Coulomb-type friction, and additional nonlinear friction to adaptively compensate the nonlinear behavior of the feed-drive system. The proposed models are presented in chapter 2. For parameter identification, this thesis consider a hybrid identification method whose details are presented in chapters 3 and 4.

1.3 Control of Uniaxial Feed Drive Systems

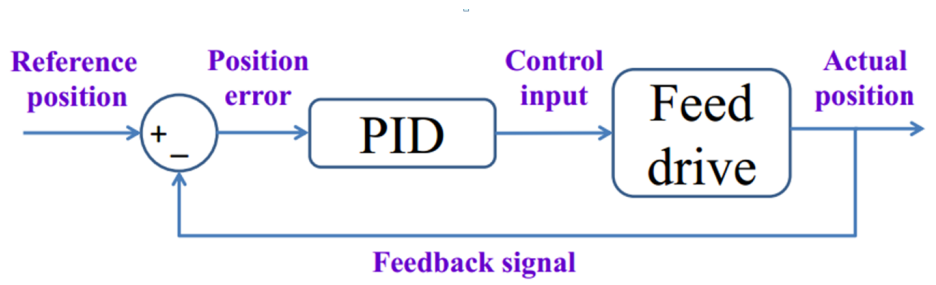


FIGURE 1.9: Feedback controller for a uniaxial feed drive systems

Uniaxial feed-drive control often refers to tracking control problems in which the feed-drive system is simplified as a second-order linear system. The

linear properties can be confirmed experimentally when the magnitude of the steady-state tracking error is directly proportional to the command desired command velocity and inversely proportional to the square of the closed-loop control bandwidth [33]–[35].

In commercial controllers, simple control strategies such Proportional-Derivative (PD), Proportional-Integral (PI), or Proportional-Integral-Derivative (PID) control are often used in the design of feedback control systems [36], [37] and to tune the control gains to achieve the fastest possible response with acceptable overshoot. A typical PID feedback controller is shown in Fig. 1.9. In a PID controller, the control signal is a combination of three components: proportional, integral, and derivative of the position error. The PID control method is more popular than other control method because it is simple to install and program, is stable, and is easily understood by most control engineers. However, the use of feedback control such as PID approaches alone results in relatively limited bandwidth and poor tracking performance at corners or in high-speed or nonlinear contour-tracking problems. For this reason, a feed-forward controller is added to the control loop to predict the desired control signal and to enable accurate tracking of tool paths at high feed-rates. Feed-forward control takes advantage of prior knowledge about the reference trajectory to predict an approximate control signal and incorporate it with the feed-back controller to attain accurate tracking at high speeds and on highly curved contours. The basic feed-back control with feed-forward control strategy is shown in Fig. 1.10. The feed-forward control block aims to predict an approximate control signal with which to cancel the almost dominant control force, thereby enabling the feed-back control to focus on compensating for minor disturbances or small differences between the predicted and actual control signals.

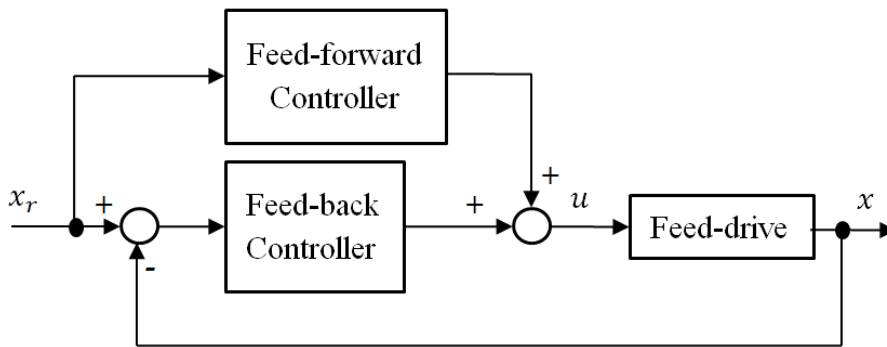


FIGURE 1.10: Feed-forward and feed-back controller for a uniaxial feed drive system

The main contribution to feed-forward tracking control was made by Tomizuka [38], who proposed the Zero Phase Tracking Error Control (ZPETC) scheme that achieves a wide bandwidth with zero phase (i.e., time) delay. By excluding the unstable zeros, the closed-loop transfer function is canceled with a feed-forward filter. Theoretically, ZPETC has an excellent ability to track complex trajectories, because of its zero phase delay and higher overall

bandwidth. However, the control method requires very accurate identification of the feed drive's transfer function which must be time invariant. Pritschow and Philipp [39] have pointed out that a significant degradation in tracking accuracy is caused by the variation of the feed-drive parameters when ZPETC or other feed-forward control strategies are used. Tsao and Tomizuka [40] have implemented adaptive zero-phase error-tracking control to deal with this problem.

1.4 Control of Multi-Axis Feed Drive System

1.4.1 Introduction

Motion control in multi-axis feed-drive systems or machine tools falls into one of two major categories: tracking and contouring control. In multi-axis machines, tracking control refers to independent position control of each axis drive using its own feedback. In contrast, contouring control is the case in which the contour error (i.e., the geometric deviation from the desired tool path) is estimated directly and used in the feedback control law.

1.4.2 Tracking Controller

The tracking controller in a multi-axis feed-drive system is similar to that in a single feed drive system in which there is independent position control on each axis. However, the desired contour in multi-axis control is not a straight line, but could be a circular contour, a non-circular contour, or a five-axis contour that requires orientation to generating the path. So, the tracking control problem with multiple axes requires a more advanced tracking controller for adaptive and robust control with feed-forward and disturbance compensation. Khalick et al. [32] proposed nonlinear sliding-mode control with a nonlinear sliding surface to improve the tracking performance and energy efficient. Erkorkmaz [5] combined feed-rate optimization, modeling, and identification of feed drive dynamics and adaptive sliding-mode control design to achieve fast and accurate control performance. The above approaches can be applied to effectively reduce tracking errors for uniaxial or decoupled motion applications. However, they do not guarantee contouring performance when applied to multi-axis contour-following tasks.

1.4.3 Contouring Controller

In the control of multi-axis feed-drive systems such as machine-tool control, the position error with respect to each feed-drive axis is generally used as a feed-back signal. However, with regard to machining, error components orthogonal to the desired contour curves are more important than errors related to the individual feed-drive axes. Error components orthogonal to the contour curves are called contour errors. Reduction of these error components is an effective method for contour following in multi-axis machining tasks. Many studies have proposed ways to estimate contour errors and design an effective contouring controller. Koren proposed a cross-coupling controller that calculates contour errors from the drive-axis tracking errors and applies contour-control gain to those components to improve the contour performance while restricting the magnitude of the tracking errors [41]. Ho

et al. decomposed the contour error into a normal tracking error and an advancing tangential error, after which a dynamic decoupling procedure is applied to the system dynamics [42]. Cheng et al. [43] proposed an integrated control scheme that consists of a feedback controller, a feed-forward controller, and a modified contour-error controller (i.e., a CCC equipped with a real-time contour-error estimator). In addition, they proposed a fuzzy-logic-based feed-rate regulator to further reduce the contour error. Cheng and Lee proposed a real-time contour-error estimation algorithm [44]. Tarn et al. presented a cross-coupled fuzzy-feedrate control scheme [45] that uses a genetic algorithm to optimize the controller parameters. Chin et al. proposed a fuzzy-logic controller with a proven algorithm in the cross-coupled pre-compensation method, and using both the position and the contour error to generate a compensation term [46] for friction. Yeh and Hsu [47] proposed an adaptive federate interpolation algorithm based on the geometric relationship between chord error and curvature constraints. Jee and Koren proposed an adaptive fuzzy-logic controller to reduce the contour error [48]. They adjusted both input and output membership functions simultaneously within a stable range derived from a stability analysis.

Advanced optimal and nonlinear controllers applied to contouring-controller design have had their effectiveness verified [49], [50]. Nevertheless, they have a disadvantage that both the contour and tracking errors in the feed-drive axis are used to calculate the control input, and this compromises the contour-tracking performance. Considering the contour and tracking errors simultaneously creates difficulties in adjusting the controller parameters. Lo and Chung proposed contouring control for biaxial feed drives based on a coordinate transformation [51], in which the tracking error of the feed-drive axis is converted to error components that are orthogonal and tangential to the desired contour curve. This obtains two decoupled single-input/output systems for the orthogonal and tangential directions, and enables controllers for each direction to be designed independently, hence simplifying adjustment of the controller parameters. Chiu and Tomizuka proposed a similar approach in which a task coordinate frame is defined at the desired position of the feed-drive system. The control-system dynamics are reformulated with respect to this coordinate frame, corresponding to the orthogonal and tangential directions of the desired contour curve. The orthogonal error component is regarded as an approximation of the actual contour error [52]. Although this approach provides control-system stability for any contour curve, the difference between the actual contour error and the determined orthogonal error component may result in an increase in the contour error. Ye et al. proposed a new cross-coupled path pre-compensation algorithm and fourth-order dynamics for rapid prototyping and manufacturing systems [53]. Uchiyama et al. designed a contouring control that was focused on reducing the consumed energy and controlling the input variance [54].

1.4.4 Sliding Mode Contouring Controller

Sliding-mode control (SMC) is a unique class of variable structure control that has nonlinear feedback that switches discontinuously in time on a specified sliding surface. SMC is also well known for its insensitivity to disturbances and parameter variations [55]. SMC originated in the Soviet Union in the late 1950s, but was not published outside the Soviet Union until 1976

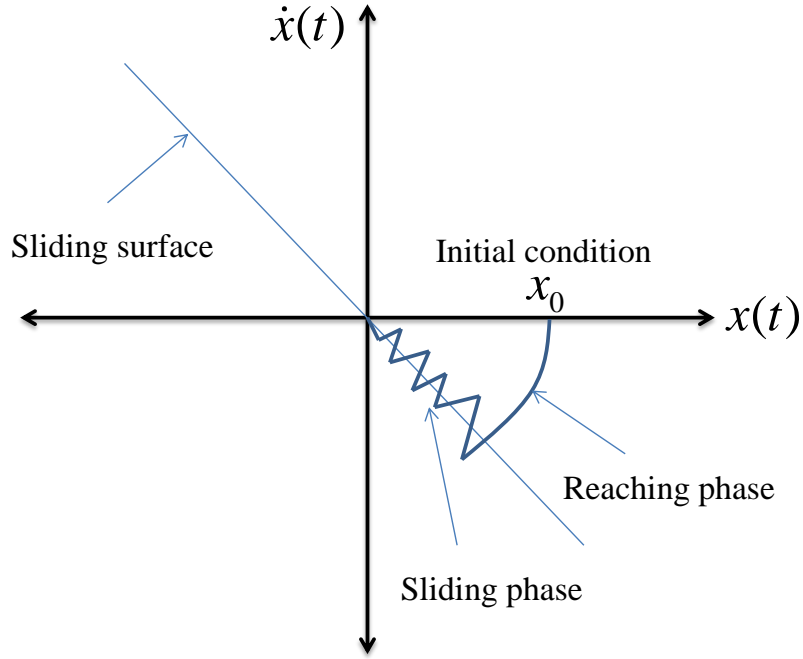


FIGURE 1.11: State trajectory during reaching phase and sliding phase in sliding mode control

when the publications [56] and [57] are released. After these publications, the list of publications concerning SMC grew rapidly and SMC has been receiving increasing attention in many control fields such as electromechanical systems, servo systems and robotic manipulators.

Sliding-mode control has several interesting properties compared with conventional control methods. These include its relatively simple design, invariance to external disturbances and system-dynamics characteristics, control of independent motion (as long as sliding conditions are maintained), and wide variety of operational modes such as trajectory control, regulation [58], model following [59] and observation [60]. Although SMC has been already addressed in many studies [61]–[64], surveys [65], or books [66]–[68], many facets of it remain to be studied from theoretical and applied perspective viewpoints [69].

In order to explain the sliding mode control approach, let us consider the following first order uncertain system [55]:

$$\dot{x}(t) = ax(t) + bu(t) + \rho(x, t). \quad (1.1)$$

where $x(t) \in R$, $u(t) \in R$ are the control variable and control input, respectively. a and b are known nonzero constants. $\rho(x, t) \in R$ refers to unknown uncertainty and only the bounds of this uncertainty are known. In order to stabilize the system in (1.1), if the initial value of $x(t)$ is positive then $\dot{x}(t)$ should be negative and vice versa. Therefore, depending on the sign of $x(t)$, control law should be altered to ensure stabilization of $x(t)$. Consider the following control law:

$$u(t) = -b^{-1}(ax(t) + Q\text{sgn}(x)). \quad (1.2)$$

where $\text{sgn}(\cdot)$ denotes the sign function, and $Q > 0$ is chosen such that

$$Q \geq \rho_{max}. \quad (1.3)$$

where ρ_{max} represents the upper bound of the uncertainty $\rho(x, t)$. With control law (1.2), system (1.1) becomes

$$\dot{x}(t) = -Q\text{sgn}(x(t)) + \rho(x, t). \quad (1.4)$$

In order to analyze the above closed-loop system, consider the following three different cases. Firstly, for an initial condition $x(0) > 0$, from (1.4) we can see that $\dot{x}(t) < 0$. Therefore, $x(t)$ is decreasing and moving towards the origin $x(t) = 0$. Secondly, for an initial condition $x(0) < 0$, then from (1.4) we have that $\dot{x} > 0$. Therefore, $x(t)$ is increasing and approaching $x(t) = 0$. Thirdly, for $x(t) = 0$, the discontinuous part of the control law is not defined. However, the moment the trajectory crosses the surface $x(t) = 0$ from either direction, again it is forced back on $x(t) = 0$ according to the aforementioned two cases. Therefore, in all cases, $x(t)$ is moving toward the point $x(t) = 0$. Thus, the control law (1.4) forces the system state $x(t) = 0$ regardless of the initial conditions.

In order to understand more physically what is happening during sliding-mode control, let us consider the following sliding surface for a second-order system:

$$s(x, t) = kx + \dot{x}. \quad (1.5)$$

where x and \dot{x} are the states of the system, and k is a positive constant. Figure 1.11 shows the state trajectories in the vicinity of the sliding surface $s(x, t) = 0$. The sliding-mode control has two phases as shown in Fig. 1.11: the initial phase in which the trajectory is forced toward $s(x, t) = 0$ this is known as the *reachingphase*, and the secondary phase in which when $s(x, t) = 0$ (this is known as the *slidingphase* or *slidingmode*). During the reaching phase, external disturbances can affect the system performance, whereas during the sliding phase the system motion is insensitive to external disturbances. Because the control law is discontinuous about $s(x, t) = 0$, it requires switching at very high frequency to maintain the system on the desired sliding surface. If this switching occurs at a very high frequency, then $s(x, t) = 0$ can be maintained consistently with this discontinuous control law.

1.5 Friction Modeling and Compensation Methods

In machine tool-control, there are two different types of disturbance force that can critically affect the tracking performance and the quality of work-piece finishing quality: friction [70]–[74] and cutting forces. This thesis is focused on investigating, modeling and identifying friction behavior in the feed drive of a machine tool.

For simplicity, friction in a feed-drive system is generally described as resistance to motion when two surfaces slide against each other [75]–[79]. In many cases friction play a useful role (e.g., vehicle movement and braking), but it can also cause undesirable effects (e.g., wear and tear, increased energy consumption). For example, in high-precision mechanical systems, friction can damage high-quality parts and deteriorate the performance of

the system. Possible unwanted consequences caused by friction are steady-state errors, limit cycling, and hunting. In motion control, a possible way to minimize the influence of friction is to reduce and compensate it with a friction model. In order to be able to compensate the effect of friction, it is necessary to describe the frictional behavior precisely. Because there is no exact formula with which to represent a frictional force, friction is normally described with an empirical model. By canceling the frictional effect, the nonlinearity in the system (assuming no other nonlinear behavior is present) is removed. This is beneficial for classic control that is based on linearity and in which the feedback is therefore not able to compensate for frictional effects completely.

Conventional friction models usually model friction as being linear at high speeds and nonlinear at very low speeds or before the onset of sliding. At high speeds, the friction force depends mainly on the velocity. At very low speeds or before the onset of sliding, the frictional behavior is nonlinear because of various nonlinear phenomena (e.g., the Stribeck effect and frictional lag). Typical friction models contain the Stribeck effect, Coulomb friction and linear viscous damping [80]–[86]. Some controllers designed with friction compensation [87]–[89] have been proposed. There are also some adaptive friction designs that compensate for the nonlinear properties [85], [90]–[93]. In this thesis, the friction is assumed to stem from both linear and nonlinear friction sources. Two nonlinear friction models are proposed in chapter 2.

1.6 Contributions

This thesis presents work about modeling and identifying nonlinear friction properties in feed-drive systems. In addition, a contouring controller with feed-forward nonlinear friction compensation is proposed to achieve accurate contouring motion control. Such highly accurate motion of the feed-drive axis will also contribute to high-precision machining. Experimental results of control with the proposed nonlinear friction-compensation model show the effectiveness of reducing the contouring errors and the control input variance. Consequently, this reduces vibrations, energy consumption, wear, and maintenance costs of industrial machines, thereby contributing to higher productivity, lower costs, and longer operating life. The main contributions are listed as follows:

- (1) Based on the noted mismatch between conventional models of feed-drive systems and experimental results, the complicated structure of feed-drive systems in machine tools is investigated and analyzed further. Sinusoidal reference experiments, velocity–friction maps and position–friction maps are proposed in this thesis to determine the dynamical properties, especially the friction properties in feed-drive systems. These approaches reveal that nonlinear friction phenomena appear not only before sliding or at low speeds but also at high speeds. In addition, the nonlinear properties depend on the type and structure of the feed-drive system. In a ball-screw feed-drive system, because of the high transmission ratio, the system is stable and the nonlinear properties are not appreciable. This thesis proposes a Gaussian augmented friction model of the nonlinear friction properties in a ball-screw feed-drive system; such a model has Gaussian functions

incorporated with a conventional static friction model. In lead-screw feed-drive system, the wear phenomenon is made much more serious because of low-quality material and insufficient lubrication. This leads to eccentric motion between the lead-screw and the nut of a lead-screw feed-drive system, and this motion is a dominant source of nonlinear friction. Experimental results from a triaxial machine-tool setup confirm the hypothesis of this thesis, for which the velocity–friction map shows the high deviation and repetitive sign of the friction value. This thesis proposes a friction model that takes eccentricity into consideration in order to compensate for the eccentric friction properties in a lead-screw feed-drive system. The model uses the sinusoidal component combined with the conventional static friction model to describe the frictional behavior.

- (2) Design the tracking controller and the contouring controller using different friction-compensation techniques is proposed to achieve accurate contour motion. Both simulations and experiments are conducted for a uniaxial ball-screw feed drive, a biaxial table, and a triaxial machine tool. Experimental results show that the performance can be improved by using the proposed nonlinear friction-compensation model.
- (3) An adaptive nonlinear friction model is designed to compensate for the nonlinear friction properties in a triaxial machine tool feed drive. In addition, we propose a robust sliding-mode contouring controller with adaptive friction compensation to deal with parametric uncertainties, nonlinear friction sources, and other unknown disturbances. Furthermore, this reduces control-input chattering, contouring errors, and energy consumption.

1.7 Outlines

The main research in this thesis is concerned with nonlinear friction modeling, identification, and application in the design of a contouring controller with nonlinear friction compensation to improve the contouring performance of machine tools. The remainder of this thesis is organized as follows. Chapter 2 begin with a literature review about the conventional static friction model and identification. After that, this chapter proposes a method for constructing high-density velocity–friction and position–friction maps that are based on sinusoidal-reference experimental results. This chapter also presents two nonlinear friction models that describe the nonlinear properties in ball-screw feed-drive systems and lead-screw feed-drive systems. The first one, the Gaussian augmented friction model, is proposed to compensate for the nonlinear friction in a ball-screw feed-drive systems. This Gaussian-augmented friction model includes a nominal conventional static friction model and a number of Gaussian functions that approximate sensitive nonlinear friction sources in a ball-screw feed-drive system. The second one, the eccentric-consideration friction model, is proposed to compensate for nonlinear friction in a lead-screw feed-drive systems. The eccentric-consideration friction model uses the sinusoidal component combined with the conventional static friction model to describe the eccentric friction between the

lead-screw and the nut in the lead-screw feed-drive system of triaxial machine tools. Uniaxial feed-drive control with friction compensation is presented in section 3.1 of chapter 3. Biaxial table control with friction compensation is presented in section 3.2 of chapter 3. Chapter 4 present two controller designs for triaxial machine tools. These are contouring control with eccentric-consideration friction compensation, and robust sliding-mode contouring control with adaptive friction compensation. Simulations and experiments are conducted and confirm the effectiveness of the proposed methods. Conclusions and future work are given in chapter 5.

Chapter 2

Mathematical Modeling of Feed Drive Systems with Friction and Identification

2.1 Introduction

In machine-tool control, understanding and precisely modeling the system dynamics are important processes for improving the control performance. Modeling the system dynamics includes modeling the feed-drive dynamics, the friction, and the cutting force. Although the feed-drive dynamics are often simplified as a second-order linear system, the friction and cutting force components are nonlinear and time variant. This chapter is focused on the identification of a feed-drive system with nonlinear friction properties, and the method for extracting frictional behavior from the disturbance and chattering signals.

As defined in Chapter 1, friction is a common physical phenomenon in mechanical system. It comes from moving parts and results in unexpected effects on the feed-drive motion, such as stick-slip oscillations, steady-state errors, and low tracking accuracy and contouring performance. In order to attenuate these adverse effects and achieve high-precision motion, model-based friction compensation methods are usually used in the design of motion control systems for compensating the friction phenomena [26], [94]–[99]. Therefore, suitable friction models are required for motion control design, and the friction compensation performance mostly depends on the correctness of the selected friction models. In general, a friction model is usually developed from basic knowledge about the frictional behavior of a mechanical system. However, it is not easy to determine friction model because there are many factors affecting the friction behavior, such as the surface texture, material and lubrication of the bodies in contact [100]–[107]. Therefore, a simpler friction model is preferred, and many simplified friction models have been proposed for motion control and compensation design [26], [96], [100], [107], [108]. Optimization methods are often used in the identification process to identify the parameters of friction models. For instance, Kim et al. [109] proposed an experimental identification method that used accelerated evolutionary programming to identify the parameters of the seven-parameter friction model presented by Armstrong-Helouvry et al. [26]. Cheok et al. [110] used the simplex method to optimize the parameters of the Karnopp friction model [111]. To experimentally obtain the friction-velocity map, Canudas-de-Wit and Lischinsky [112] also used the simplex method to obtain the optimal parameters of the LuGre friction model [6].

Conventionally, for particular experimental setup, the friction and velocity data values are often used for the identification process [108], [112], [113]. To obtain data values, two experiments are performed: a breakaway experiment and a constant-velocity experiment. The breakaway experiment begins by halting the moving parts of a mechanical system at certain positions for a given duration, and then slowly increasing the driving torque and measuring it at the point at which the parts begin to move. Therefore, the breakaway experiment, which involves sampling the static friction at a suitable frequency, can be utilized to identify static friction and develop a nonlinear friction model at low speeds for motion reverse friction compensation. In the constant-velocity experiment, data measured during the constant-velocity motion of a moving part are used to construct a friction-velocity map at both low and high speeds. Linear or nonlinear optimization algorithms are then used to identify the parameters of a friction model by fitting the model to the friction-velocity data map so obtained. Although velocity control-loop methods can be employed to obtain data values for friction identification processes, position-dependent perturbations that exist in mechanical systems can deteriorate the obtained friction-velocity map. In addition, unmodeled dynamics, usually induced by several flexible and inertia elements in a mechanical system, increase the uncertainties in the estimated friction characteristics. Yeh et al. [114] consider the merits of Disturbance Observer (DOB) feed back control [115] and integrated it into a velocity control loop to compensate for the speed perturbation induced by external disturbances and system uncertainties. They developed a friction extraction method that involves subtracting different torque values measured at the same position of the moving part.

Besides introducing the conventional approach, this chapter presents a new experimental method for obtaining a precise friction-velocity map to further understand the characteristics and nonlinear behavior of friction. The method based one sinusoidal reference experiment and controller with DOB. By using some filters and a nonlinear optimization method, a precise continuous friction-velocity map is obtained. Based on the proposed method, some nonlinear friction models are proposed to describe the nonlinear frictional behavior in a feed-drive system. To identify the friction in a feed-drive system, we first need to model the feed-drive system with friction and deal with its complexity. Details about feed-drive dynamics with friction will be presented in the next section.

2.2 Feed Drive Dynamics with Friction

The experimental setup used to identify friction models and verify the control algorithms developed in chapter 3, is a typical biaxial feed-drive system as shown in Fig. 2.1. A rotary encoder whose resolution for position measurement is 25nm is attached to the end of each servomotor to measure the actual position of the feed-drive system. The table is instrumented with linear encoders (100nm). Because there is no velocity sensor, a velocity signal is calculated by means of numerical differentiation of the position measurements. The system is controlled by the self-developed RmechCNC software on a personal computer (OS: Windows, CPU: 1GHz) with a sampling time of 5ms. The control program is written in C++. In order to provide a fixed

sampling period in a Windows environment, we employ a timer on a counter board with four channels of 24-bit up/down counters.

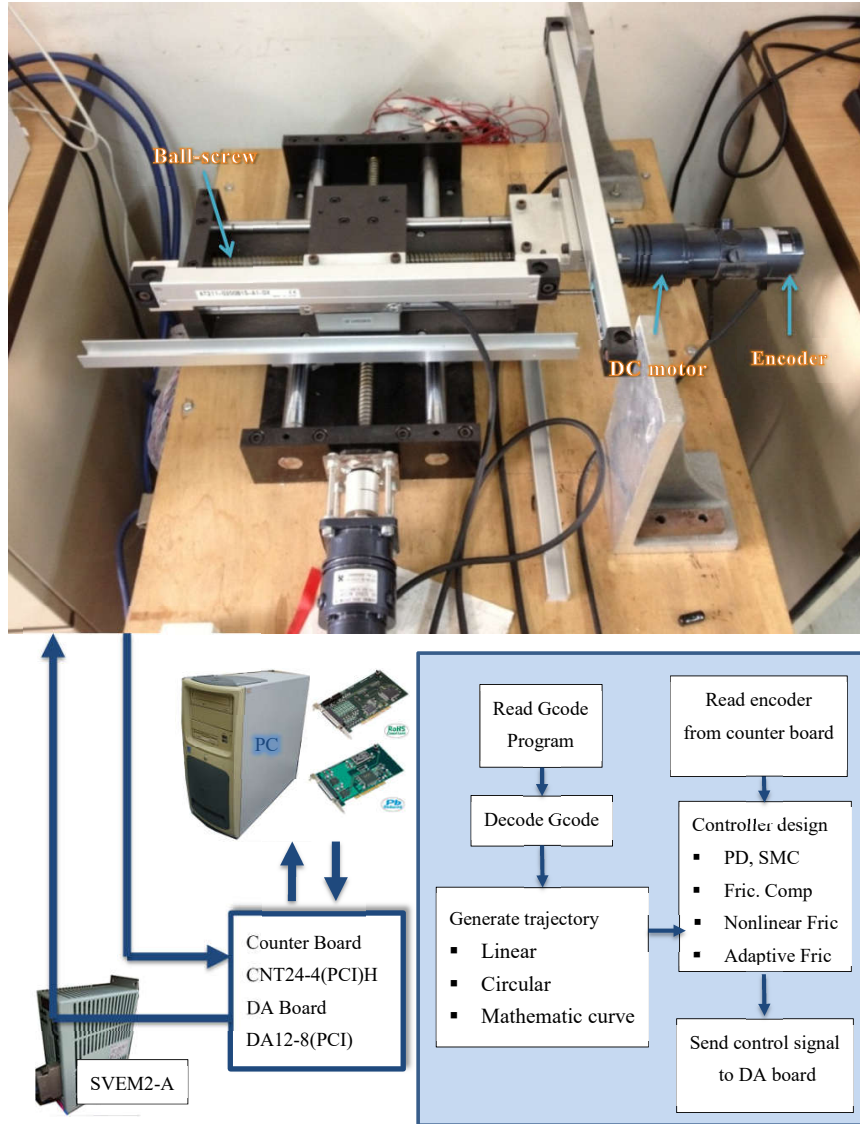


FIGURE 2.1: Bi-axial table system

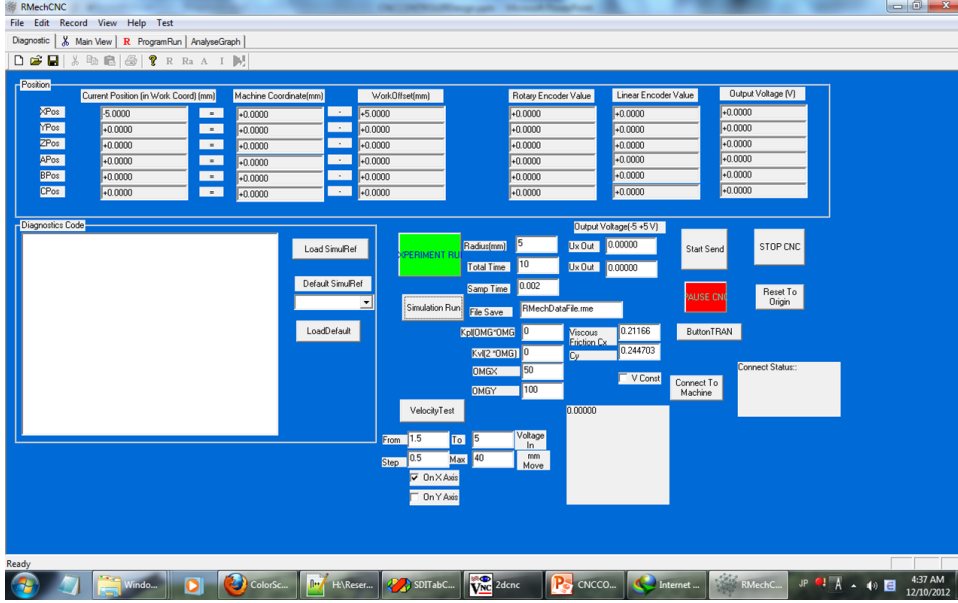


FIGURE 2.2: Bi-axial table RmechCNC controller user interface

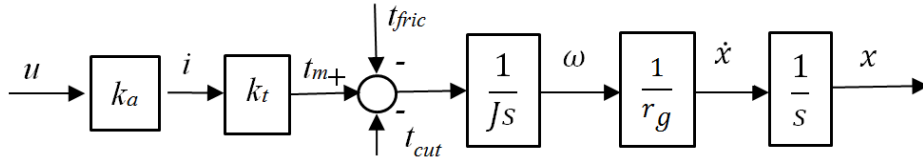


FIGURE 2.3: General feed drive dynamics

Generally, the feed-drive dynamics comprise the motor dynamics and the table dynamics, as shown in Fig. 2.3. Here, u (V) is the control signal applied to the input of the current amplifier, whose gain is k_a (A/V). The amplifier produces a current i (A) in the motor armature, resulting in a motor torque t_m that is linearly proportional to i with the motor torque constant k_t (Nm/A). The motor torque generates a driving force f_u (N) that is linearly proportional to t_m with the lead screw gain r_g (rad/mm). The feed drive is also subjected to a disturbance force that contains the effects of friction in the linear guide ways (f_{fli}) and ball screw (f_{fle}), as well as the cutting force f_c . The difference between f_u and $f_c + f_{fli} + f_{fle}$ is used to actuate the mechanical system consisting of the equivalent axis mass m (kg) of the corresponding axis. In this case, the amplifier is configured to operate in current-control mode, the torque loss due to back EMF is compensated by the current-control loop in the amplifier. Hence, neither the effects of back EMF nor the electrical armature dynamics are considered in this model. The lead screw gain r_g is calculated as follows:

$$r_g = \frac{2\pi}{L}, \quad (2.1)$$

where L is the lead of the screw. This gain is used in a lead-screw system to translate rotational motion to linear motion and motor torque to driving

force. This model was developed by Erkorkmaz [5]. In this thesis, we implement the identification method to estimate nominal mass and conventional friction parameters. This thesis also propose a density velocity–friction and a position–friction map construction method base on sinusoidal-reference control. This method figure out the mismatch between convention feed drive model and actual feed drive response. It can be explained that the friction is not only came from sliding motion between two simple surface but also came from nonlinear sources as torque disturbance t_d in Fig. 2.4.

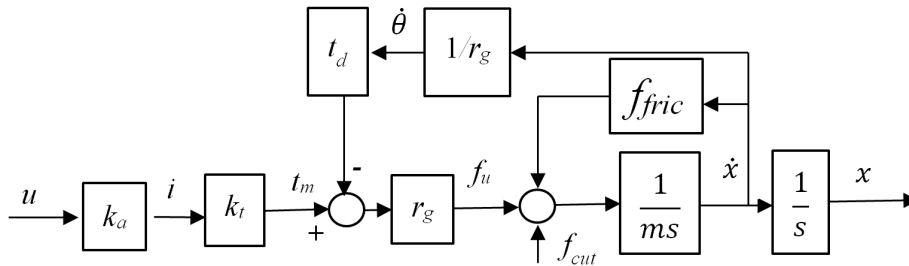


FIGURE 2.4: Feed drive dynamics with various friction sources

To model the precise effect of friction on the feed-drive system, we model the feed drive as shown in Fig. 2.4, where friction come variously from the motion associate with the motor shaft, the ball-screw nut, and the guide ways. The torque losses due to back EMF and friction act on the circular motion of the ball-screw to affect the system through a disturbance torque t_d . The friction from the guide-way motion and the cutting force affect the system directly through f_{fric} and f_{cut} , respectively. The general feed-drive dynamics include the motor dynamics and the ball-screw feed-drive dynamics. The motor dynamics are represented in Fig. 2.4 as a block diagram from u to t_m , which translates the control input u to a torque t_m acting on the ball-screw system.

Fig. 2.5 describe motor dynamics and represent by following equation:

$$\begin{aligned} L \frac{di}{dt} + Ri &= u - K_e \dot{\theta} \\ J \ddot{\theta} + t_m &= K_t i, \end{aligned} \quad (2.2)$$

where I is the motor current, L is the armature induction, R is the armature resistance, K_e is the back EMF coefficient, and u is the control input. As for the physical parameters of the motor, J is the motor inertia, t_d is the friction on the motor shaft, t_m is the torque that results from the active driving force from the ball screw to the motor shaft, K_t is the proportion of the current i to the motor torque output, and p is the pitch of the ball screw (5 mm). Although there is a physical current-feedback loop in the motor armature

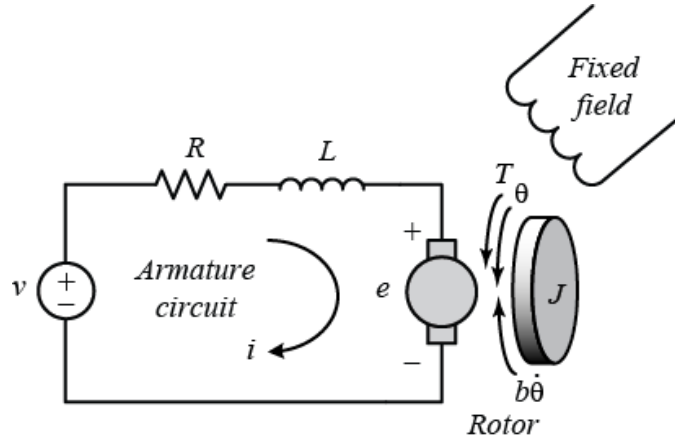


FIGURE 2.5: Modeling of DC motor in feed drive systems
Control tutorials for MATLAB and Simulink (CTMS)

circuit, its typical bandwidth is around only a few kiloHertz. This allows the current amplifier to be model as a linear gain because the discrete-time sampling frequency in most control systems is around 1-2 kHz. It means:

$$\frac{d_i}{d_t} \approx 0 \rightarrow i = \frac{u - K_e \dot{\theta}}{R} \rightarrow k_a = \frac{1}{R}, \quad (2.3)$$

Here we concern the torque loss due to back EMF as a friction component in t_d so we have:

$$t_d = t_{fric} + \frac{k_t K_e \dot{\theta}}{R}, \quad (2.4)$$

Fig. 2.7 shows the translation the friction acting on the ball-screw and the motor to an equivalent friction acting on the feed-drive table. The total friction acting on the feed drive is as follows:

$$f_{fric} = t_{fric} r_g + f_{gfric}, \quad (2.5)$$

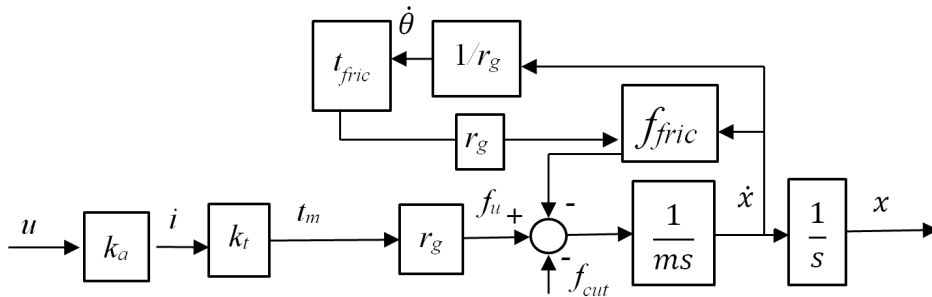


FIGURE 2.6: Feed drive dynamics with unified friction

Finally the feed-drive dynamics can be reduced to a simplified model as shown in Fig. 2.7, where the driving force f_u is assumed to be directly

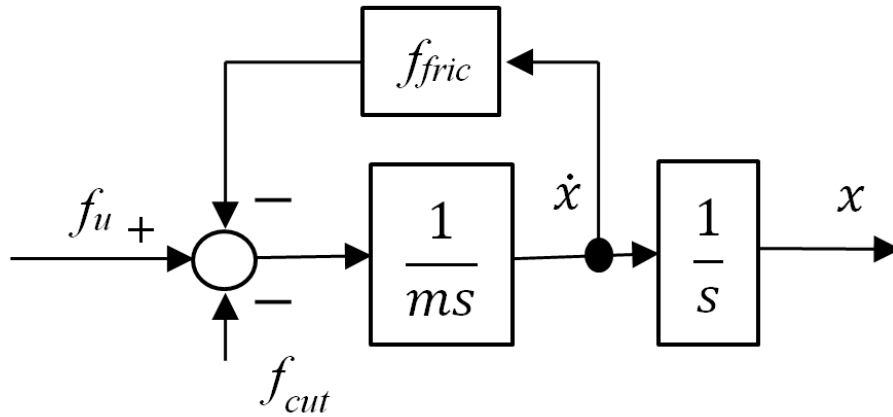


FIGURE 2.7: Combined friction sources in feed drive dynamics

proportional to the control signal u . Converting between f_u and u done easily with the following relationship:

$$f_u = k_a K_t u, \quad (2.6)$$

where k_a and K_t are motor designed parameters as in Fig. 2.6. The simplified feed drive dynamics is represented as follows:

$$f_u = m\ddot{x} + f_{fric} + f_{cut}, \quad (2.7)$$

The axis position $x(s)$ in uniaxial feed drive systems can be written in terms of the driving force f_u , friction f_{fric} and cutting force f_{cut} as,

$$x(s) = \frac{1}{ms^2} (f_u(s) - f_{fric}(s) - f_{cut}(s)), \quad (2.8)$$

In the next section, we present two conventional methods for identifying the feed-drive dynamics with a conventional friction model.

2.3 Conventional Friction Model and Identification

2.3.1 Conventional Friction Model

The conventional friction-compensation method [27] is based on the typical characteristics of lubricated metallic surfaces, which are described by the Stribeck curve. It models the total friction (friction in the linear guide ways and ball screw) in the feed-drive system by the Coulomb–viscous–Stribeck friction model as shown in Fig. 2.8. The mathematical equation is given as

$$f_r(\nu) = f_{fli} + f_{fle} = \left[\alpha_0 + (\alpha_1 - \alpha_0) e^{-(\nu\nu_0^{-1})^\delta} \right] \text{sgn}(\nu) + \alpha_2\nu, \quad (2.9)$$

where f_r , ν , α_0 , α_1 , and α_2 represent the total friction force, motion velocity, the Coulomb, static, and viscous friction coefficient, respectively. The Stribeck friction model parameters are the Stribeck velocity ν_0 and the

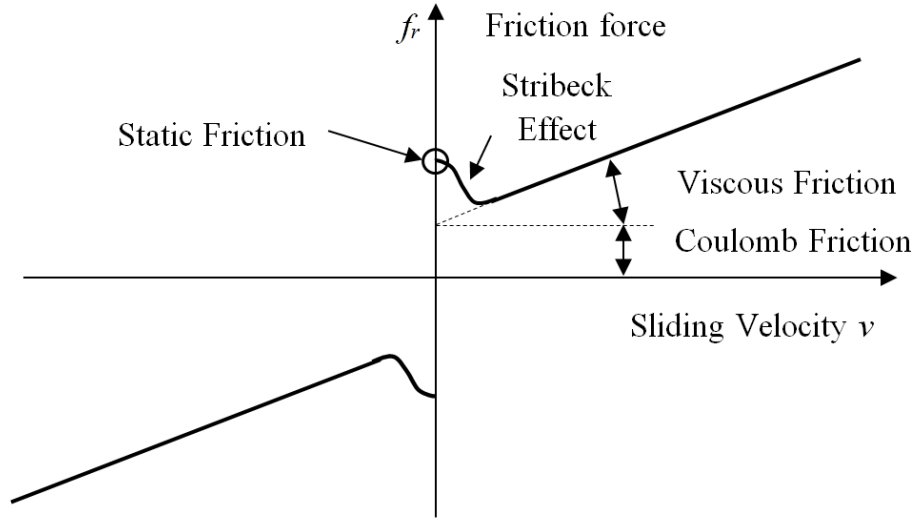


FIGURE 2.8: Coulomb-viscous-Stribeck friction model

Stribeck sharp-factor δ .

2.3.2 Identification Method by Unbiased Least Squares Scheme and Kalman Filter

This subsection presents identification of feed drive dynamics in Fig. 2.2 by using eq. 2.7 with friction model as in eq. 2.9. Firstly, the feed-drive dynamics is changed to discrete time and transform the identification of nominal mass and viscous and Coulomb friction to be a LS problem. Secondly, a PD controller is used with DOB to identify non-viscous and to correlate the viscous coefficient. Finally, the velocity constant in the Stribeck effect is identified by testing a range of values to choose the value that result in the lowest value of the cost function.

The feed driving force is generated from the control signal u through a D/A converter. Hence, the velocity expression in Eq. 2.8 can be rewritten in the discrete-time domain with a zero-order hold at the input stage as [27],

$$\dot{x}(k) = T_s \frac{z}{z-1} \frac{(f_u(k) - f_{fric}(k) - f_{cut}(k))}{m}, \quad (2.10)$$

where k is the sample counter, T_s (seconds) is the discrete sampling period, m is the normalized weight, and z is the forward shift operator. The discrete-time feed-drive dynamics given by Eq. 2.10 have friction and cutting disturbances, but we conduct no cutting identification experiments in using the LS identification technique so $f_{cut}(k) \approx 0$. The disturbance due to friction f_{fric} considering a simple Coulomb-viscous friction model is of the following form:

$$f_{fric}(k) = \alpha_0 \text{sgn}(\dot{x}_k) + \alpha_2 \dot{x}_k, \quad (2.11)$$

where the Stribeck effect is eliminated. Because the Stribeck effect appears at low speeds or then the velocity is reversed, a dead-band ν_d is introduced that is above the low speed region. This also avoids undesirable ringing in the friction model due to velocity measurement noise while the axis is at

rest. Defining the signum function with a deadband:

$$\sigma(\dot{x}, \nu_d) = \begin{cases} 1 & \text{if } \dot{x} > \nu_d, \\ 0 & \text{if } |\dot{x}| \leq \nu_d, \\ -1 & \text{if } \dot{x} < -\nu_d. \end{cases} \quad (2.12)$$

The friction model in Eq. 2.11 is written as,

$$f_{fric} = PV(\dot{x})\alpha_0^+ + NV(\dot{x})\alpha_0^- + \alpha_2\dot{x}, \quad (2.13)$$

where,

$$\begin{aligned} PV : \text{Positivevelocity} &= \frac{1}{2}\sigma(\dot{x}).(1 + \sigma(\dot{x})) \\ NV : \text{Negativevelocity} &= -\frac{1}{2}\sigma(\dot{x}).(1 - \sigma(\dot{x})), \end{aligned} \quad (2.14)$$

The friction model in Eq. 2.13 is combined with the discrete axis model in Eq. 2.10, resulting in the difference equation:

$$\dot{x}(k) = \dot{x}(k-1) + T_s \frac{(f_u(k-1) - PV(k-1)\alpha_0^+ - NV(k-1)\alpha_0^- - \alpha_2\dot{x}(k-1))}{m}, \quad (2.15)$$

where $PV(k-1) = PV(\dot{x}(k-1))$ and $NV(k-1) = NV(\dot{x}(k-1))$, or separating the signals from the parameters:

$$\dot{x}(k) = [\dot{x}(k-1)f_u(k-1) - PV(k-1) - NV(k-1)] \quad (2.16)$$

Considering the available measurements of the driving force $f_u = k_a K_t u = [f_u(1)f_u(2)...f_u(N-1)]$, and feed-drive velocity $\dot{x} = [\dot{x}(2)\dot{x}(3)... \dot{x}(N)]$. Defining the vector of parameters to be estimated as $\theta = [\frac{m-T_s\alpha_2}{m} \frac{T_s}{m} \frac{T_s\alpha_0^+}{m} \frac{T_s\alpha_0^-}{m}]$, the parameter estimation is given as an LS problem. The output prediction for all measurements is written as,

$$Y = \phi\theta + E, \quad (2.17)$$

where E is the vector of output prediction error, and ϕ is the regressor matrix, defined as,

$$\phi = \begin{bmatrix} \dot{x}_m(1) & f_u(1) & -PV(1) & -NV(1) \\ \dot{x}_m(2) & f_u(2) & -PV(2) & -NV(2) \\ \dots & \dots & \dots & \dots \\ \dot{x}_m(N-1) & f_u(N-1) & -PV(N-1) & -NV(N-1) \end{bmatrix} \quad (2.18)$$

The objective is to find the optimal set of parameters θ which minimizes the sum of squares of prediction errors,

$$\min \frac{1}{2} E^T E = \min \frac{1}{2} (Y - \phi\theta)^T (Y - \phi\theta), \quad (2.19)$$

which is solved as [116],

$$\theta = (\phi^T \phi)^{-1} \phi^T Y, \quad (2.20)$$

The feed-drive normalized mass, viscous coefficient and Coulomb friction are extracted from the parameter vector θ . Prior to the identification tests, both axes are driven by RHS-14-6003 DC brush motors, for which the torque gain is given as $K_{tx} = K_{ty} = 8.9[Nm/A]$. The ball-screw pitch length for both axes is $L = 5$ [mm], resulting the in a ball-screw gain ratio of $rg = (2\pi)/L = 1.256$ [rad/mm].

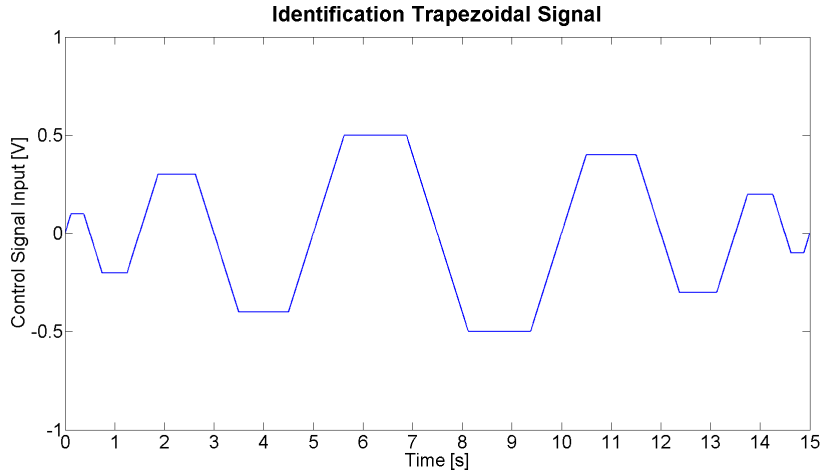


FIGURE 2.9: Input signal used in identification tests

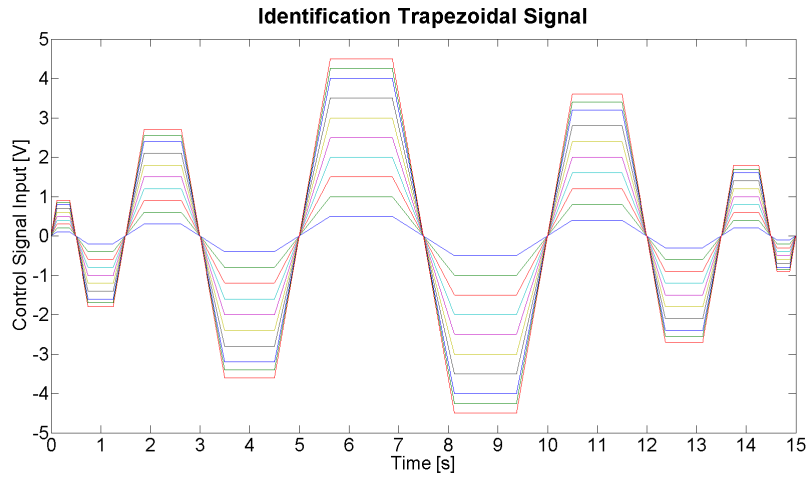


FIGURE 2.10: Input signal used in identification tests

Identification tests were conducted on the x and y axes of the biaxial feed-drive system, which involved trapezoidal inputs, as shown in Fig. 2.9. For each different test, the amplitude of the input signal was scaled with the factors $K_u=1, 1.5, 3, 4, 5, 6, 7, 8, 8.5$, and 9, which are represented in Fig. 2.10. In addition, the parameters m , α_2 , α_0^+ and α_0^- were estimated for the cases in which sufficient excitation was achieved to overcome static friction and

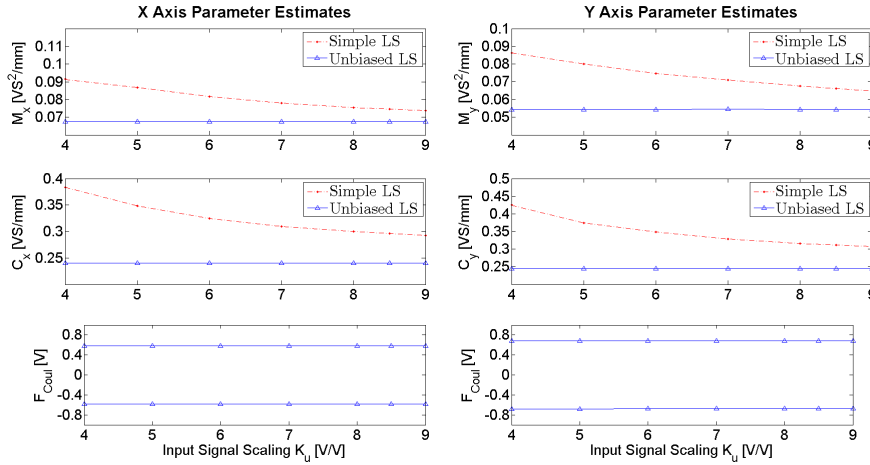


FIGURE 2.11: X and Y axes parameters - Use simple least squares and unbiased least squares identification techniques

TABLE 2.1: Estimated feed drive dynamics with conventional friction

	m (Kg)	α_0 (N)	α_1 (N)	α_2 (Ns/mm)	ν_0	δ
x	57.65	1255.38	1255.38	105.54	0.0	0
y	58.93	1066.05	1066.05	138.86	0.0	0

the Stribeck effect (i.e. $K_u = 4$) (Fig. 2.11). The velocity deadband was set to 0.5 [mm/s], to exceed the noise level when the axes were in the low speed regime. Because Stribeck friction and the pre-sliding effect are less significant at higher control-signal scalings, the parameter estimates corresponding to the case of $K_u = 4$ have been chosen, resulting in Table. 2.1.

Following the identification of the feed-drive dynamics by least square method, friction model verification tests were conducted by jogging the axes back and forth at various speeds by using a PD controller. No cutting was done during these tests, leaving the feed-drive friction as the only source of disturbances to the feed-drive system. The friction was observed using a DOB designed for the dynamic model in Eq. 2.21. A PD controller with a disturbance observer is designed based on the dynamics in Eq. (2.10) as follows:

$$\begin{aligned} f &= m_x(\ddot{r} - k_p\dot{e} - k_d e) + \hat{d} \\ e &= x - r \end{aligned} \quad (2.21)$$

where m_x, k_p, k_d, e and r are the nominal mass, proportional gain, derivative gain, tracking error and reference position, respectively. The disturbance force \hat{d} is estimated from a disturbance observer design [117] as follows:

$$\begin{aligned} \dot{\hat{v}} &= \frac{1}{m_x}(f - \hat{d}) + k_{ev}(\hat{v} - \dot{r}) \\ \dot{\hat{d}} &= k_{ed}(\hat{v} - \dot{r}) \end{aligned} \quad (2.22)$$

where \hat{v} is the estimated velocity, and k_{ev} and k_{ed} are DOB gains.

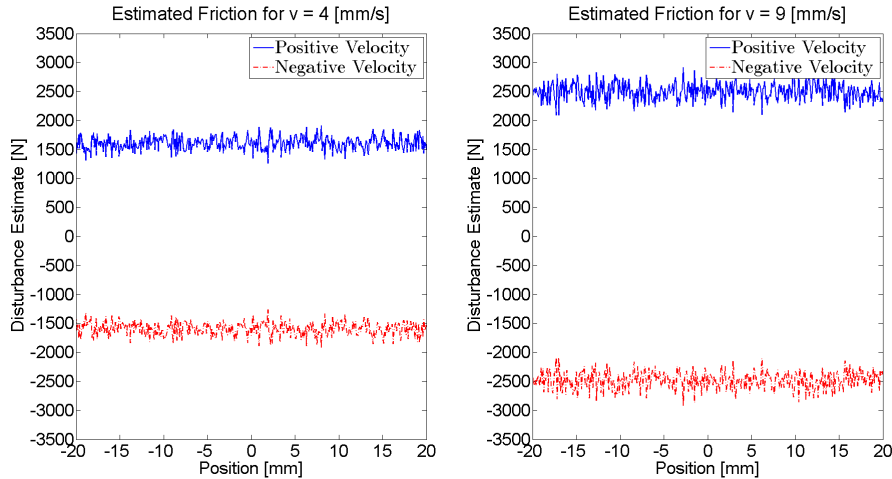


FIGURE 2.12: Input signal used in identification tests

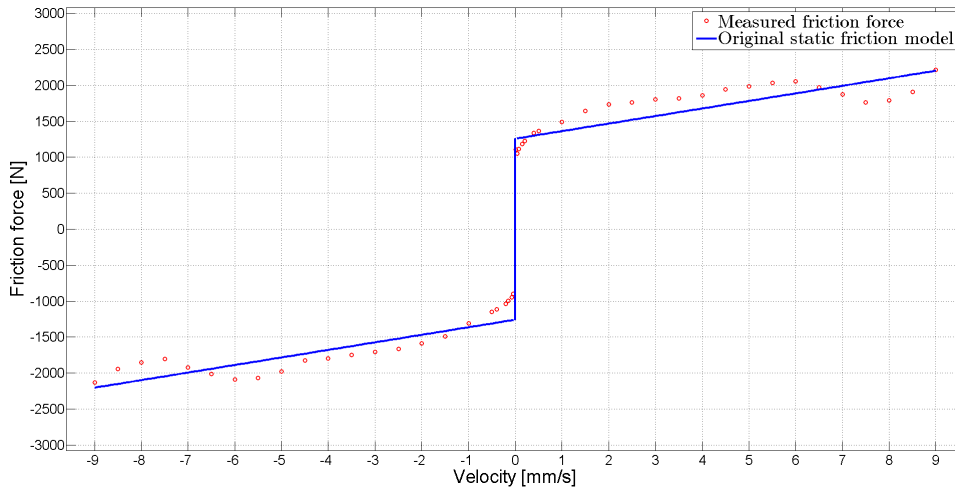


FIGURE 2.13: Observed and original modeled friction of the X axis

The friction was observed while jogging the axes at constant speeds ranging from 0.1 [mm/s] to 10 [mm/s]. More tests were conducted in the lower speed region (i.e. $\pm 0.1, \pm 0.2, \pm 0.3, \pm 0.5$ [mm/s]) to accurately capture the transition from static to sliding friction regions. Six high-speed points ($\pm 1, \pm 2, \pm 4, \pm 6, \pm 8, \pm 10$ [mm/sec]) were sufficient for characterizing the viscous friction range. Typical observed friction profiles for the x at axis speeds of 4 [mm/s] and 9 [mm/s] are shown in Fig. 2.12. As can be seen, the friction estimates are not significantly position dependency. By computing the average friction values for the positive and negative directions of motion in each test, and scaling them in terms of the friction torque ($T_f = K_t K_a d_f$), the plots of observed friction versus axis velocity were obtained, as shown with the 'o' marks in Fig. 2.13.

This identification technique involves two steps to identify a conventional static friction model. The first step involves reducing the friction model to Coulomb and viscous friction and incorporating it in the feed-drive dynamics, then designing a vector of parameters and changing the parameter estimation to be a LS problem. The second step involves using the disturbance-observer technique to observe the non-viscous friction value. It

shows a slope in the observed values and correct the extra viscous effect. The velocity constant is estimated based on the curve fitting Nelder-Mead downhill simplex method [118]. This identification method give us a good understand of using the LS method to deal with the identification of friction parameters, and of using a Kalman filter to correct the mismatched viscous friction parameter. However, this method is somewhat complicated and requires a deep understanding of feed-drive systems, sensor resolution, DAC, and error distributions. In next section, we apply a simpler method that uses a simple PD controller with a DOB to conduct various velocity joggings, measure friction values and use nonlinear optimization algorithms to identify the parameters of a conventional friction model.

2.3.3 Identification Method by Velocity Control and Disturbance Observer

The method in this subsection is somewhat different from the previous method when we use an inverse identification technique. Firstly, a PD controller with a DOB is used to conduct the constant-velocity experiments. Nonlinear optimization algorithms are then used to identify parameters of nonlinear friction sources. Secondly, the identified friction model is used in sinusoidal-velocity experiments to estimate the nominal feed-drive mass.

This identification method is applied to the feed drive dynamics of biaxial table in Fig. 2.2. When the feed drive in Fig. 2.2 with dynamics as in Eq. 2.7 is operated at a constant velocity, the driving force equals the friction force. Hence, constant velocity motion is enforced using a PD feed drive controller Eq. 2.21 with a disturbance observer Eq. 2.22. This experiment is repeated for the constant velocities of 0.01, 0.04, 0.08, 0.15, 0.2, 0.4, 0.5, 1.0, 1.5, 2.5, 3.0, 3.5, 4.0, 4.5, 5.0, 5.5, 6.0, 6.5, 7.0, 7.5, 8.0, 8.5 and 9.0 mm/s. A controller with PD feedback gains $k_p = 1600\text{s}^{-2}$ and $k_d = 80\text{s}^{-1}$, and disturbance gains $k_{ev} = 40\text{s}^{-1}$ and $k_{ed} = 20\text{kgs}^{-1}$.

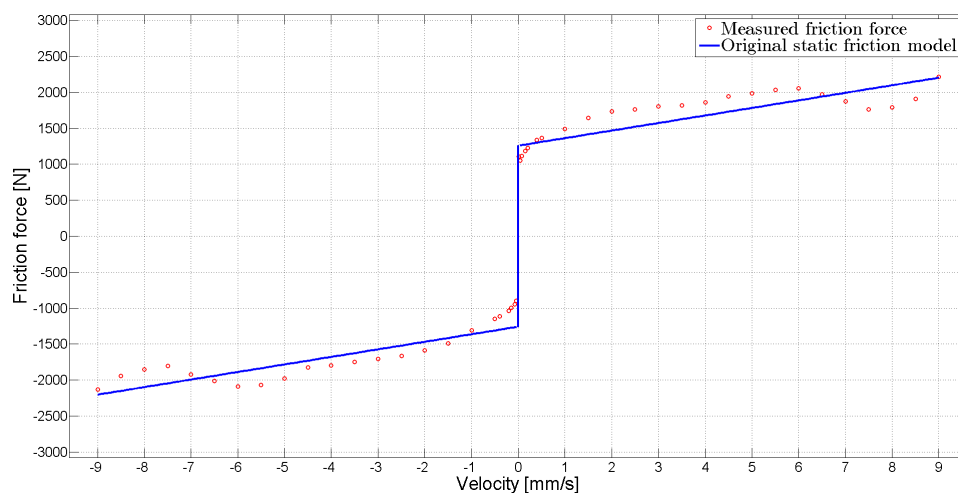


FIGURE 2.14: Observed and original modeled friction of the X axis use velocity control method

Fig. 2.14 shows the measured and the fitted friction force represented by Eq. 2.9. The Stribeck effect does not clearly appear in the experimental results, and it is assumed to be zero. The least square method is used to optimally obtain the friction model parameters. After that, the identified friction model are used in sinusoidal velocity experiment to estimated nominal feed drive mass. The obtained parameters are present in Table. 2.2

TABLE 2.2: Estimated feed drive dynamics with conventional friction

	m (Kg)	α_0 (N)	α_1 (N)	α_2 (Ns/mm)	ν_0	δ
x	56.61	1352.63	1185.45	113.54	0.0	0
y	59.03	1162.05	1066.23	111.86	0.0	0

2.4 Gaussian Augmented Friction Model and Identification Method

2.4.1 Tracking Controller with Disturbance Observer

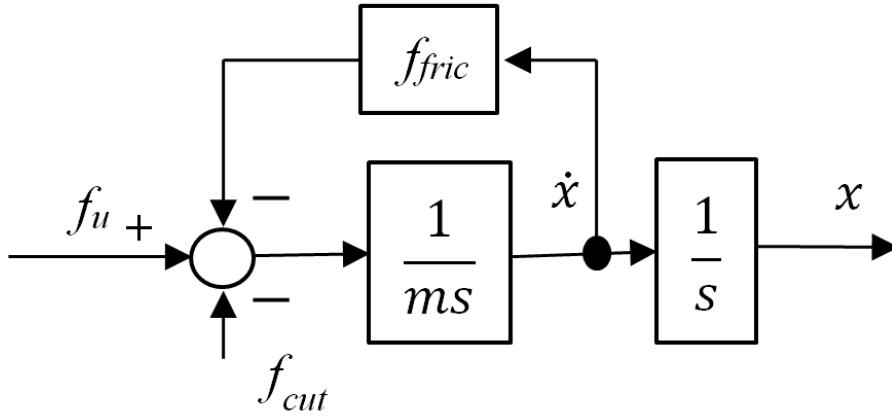


FIGURE 2.15: Simplified Feed drive dynamics with unified friction

The feed drive dynamic in time domain,

$$\begin{aligned} f_u - d &= m\ddot{x}, \\ f_u &= m\ddot{x} + d, \end{aligned} \tag{2.23}$$

The tracking error of the feed drive system:

$$e = x - r, \tag{2.24}$$

We design a PD feedback controller for non-cutting experiment as following:

$$f_u = m(\ddot{r} - k_v\dot{e} - k_p e) + f_{fric}, \tag{2.25}$$

Where k_v , k_p are velocity and position feedback gain. The following relations are derived from Eq. 2.24:

$$\begin{aligned} \dot{e} &= \dot{x} - \dot{r}, \\ \ddot{e} &= \ddot{x} - \ddot{r}, \end{aligned} \quad (2.26)$$

Substituting Eqs. (2.6), (2.7) into (2.3) yields

$$m(\ddot{r} - k_v\dot{e} - k_p e) + f_{fric} = m\ddot{x} + d, \quad (2.27)$$

Assumed $d \approx 0$ we have

$$-(\ddot{x} - \ddot{r}) - k_v\dot{e} - k_p e = 0, \quad (2.28)$$

Error dynamics for error e

$$\ddot{e} + k_v\dot{e} + k_p e = 0, \quad (2.29)$$

So by assigning feedback gain k_v and k_p appropriately, $e \rightarrow 0$ as $t \rightarrow \infty$ is concluded to be achievable.

In order to robust to parameter uncertainty, nonlinear disturbance we add a disturbance observer in controller as,

$$f_u = m(\ddot{r} - k_v\dot{e} - k_p e) + f_{fric} + \hat{d}, \quad (2.30)$$

Disturbance \hat{d} is estimated as,

$$\dot{\hat{v}} = m^{-1}(f_u - m\ddot{r}_{fric} + \hat{d}), \quad (2.31)$$

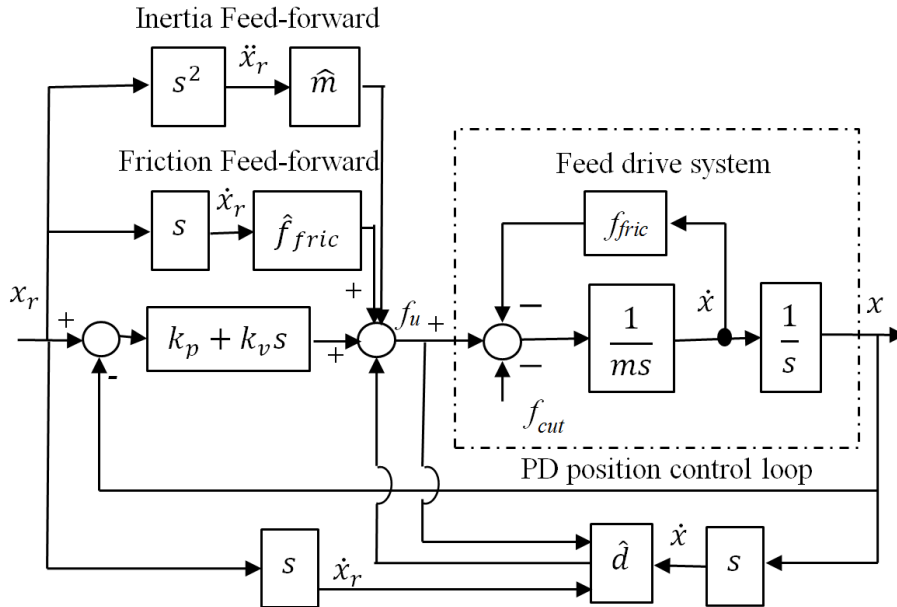


FIGURE 2.16: Controller design with disturbance observer for feed drive systems

2.4.2 Gaussian Augmented Friction Model

Although the friction model in Eq. (2.9) can be applied widely, it considers only three terms with fixed structures, and therefore the predicted performance of the friction behavior is limited. Based on experimental results with the biaxial table, the velocity–friction map in the x axis are shown in Fig. 2.16 demonstrates that the conventional model is not sufficient to capture the nonlinear friction properties in the high-velocity regime. So, we presents a new friction model that considers a number of friction sources with complicated and nonlinear properties as follows:

$$F_f(\nu) = \eta_0 \text{sgn}(\nu) + \eta_1 \nu + \sum_{i=1}^n g_{ia} \exp \left[- \left(\frac{\nu - g_{ib}}{g_{ic}} \right)^2 \right] \quad (2.32)$$

where $\eta_0 (> 0)$ and $\eta_1 (> 0)$ are the nominal Coulomb force and the nominal viscous coefficient of the feed drive, respectively. The nonlinear properties of friction are defined by the sum of n Gaussian equations in which g_{ia} , g_{ib} and g_{ic} denote the height of the Gaussian curve's peak, the position of the center of the peak, and the width of the "bell", respectively. The number n of Gaussian functions depends on the nonlinear properties of the estimated friction, as is explained in the next section.

2.4.3 Identification Method with Continuous Velocity-Friction Map

Because the conventional friction model has a relatively simple structure, it describes the friction properties poorly in both the low-speed and high-speed regimes. To obtain the friction property more precisely, we propose an identification method for the proposed friction model in Eq.(2.32) with sinusoidal tracking results. A PD controller and a DOB as shown in Fig. 2.19 are used for this control, and the driving forces are measured. Next, the friction force at each sampling time is estimated.

We explain the method for the x axis case, which is similar to that applied to the y axis. The following sinusoidal reference is used for the identification experiments:

$$\begin{aligned} r &= -20 + 20 \cos(0.475t) \\ t &= \left[0.0, \frac{4.0\pi}{0.475} \right] \text{ s} \end{aligned} \quad (2.33)$$

where r is the reference position of the X axis. The reference sinusoidal signal is repeated several times to eliminate the uncertainty. The controller gains for the PD control are $k_p = 1600\text{s}^{-2}$ and $k_d = 80\text{s}^{-1}$, and the disturbance-observer gains are $k_{ev} = 40\text{s}^{-1}$ and $k_{ed} = 20\text{kg}\text{s}^{-1}$.

Although the reference signal is well tracked in Fig. 2.17, a tracking error with a maximum magnitude of around 5 m still remains. The measured driving force is shown in Fig.2.18, in which chattering exists. In order to avoid the noise effect in the identification, we assume that $\dot{r} \simeq \dot{q}$ and $\ddot{r} \simeq \ddot{q}$,

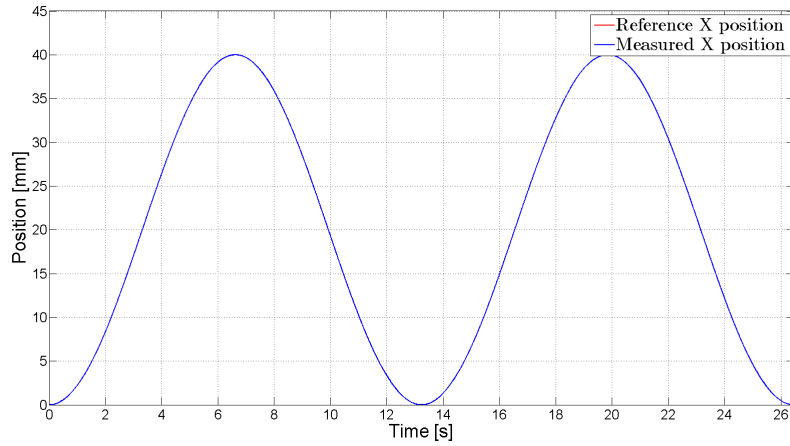


FIGURE 2.17: Reference and measured position

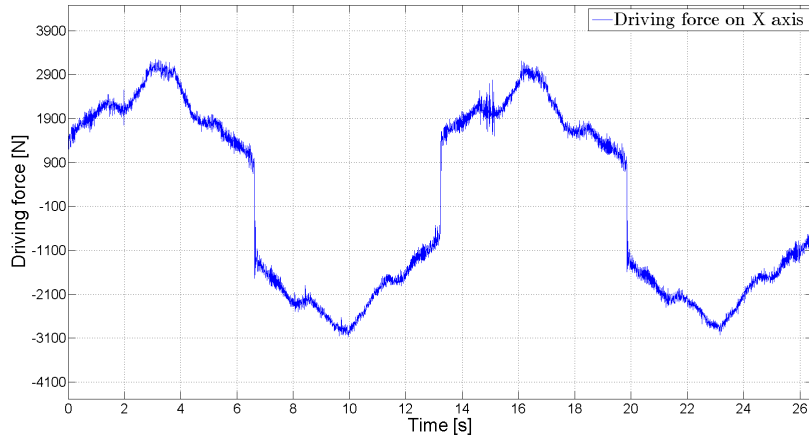


FIGURE 2.18: Driving force

and then the disturbance force is estimated as follows:

$$d = f - m_x \ddot{r} \quad (2.34)$$

The fluctuating green line in Fig. 2.20 denotes the disturbance force obtained by using Eq. (2.34). We assume that the estimated disturbance in the x axis comprises only friction and white noise with zero mean value. The LS method is used to eliminate this noise and to obtain the friction property as shown by the blue dotted line. From Fig. 2.20, we can see that the actual friction force is non-linear in not only the low-speed regime but also the high-speed one. Therefore, the conventional friction model is not sufficient for describing the actual friction property in feed-drive systems. Hence, the nonlinear static friction model Eq. (2.32) is proposed. The Gaussian function is used in this model because it can consider multiple nonlinear effects (e.g., gear and ball-screw friction) simultaneously. The number of Gaussian functions used is equal to the number of peaks of the estimated friction (circles in Fig. 2.20). For curve fitting in Fig. 2.20, the Nelder-Mead downhill simplex method [118] is employed, and the result is represented by a red line.

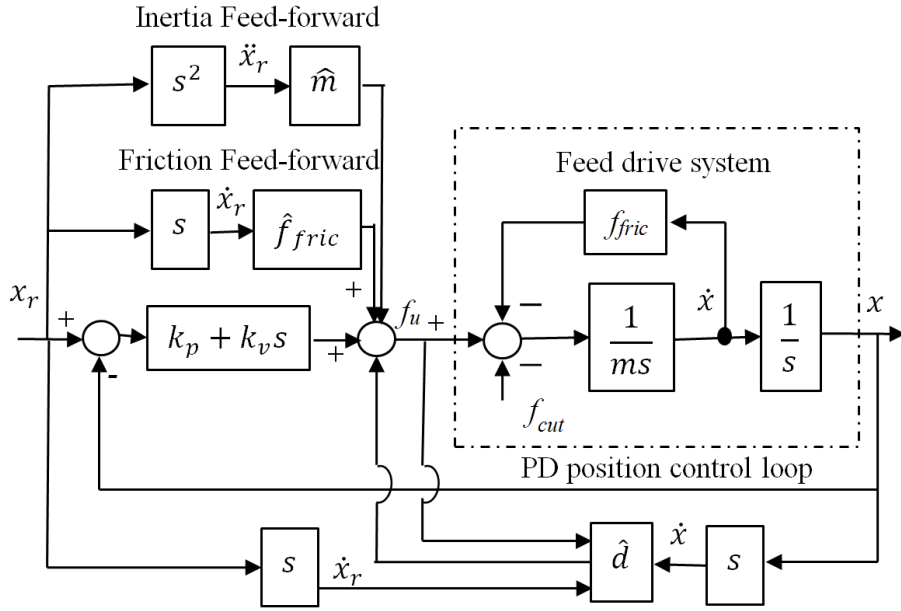


FIGURE 2.19: PD Controller with disturbance observer for feed drive systems

TABLE 2.3: Estimated Gaussian augmented friction model parameters

Estimated parameters	X Axis						Y Axis					
	$\dot{x} \geq 0$			$\dot{x} < 0$			$\dot{y} \geq 0$			$\dot{y} < 0$		
η_0, η_1, n	768.6	102.48	3	-768.6	102.48	3	640.5	140.91	3	-640.5	140.91	3
g_{1a}, g_{1b}, g_{1c}	517.4	1.763	3.091	-378.2	-2.163	2.265	518.0	1.766	1.986	-371.34	-1.963	2.997
g_{2a}, g_{2b}, g_{2c}	509.3	5.806	1.825	-547.5	-5.912	1.761	852.0	5.872	2.733	-236.1	-5.804	1.223
g_{3a}, g_{3b}, g_{3c}	1995.9	10.668	1.876	-4472	-13.99	3.659	1059.1	10.27	1.744	-354.97	-9.311	0.475

The parameters in Eq. (2.32) for the x and y axes are estimated in Table 2.3.

2.5 Eccentric Consideration Friction Model and Identification Method

2.5.1 Triaxial Machine Tool and Frictional Properties

The experimental system used in this section is a desktop triaxial machine tool as shown in Fig. 2.21. It consists of three axes driven by DC servo motors (15 ~ W, 24 ~ V DC) that are coupled to and drive three lead screws. It has a spindle that is attached to z axis and a table is attached to y axis. In addition, a linear encoder (resolution $0.1 \sim \mu\text{m}$) is attached to each feed-drive axis to measure the real position of the feed-drive system. Modeling the feed drive on each axis shown in Fig. 2.24 involves a linear guide and a lead-screw/nut system to translate the rotation of the motor into the linear motion of the feed drive.

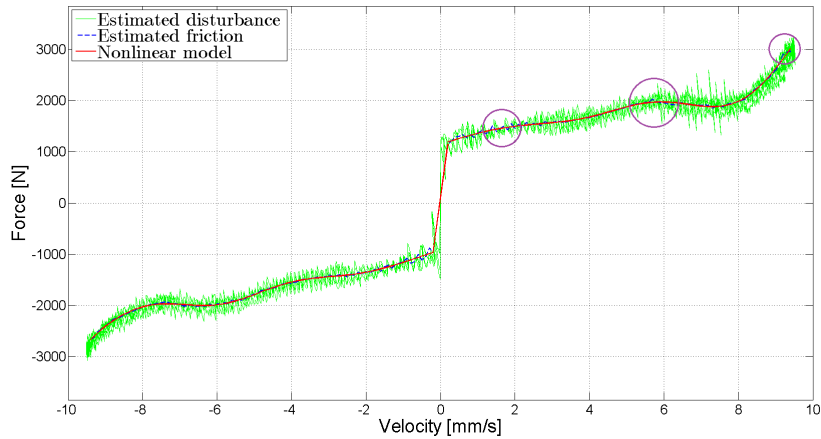


FIGURE 2.20: Measured and estimated non linear static friction model

The friction model discussed in Section 2.4 has better described nonlinear friction behavior in the high-speed regime with suitable Gaussian functions than conventional one. However, from the velocity map of the y axis of the triaxial machine tool in Fig. 2.23, we can see that the friction–velocity map is somewhat more complicated. If we use the friction model discussed in Section 2.4, numerous Gaussian functions are needed. This results in problems with the identification time and in practical applications. Instead, we used the friction–position and friction–velocity maps to help clarify the friction sources. We reason that there are eccentric friction effects in our experimental feed-drive system, so we propose a sinusoidal function to model this eccentric friction. The model and the identification are presented in the next subsection.

2.5.2 Friction Model Considering Eccentric Property

Although the friction model in Eq. (2.9) has been used widely, little consideration has been given to the development of nonlinear friction associated with the lead screws (Fig. 2.24) and the linear guide-ways under continuous working conditions, in particular insufficient lubrication. Bui and Uchiyama [119] have proposed a nonlinear friction term consisting of Gaussian functions from the assumption about the existence of several nonlinear friction sources in the feed-drive system and coupling effects between feed-drive axes. However, they only consider nonlinear properties based on friction-velocity map, and their proposed model becomes complicated for high-speed machine tools. In the present thesis, we assume that the nonlinearity arises mainly from the eccentricity between lead screw and nut as shown in Fig. 2.25. In a precise machine-tool system under continuous use, an infinitesimal gap between the lead screw and the nut results in an uncertain friction value. Based on this assumption, we propose a spring-like model to describe the friction behavior inside the screw/nut system. The normal force N varies

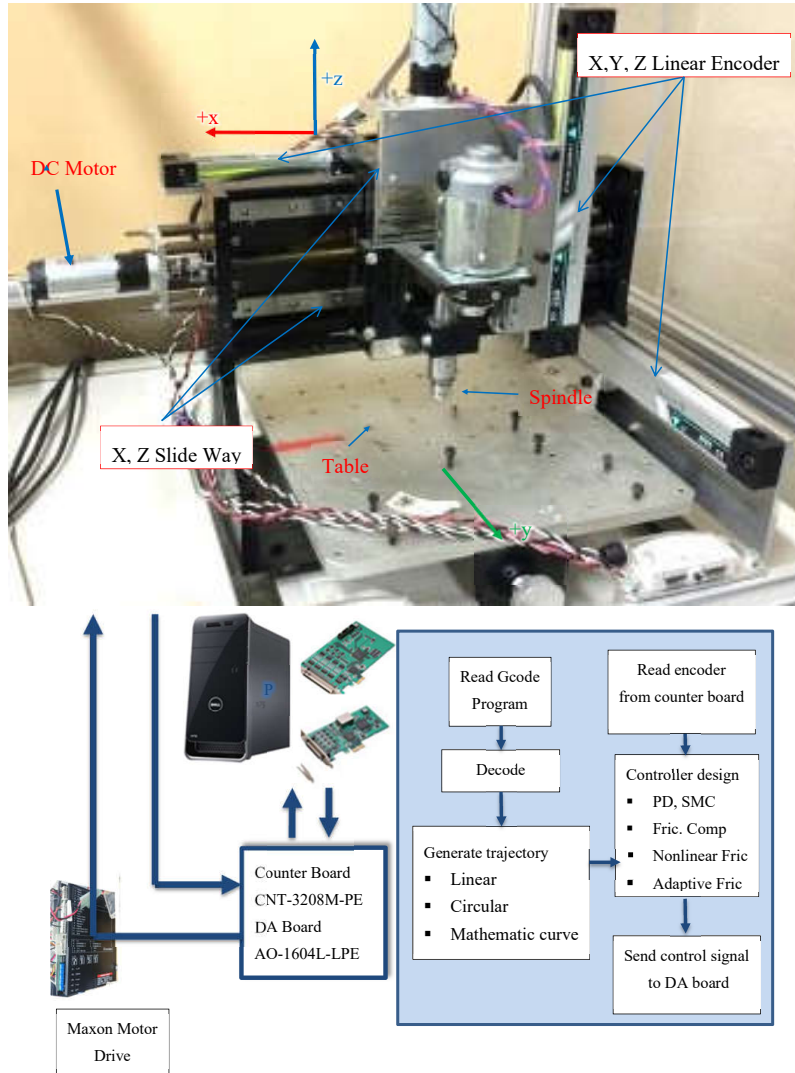


FIGURE 2.21: Triaxial machine tool

when the screw rotates, and the friction caused by this normal force varies depending on the angular position θ of the screw. This variation of the normal force results in a sinusoidal friction term that is described as follows:

$$f_{ec}(\theta) = k\sin(\theta - \theta_0), \quad (2.35)$$

where f_{ec} , k , θ and θ_0 are the eccentric friction, the maximum absolute value (amplitude) of the eccentric friction in the lead screw, the current angular position, and the initial angular position, respectively. From the relationship between θ and x as $\theta = x2\pi/L$, Eq. (2.35) becomes:

$$\begin{aligned} f_{ec}(x) &= \eta_2\sin(x2\pi/L - \eta_3) \\ \eta_2 &= k \\ \eta_3 &= \theta_0. \end{aligned} \quad (2.36)$$

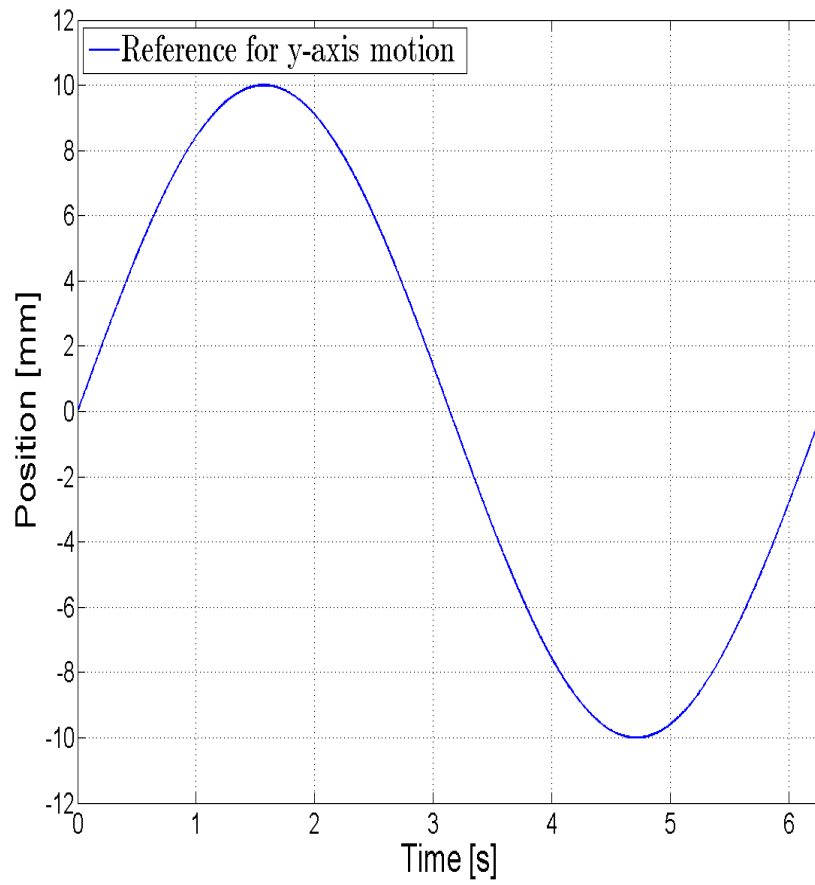


FIGURE 2.22: Reference for y-axis motion

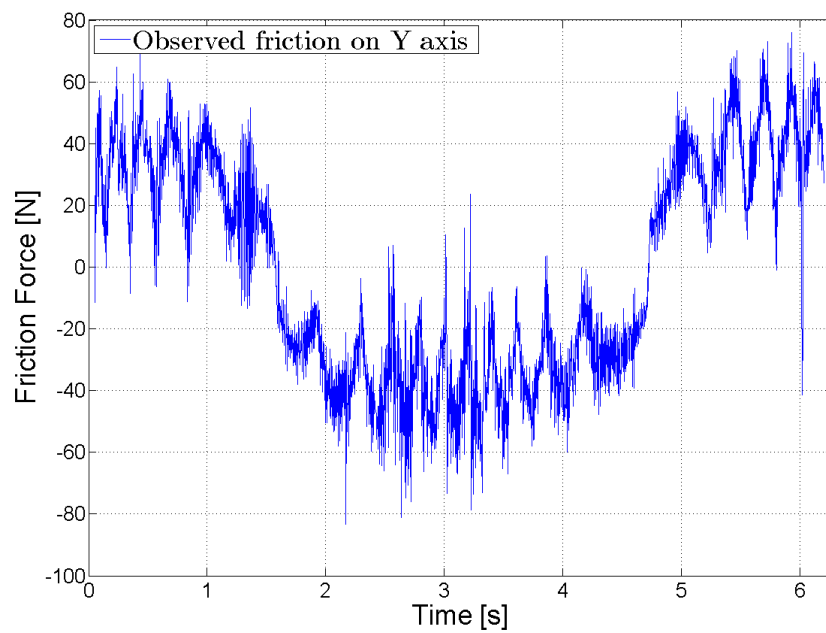


FIGURE 2.23: Observed friction on y-axis

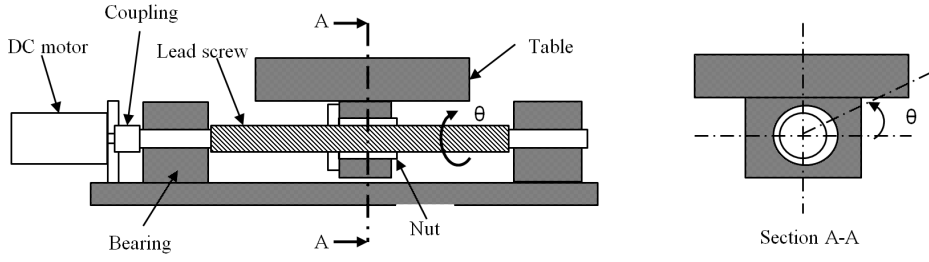


FIGURE 2.24: Eccentric friction in feed drive system

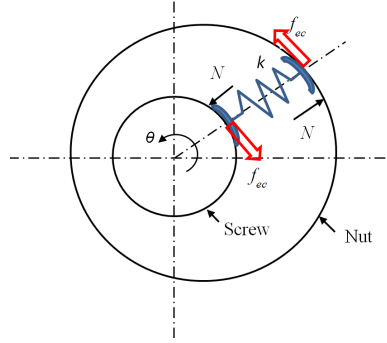


FIGURE 2.25: Modeling of eccentric phenomenon between lead screw and nut

From the assumption about the eccentric friction part, we proposed a nonlinear friction model that includes Coulomb–viscous friction and the nonlinear friction term f_{ec} as follows:

$$f_r(\nu) = f_{fli} + f_{fle} = \eta_0 \text{sgn}(\nu) + \eta_1 \nu + f_{ec}(x), \quad (2.37)$$

where $\eta_0 (> 0)$ and $\eta_1 (> 0)$ are the Coulomb force and the viscous coefficient of the feed drive, respectively. Equation (2.37) does not include the Stribeck effect since it only affects the low-speed regime, and we add the eccentric-friction part to describe more precisely the frictional behavior of the lead screw in the high-speed regime. Eccentric friction is concerned with part of the lead-screw friction f_{fle} . The eccentric friction and its estimation method are explained in the next section.

2.5.3 Identification Method with Velocity-Friction Map and Position-Friction Map

Because the conventional friction model has a relatively simple structure, it can be identified easily by the previous method. To identify the proposed friction model, a sinusoidal tracking controller is applied [119]. The following sinusoidal reference is used for the identification experiment:

$$\begin{aligned} r &= 10 \sin(t) \text{ mm} \\ t &= [0.0, 2.0\pi] \text{ s.} \end{aligned} \quad (2.38)$$

We explain the method for the y axis case because this axis contains the machining table for the mass the brings an unstable property in our

experimental setup as shown in Fig. 2.21. A similar method is applied to the feed drives of the x and z axes.

The reference for the y axis motion and the observed friction values are shown in Figs. 2.26 and 2.27, respectively. We assume that the effect of the eccentric friction includes high-frequency noise, and a low-pass filter eliminates this effect. The LS method is used to identify the nominal Coulomb force η_0 and the nominal viscous coefficient η_1 as in [119]. The estimated values are shown in Table 2.4. After obtaining the values of η_0 and η_1 , the observed eccentric friction value is calculated as follows:

$$f_{ec}(\nu) = f_{ob} - \eta_0 \text{sgn}(\nu) - \eta_1 \nu, \quad (2.39)$$

where f_{ob} is the observed friction force in Fig. 2.27.

The observed eccentric friction is shown in Fig. 2.28. It consists of very high-frequency chattering that results mainly from the unstable system and the analog-to-digital converters, and a lower frequency sinusoidal profile that results from the eccentric friction. We can see that this friction term has a sinusoidal shape and a period of roughly $2 \sim$ mm, which corresponds to the lead of the screw. This agrees with our proposed spring-like behavior model with a sinusoidal function. The Nelder-Mead downhill simplex method with the MATLAB function “fminsearch” is used to identify the parameters in Eq. (2.36), and the result is shown as the red line in Fig. 2.28. Finally, the total friction model from Eq. (2.32) is shown as the red line in Fig. 2.29. In addition, the conventional friction model is shown as the blue line for comparison purposes. From the identification result, we confirm that the proposed friction model describes the friction behavior well. The parameters in Eq. (2.32) for the x , y and z axes are shown in Table 2.4.

TABLE 2.4: Estimated nonlinear friction model parameters

	$\eta_0(\text{N})$	$\eta_1(\text{Ns/mm})$	$\eta_2(\text{N})$	$\eta_3(\text{rad})$
x	18	4.5	4.2	0.28
y	15	3	11.2	-0.27
z	24	4	2.5	+0.31

2.6 Verification Experiment

We summarize the method for identifying the feed-drive dynamics as follows,

- (1) Model A: Feed-drive dynamics with friction model from the unbiased LS parameter estimation and viscous-coefficient correlation.
- (2) Model B: Feed-drive dynamics with friction model from velocity jogging and nonlinear optimization method.

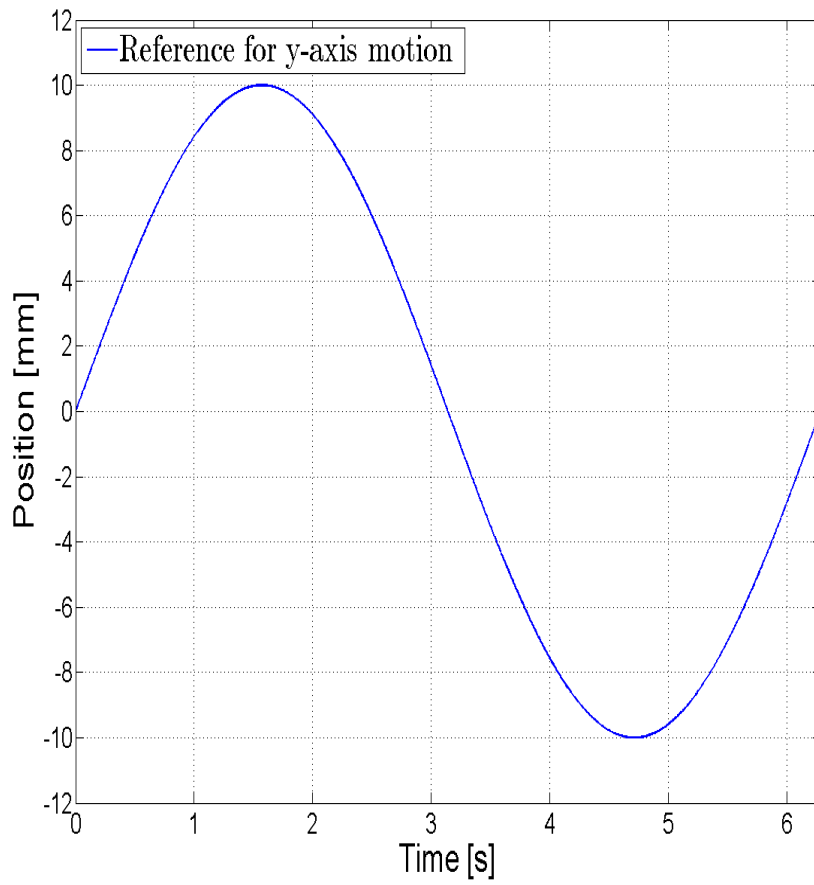


FIGURE 2.26: Reference for y-axis motion

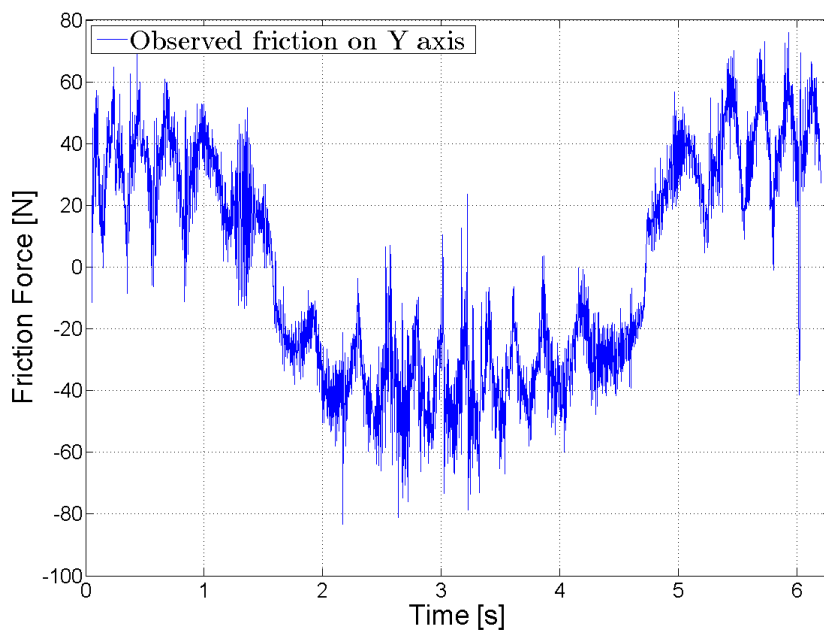


FIGURE 2.27: Observed friction on y-axis

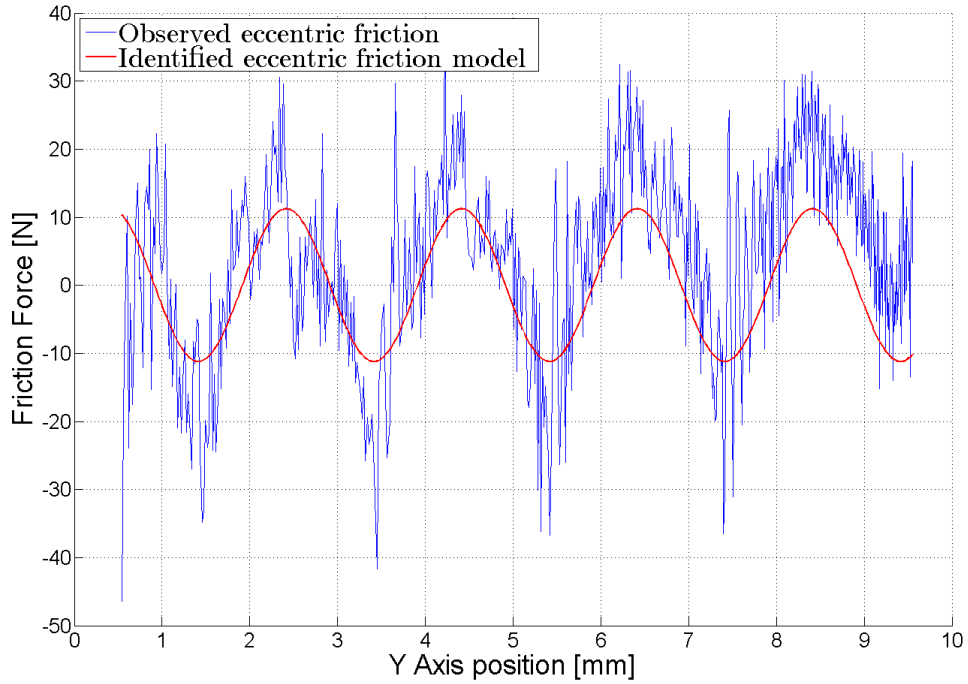


FIGURE 2.28: Observed eccentric friction

- (3) Model C: Feed-drive dynamics with friction model including nonlinear Gaussian functions.
- (4) Model D: Feed drive dynamics with friction model including eccentric friction.

Both the unbiased LS parameter estimation and the velocity-jogging technique explained above were used to allow comparison with the nonlinear friction model proposed in section 2.4. The experimental results of verification on the x axis of the biaxial feed drive show the effectiveness of proposed model.

For the triaxial machine tool, identification on our experimental setup represents the dominant effect of eccentric friction, so a friction model with nonlinear eccentric friction is proposed in section 2.5. Same verification method as in biaxial feed-drive system, both the unbiased LS parameter estimation, as well as the velocity jogging technique explained in previous sections was used to allow comparison with proposed eccentric friction model in section 2.5. The experimental results of verification on the y axis of the triaxial machine tool show the effectiveness of the proposed model.

2.7 Conclusions

This chapter discusses the characteristics of the friction force considered in this thesis. Three friction models are discussed: the widely known static friction model, the Gaussian-augmented friction model, and the eccentric-augmented friction model. Unlike the conventional static friction model, the

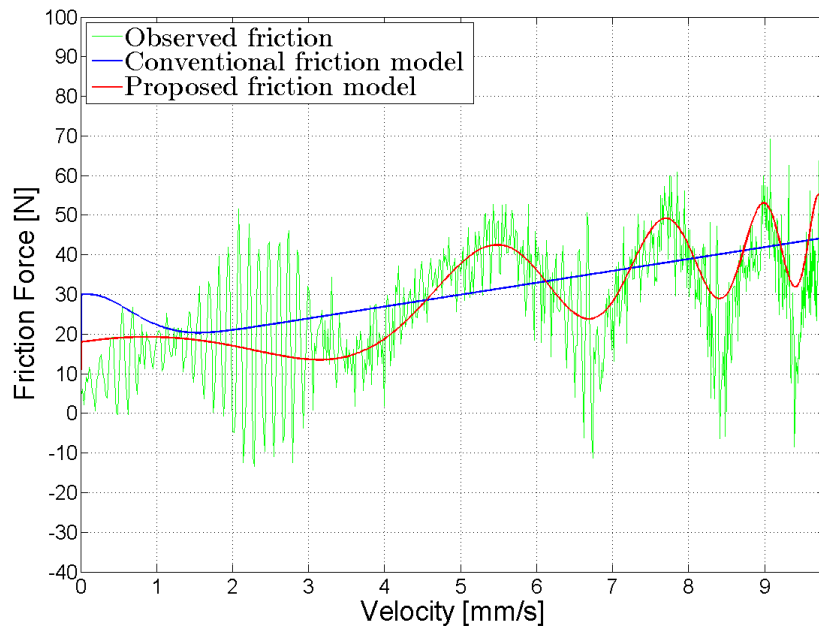


FIGURE 2.29: Comparison with conventional friction model

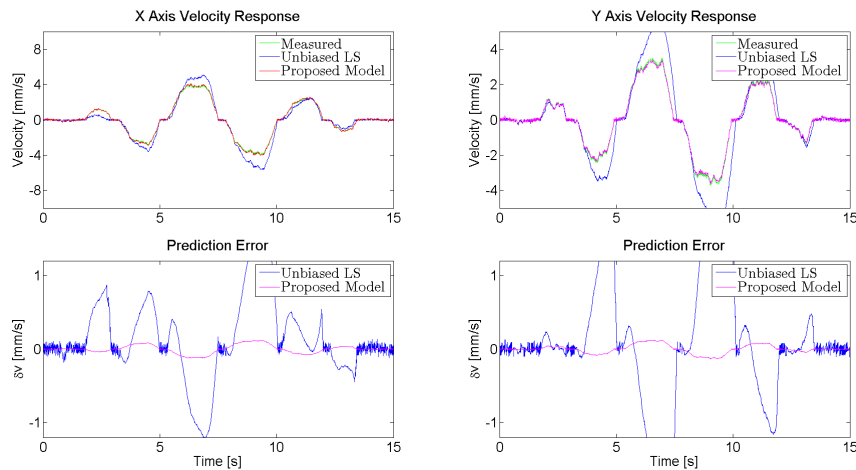


FIGURE 2.30: Real velocity and Velocity prediction from model A, B and C for ball-screw in x axis of bi-axial table

proposed friction models concern about the system structure and mechanical effects and therefore accurately describe the nonlinear friction behavior. The proposed friction model is somewhat complex and is difficult to identify. The identification of the three friction models for the uniaxial ball screw, the biaxial table, and the triaxial machine tool of the experimental test setup considered in this thesis is presented in detail. Simulation and experimental validation of controllers using these friction models are discussed in Chapter 3, 4, .

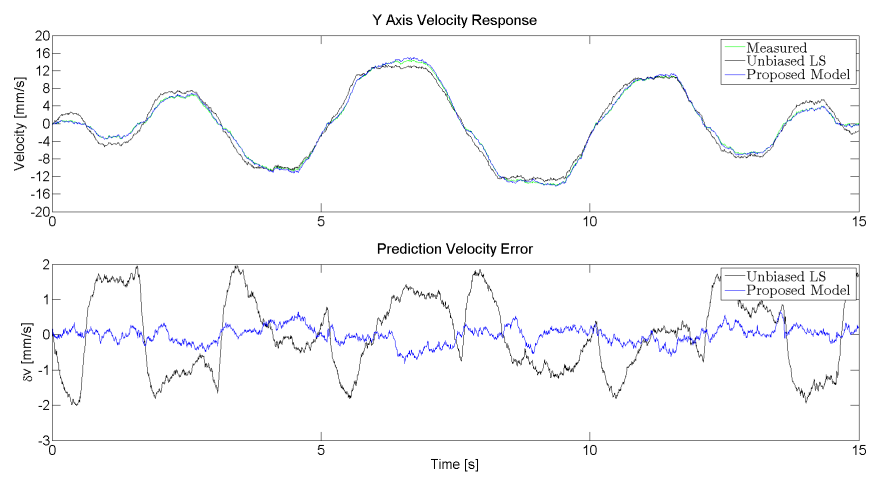


FIGURE 2.31: Real velocity and Velocity prediction from model A, B and D for lead-screw in y axis of triaxial machine tool

Chapter 3

Uniaxial Feed Drive and Biaxial Table Control

3.1 Uniaxial Feed Drive Control

3.1.1 Introduction



FIGURE 3.1: Ball-screw feed drive system

A ball-screw-driven mechanism actuated by servo drives is commonly used in many industrial applications (e.g., CNC machines, precision assembly equipment, and industrial robots) to provide high-speed motion and positioning accuracy. The main issue in servo applications is position control, which is essential for many mechanical motion systems. A positional servo system in a high-performance industrial application must respond quickly, preferably without overshoot. It must also have high steady-state accuracy, good external-disturbance rejection, and be robust to parameter perturbations [29]. Therefore, accurate modeling and identification of the dynamics of the feed drives is an important step in designing a high-performance controller.

In this chapter, we propose a simple PD controller based on the linear feed-drive dynamic models A, B and C discussed in chapter 2 for the uniaxial feed drive shown in Fig. 3.1. The experimental results are compared between controllers. A PD controller with a DOB based on model C is also presented and shows very good tracking performance.

3.1.2 Uniaxial Feed Drive Dynamics and Identification

The unbiased LS technique [27] is used to identify the system dynamics and to construct a velocity–friction map as in Fig. 3.6 and Table 3.1. The observed velocity–friction map and the identified conventional friction model show that the conventional friction model only approximates the friction–velocity map roughly.

3.1.3 Tracking Controller Design

3.1.4 Simulation Results

To verify the effectiveness of the PD controller, a simulation is conducted in MATLAB for the following reference trajectory:

$$r = 10\cos(0.85t)[mm], \quad (3.1)$$

In order to consider the vibration of the ball screw and the effects of the disturbance force due to the change of the load, we consider the following real feed-drive system:

$$m_r\ddot{x} + c_r\dot{x} + f_{coul}\text{sign}(\dot{x}) + d_r = u[V], \quad (3.2)$$

Where $m_r = 0.045[V s^2/mm]$, $c_r = 0.10V s/mm$, $f_{coul} = 0.60V$, $d_r = \text{random}(-0.2, +0.2)V$. Coulomb friction of 0.88V equivalent magnitude is added in simulation equation. PD contouring controller design:

$$f_u = m(\ddot{r} - k_v\dot{e} - k_p e), \quad (3.3)$$

where $m = 0.055V s^2/mm$, $c = 0.21V s/mm$. Controller gain is assigned as follows:

$$K_v = 2\omega, K_p = \omega^2, \omega = 30.$$

In discrete time, we use the Rungle–Kutta method to simulate the different equation 3.2. The simulation control results are shown in Fig. 3.2.

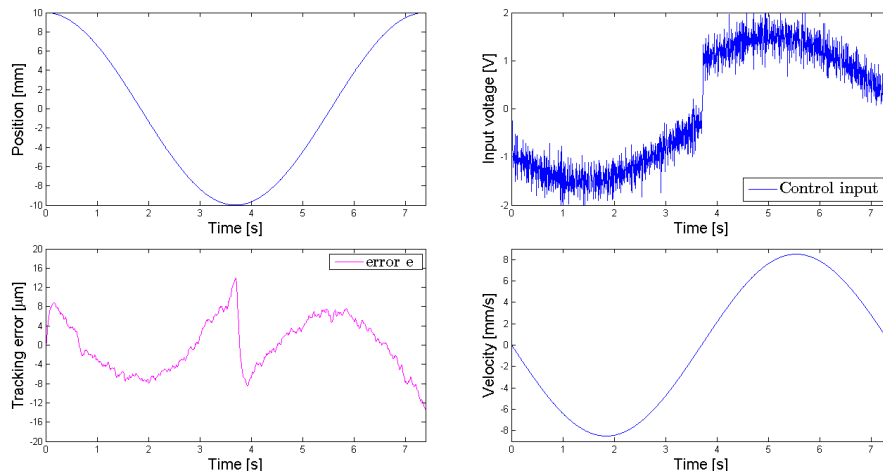


FIGURE 3.2: Simulation results, $\omega = 30$

We can see that the error in the simulation results comes from a mismatch between parameters m, c and actual one. From a lack of Coulomb-friction compensation in the design of the PD controller.

3.1.5 Experimental Results

The PD feedback controller was verified experimentally with a ball-screw feed-drive system driven by a DC servo motor as shown in Fig. 3.1. A

rotary encoder with a resolution of $0.025 \sim \mu\text{m}$ was attached to the feed drive to measure the actual position of the feed-drive system. The control law given in Eq. 3.3 was implemented using the C++ programming language on a personal computer (OS: Windows Me, CPU: 1 GHz) with a sampling time of $5 \sim \text{ms}$. In order to provide a fixed sampling period in a Windows Me environment, we employed a timer on a counter board of 24-bit up/down counters. The design of the PD feedback controller are setting similar with PD feedback contouring controller in Chapter 2.

$$f_u = m(\ddot{r} - k_v \dot{e} - k_p e) + cx, \quad (3.4)$$

where $m = 0.055 \text{Vs}^2/\text{mm}$, $c = 0.21 \text{Vs}/\text{mm}$ Controller gain is assigned as follows: $K_v = 2\omega$, $K_p = \omega^2$, $\omega = 30$. The parameter of table mass m and viscous friction c are identified by simple least square (LS) method which are present in chapter 2.

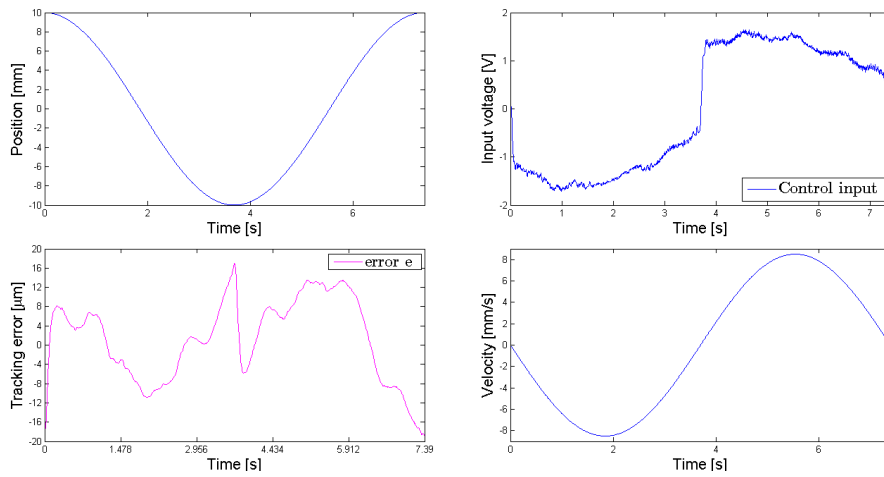


FIGURE 3.3: Simulation results, $\omega = 30$

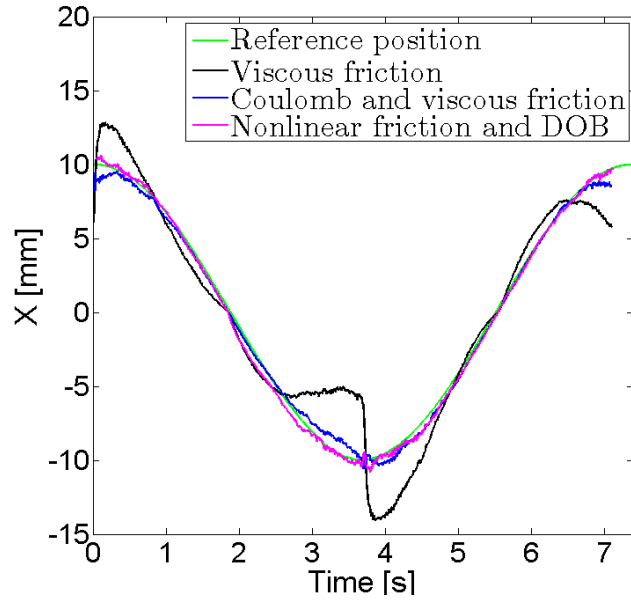
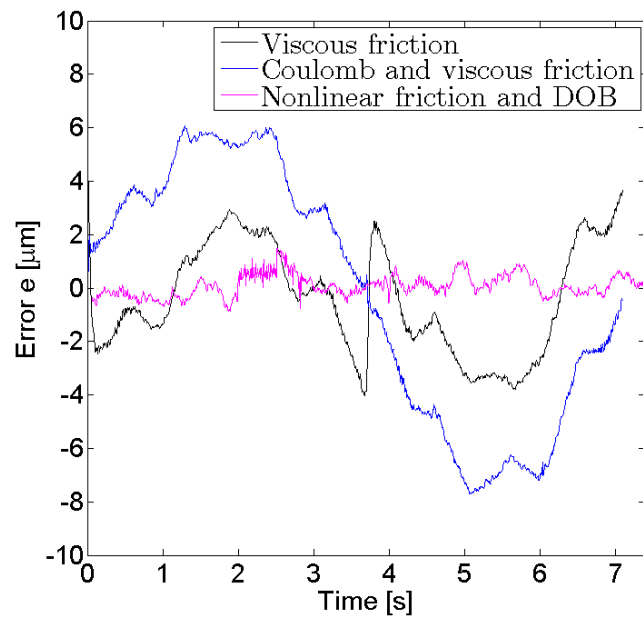
From the experimental results, we can see that the input voltage and tracking error are slightly different in comparison with the simulation results. I prove that simulation equation of feed-drive system have good define actual feed-drive system but still remain some small difference. These come mainly from the mismatched parameters, the nonlinearity of the real feed-drive system, the effect of the Coulomb force, and the phase lag. Therefore, accurate modeling and identification of the dynamics of the feed drives is an important part and is presented in chapter 2. We will compare the experimental results between PD controller use three type controllers in Eqs. ???. We conduct experiments with the following reference trajectory:

$$r=10\cos(0.85t) \text{ (mm)}$$

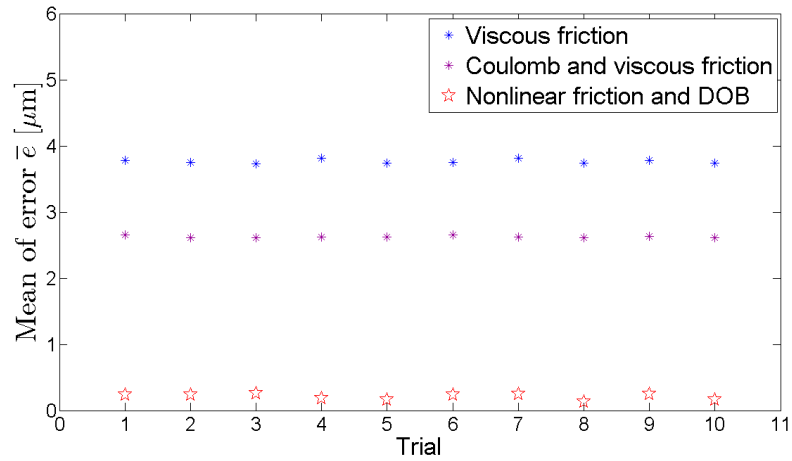
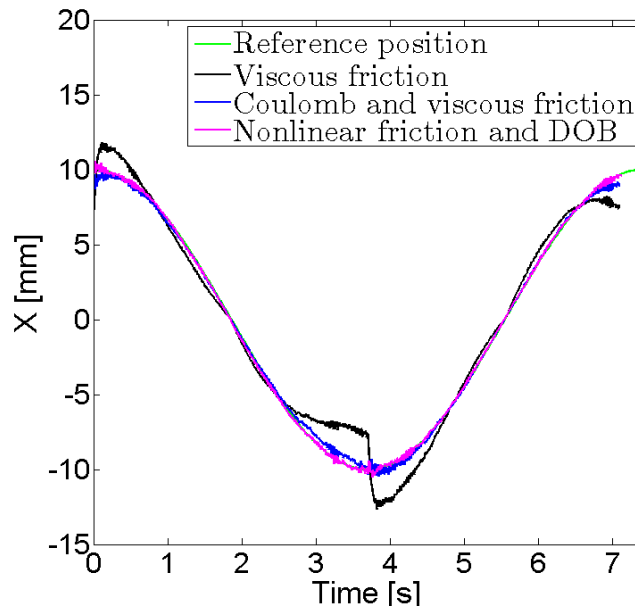
Control gains are selected following:

$$\begin{aligned} K_p &= \omega^2, K_v = 2\omega \\ \omega &= 40 \text{rad/s} \\ K_d &= 5, K_v = 10 \end{aligned} \quad (3.5)$$

Experimental results are shown in Fig. 7.3.

FIGURE 3.4: Simulation results, $\omega = 40$ FIGURE 3.5: Simulation results, $\omega = 40$

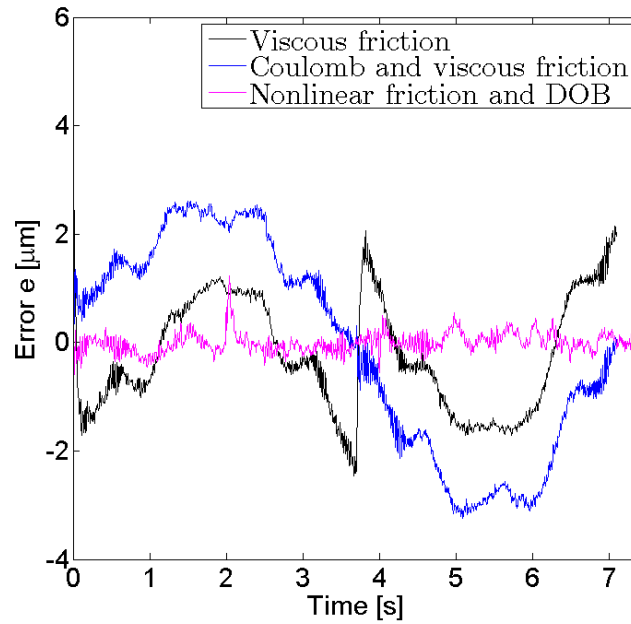
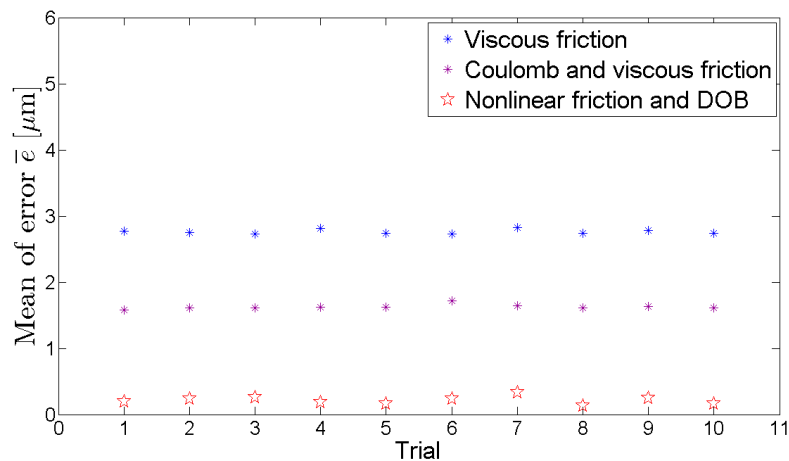
From Fig. 3.6, we have tracking error use Coulomb and viscous friction have better performance than control performance use only viscous friction in friction definition. However, the proposed nonlinear friction and DOB clearly reduce the tracking error and give the best control performance overall. We increase the control gain to $\omega = 60\text{rad/s}$ to verify the proposed method, and we obtain the following experimental results,

FIGURE 3.6: Simulation results, $\omega = 40$ FIGURE 3.7: Simulation results, $\omega = 60$

As with the results from the previous experiment, this result demonstrates the effectiveness of our proposed friction model. In addition, our proposed friction is used to identify the feed drive in the biaxial feed-drive contouring control.

3.1.6 Conclusions

In this section, we design PD feed-drive tracking control with the Gaussian-augmented friction model. The experimental results confirm clearly that our proposed controller with the Gaussian-augmented friction model and

FIGURE 3.8: Simulation results, $\omega = 60$ FIGURE 3.9: Simulation results, $\omega = 60$

the DOB gives better control performance and reduces the error. Experiments have been conducted to examine the effectiveness of the proposed Gaussian-augmented friction model. In sinusoidal reference following tasks, the effectiveness of our proposed methods has been confirmed in both simulation and experiments. The controller based on our proposed Gaussian-augmented friction model has a tracking error of less than $0.3m$.

3.2 Bi-Axial Table Control

3.2.1 Introduction

Friction in mechanical systems such as machine-tool feed drives is the main disturbance that reduces tracking accuracy and machining surface quality. Therefore, friction compensation is generally required in the design of controller for high-precision motion. A controller that compensates for friction without using high-gain control loops is inherently in need of a suitable friction model, and hence such a controller is known as a model-based friction compensator. A good friction model is also necessary in order to analyze the stability, predict the friction behavior, and perform simulation.

Many simple and advanced friction models have been proposed in the literature. Most existing model-based friction compensators use conventional static friction models that describe the static map between velocity and friction force [107]. The conventional static friction model does not describe the friction behavior in the pre-sliding regime and is insufficient for representing the friction behavior at very low speeds. A dynamical model has been proposed in order to compensate for this shortcoming [120]. The LuGre friction model is widely applied because of its simplicity and relatively good performance [6]. Swevers et al. have improved the LuGre model to yield the Leuven integrated friction model [73], which has been modified further by Lampaert et al. [80]. Recently, Al-Bender et al. developed the so-called generalized Maxwell-slip (GMS) friction model [81].

Various model-based and non model-based friction compensation schemes have been proposed thus far. Armstrong have carried out a survey on friction models and compensation methods for the control of machines with friction [26]. Canudas and Lischinsky utilized their LuGre friction model for adaptive friction compensation [112]. Tjahjowidodo et al. have shown that a nonlinear gain-scheduled controller based on the Maxwell-slip-model-based yields fast responses and low steady-state errors for friction compensation in electro-mechanical systems [121]. Tung et al. applied a non model-based friction compensation approach in the form of a repetitive controller, and demonstrated improved tracking performance and the compensation of quadrant glitches [82]. Lampaert et al. compared model-based and non model-based friction compensation for a tracking application on a dedicated test setup (a tribometer), and concluded that a combination of a GMS friction model based feed-forward and DOB yields the best performance [72].

Regarding machine-tool control, Erkorkmaz et al. proposed an unbiased identification method and demonstrated the effectiveness of static friction compensation [27]. Jamaludin et al. used a dynamic friction model (GMS friction model) for friction compensation and evaluated it experimentally on a linear-drive xy table [78], [122]. However, the GMS friction model or other dynamics friction model provides better results than those of the conventional static friction model only at low speeds.

This thesis focuses on a static friction model and assumes that nonlinear friction phenomena appear not just at very low speeds but also at high speeds. We propose a new nonlinear friction model that includes a nominal linear friction model (Coulomb friction and viscous friction) and a number of nonlinear friction sources represented by Gaussian functions. In addition,

this study presents a controller design that consists of a feed-forward compensation term with the proposed friction model and a DOB. Experiments are conducted to compare the control performance between the proposed and conventional static friction models. The proposed controller largely improves the control performance with a maximum contouring error of less than $1.6\mu\text{m}$.

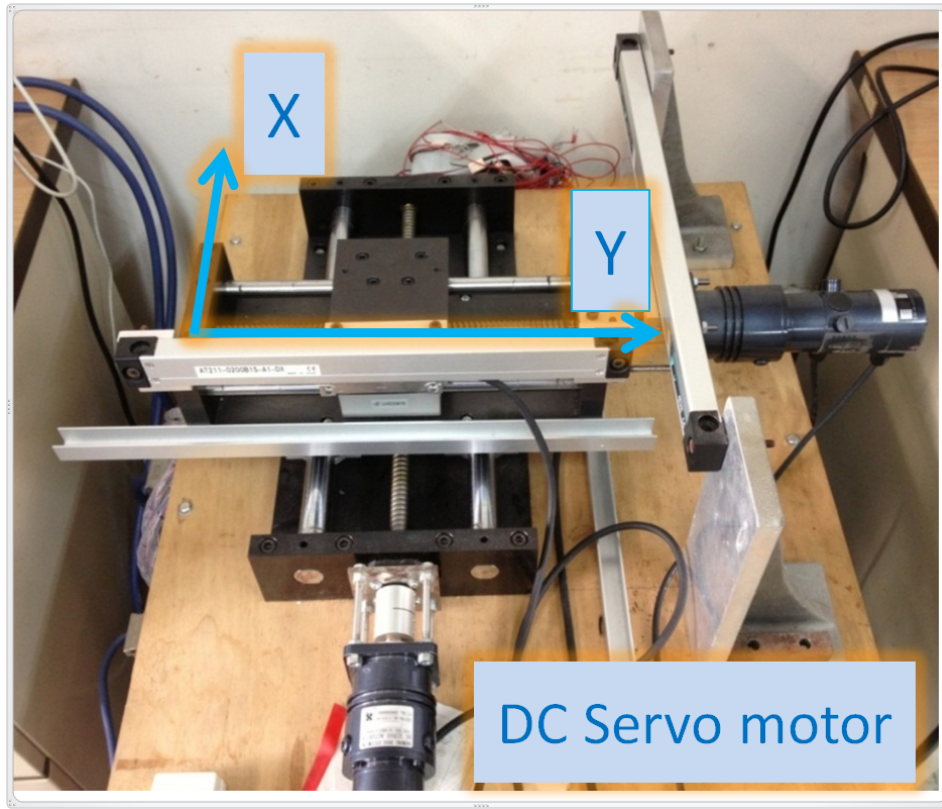


FIGURE 3.10: Biaxial feed drive system

The parameters of the friction model given by Eqs. (2.9) and (2.32) are identified experimentally. The experimental setup is a typical biaxial feed-drive system as shown in Fig. 3.10, which consists of two axes driven by DC servo motors that are coupled to drive two ball screws. We assume that the friction on each feed drive is the sum of many friction sources, such as ball bearings, gears, and ball-screws nuts. A rotary encoder whose resolution for position measurement is $0.025\mu\text{m}$ is attached to each feed-drive servomotor to measure the actual position of the feed-drive system. Because of the absence of a velocity sensor, the velocity signal is calculated by means of numerical differentiation of the position measurements. The system was controlled by a personal computer (OS: Windows, CPU: 1GHz) with sampling time of 5ms. The control program was written in the C++ language. In order to provide a fixed sampling period in a Windows environment, we used a timer on a counter board with four channels of 24-bit up/down counters. The equivalent-mass parameter values for the x and y axes of the experimental setup are $m_x = 57.65\text{kg}$ and $m_y = 58.93\text{kg}$, respectively.

3.2.2 Identification of Bi-Axial Table Dynamics

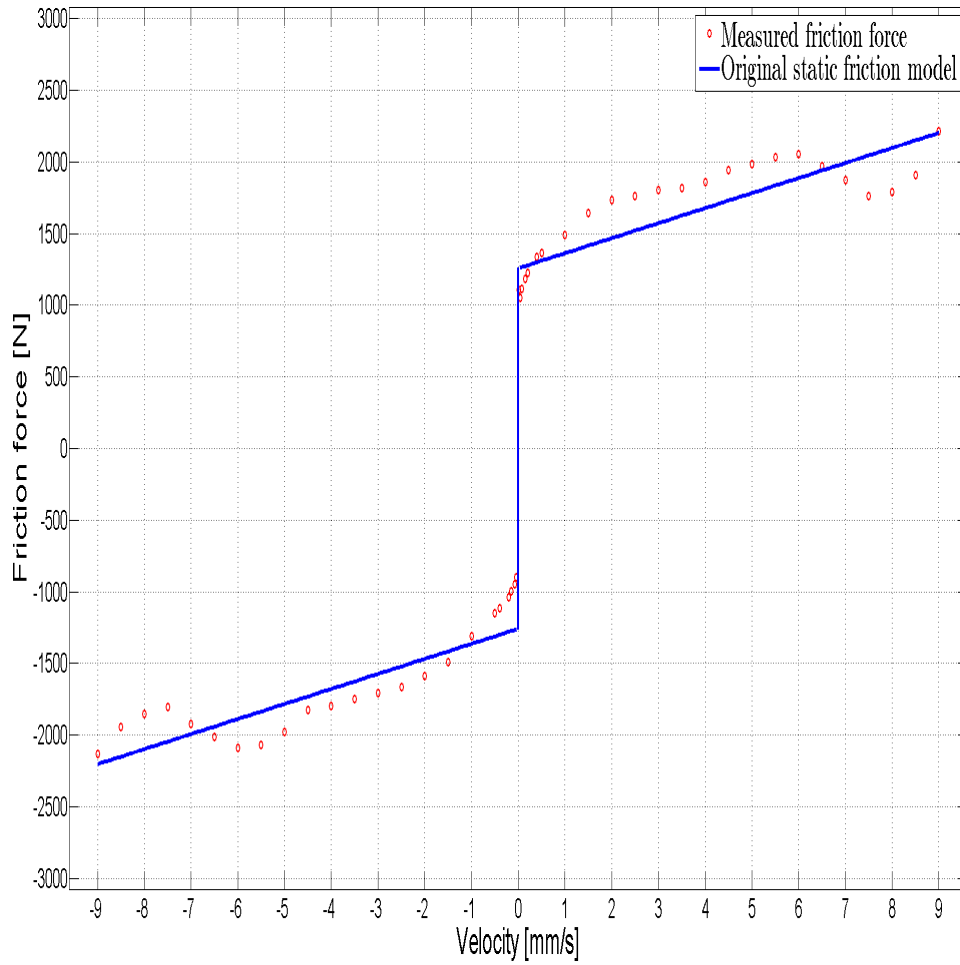


FIGURE 3.11: Original friction model and observed friction X axis

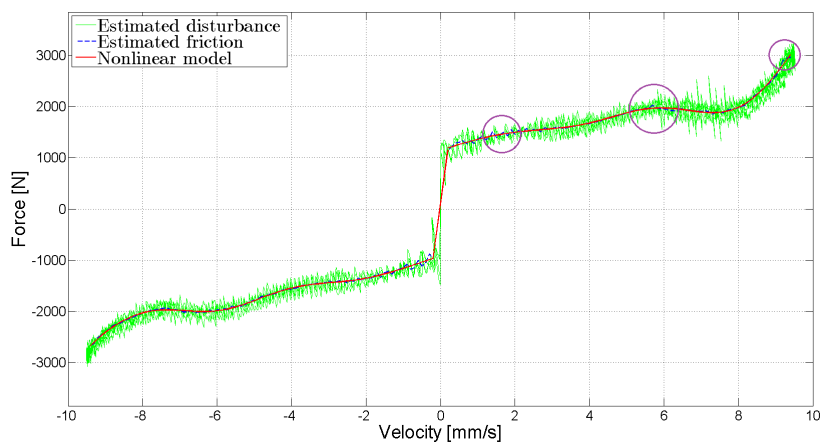


FIGURE 3.12: The Gaussian augmented friction model and observed friction X axis

The Gaussian augmented friction model is used to describe nonlinear behavior in ball-screw feed drive systems of bi-axial table, comparison with conventional friction model and observed friction is shown in Fig. 3.12 . The estimated conventional friction model and the Gaussian augmented friction model parameters are shown in Table. 2.1 and Table. 2.3, respectively.

3.2.3 Contouring Control of Bi-axial Table

3.2.3.1 Estimation of Two-Dimensional Contour

In machining, the contour error is an important criterion for the quality of the machining surface. This thesis applies the proposed friction compensation to a contouring controller [123], [124].

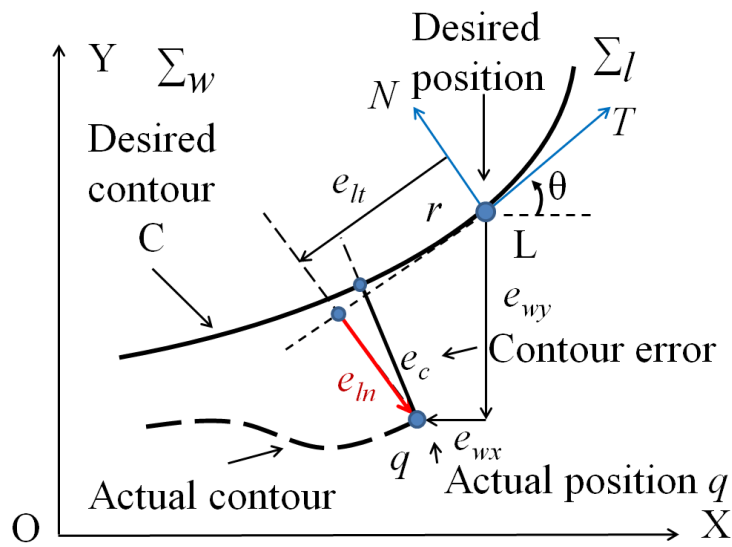


FIGURE 3.13: Definition of Contour Error

Figure 3.13 explains schematically the relationship between the tracking errors in each feed-drive axis and the contour error. The coordinate frame Σ_w , whose x and y axes correspond to the feed-drive axes, is a fixed frame. The curve C in the figure is the desired contour curve of the point of a machined part driven by the feed-drive system. The symbol $r = [r_x, r_y]^T$ is the desired position of the point of the machined part at time t , and defined in Σ_w . The actual position of the feed-drive system is assumed to be $q = [q_x, q_y]^T$, which is also defined in Σ_w . The contour error is defined as the shortest distance from q to the desired contour C and is represented by the symbol e_c , the contouring controller is concerned with reducing this error. A local coordinate frame Σ_l is also defined, the origin of which is at the desire position r and with two axes T, N , as shown in the figure. The T axis is in the tangential direction of c at r , and the direction of N is perpendicular to T at r . The tracking error vector e_w , which consists of the tracking errors of both feed-drive axes, is defined as follows:

$$e_w = [e_{wx}, e_{wy}]^T = x - r \quad (3.6)$$

This error vector can be expressed with respect to Σ_l as follows:

$$e_l = [e_{lt}, e_{ln}]^T = R^T e_w$$

$$R = \begin{bmatrix} \cos\theta & -\sin\theta \\ \sin\theta & \cos\theta \end{bmatrix} \quad (3.7)$$

where the inclination θ of Σ_l to Σ_w is shown in Fig. 3.13.

3.2.3.2 Contouring Controller Design for Bi-axial Table

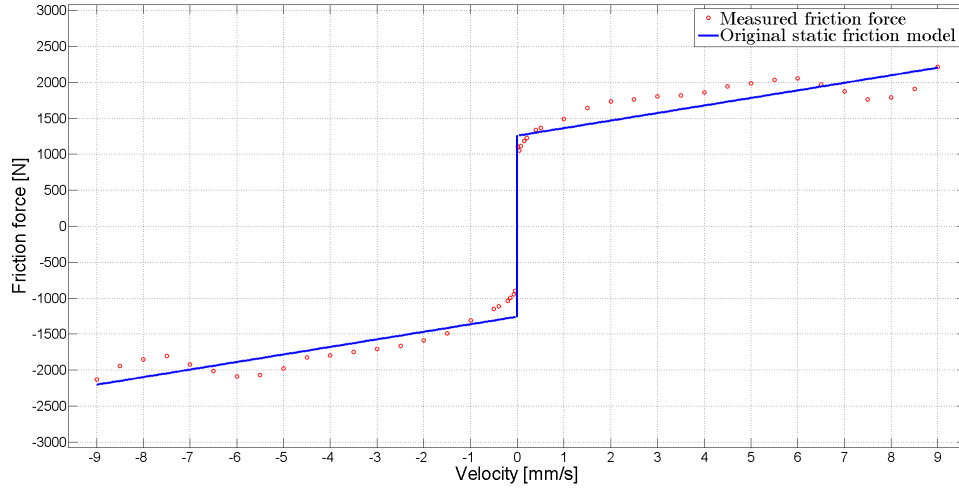


FIGURE 3.14: Identified conventional friction model, x axis

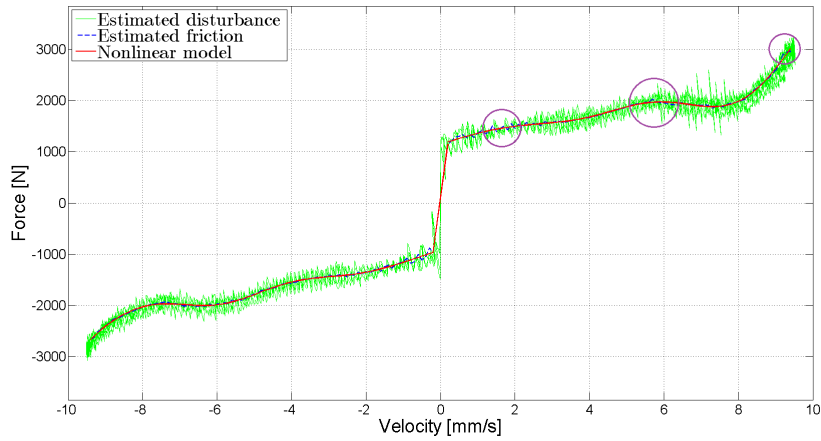


FIGURE 3.15: Identified nonlinear friction model, x axis

We have the following improved contouring controller, where a DOB and feed-forward friction compensation are included in the controller [124]:

$$\begin{aligned}
 F &= M\{\ddot{r} - R(K_{vl}\dot{e}_l + K_{pl}e_l) - \ddot{\theta}I_e e_w + \dot{\theta}^2 I_e e_w - 2\dot{\theta}I_e \dot{e}_w\} + D + F_f \\
 I_e &= \begin{bmatrix} 0 & 1 \\ -1 & 0 \end{bmatrix}, F = [f_x, f_y]^T, M = \text{diag}\{m_x, m_y\}, D = [d_x, d_y]^T \\
 F_f &= [F_{fx}, F_{fy}]^T, K_{vl} = [k_{vlt}, k_{vln}]^T, K_{pl} = [k_{plt}, k_{pln}]^T
 \end{aligned} \tag{3.8}$$

where F, M, I , and \ddot{r} are the driving force vector, the table mass matrix, a 2x2 identity matrix, and the reference acceleration vector of the desired contour, respectively. The symbols K_{vl} and K_{pl} are the velocity and position feedback-gain matrices. They are assumed to be diagonal matrices with positive elements. The disturbance d_x and d_y are estimated as in Eq.(2.22).

3.2.3.3 Experimental Results

Here, we compare experimental results between PD controller use three type feed drive controller in Eqs. (7.7), (7.8), and (7.9). We conduct experiments with the following circular reference trajectory:

$$r_x = 10\cos(0.85t)(mm), r_y = 10\sin(0.85t)(mm) \tag{3.9}$$

Controller gains are set as $K_{vl} = 2\omega, K_{pl} = \omega^2, \omega = \text{diag}\omega_i, i = t, n, \omega_{lt} = 40\text{rad/s}, \omega_{ln} = 60\text{rad/s}$ We have following experimental results.

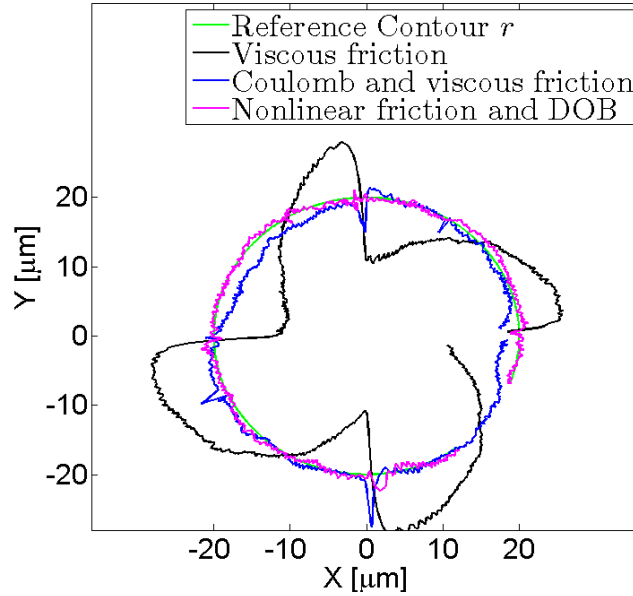


FIGURE 3.16: Reference and real circular contour

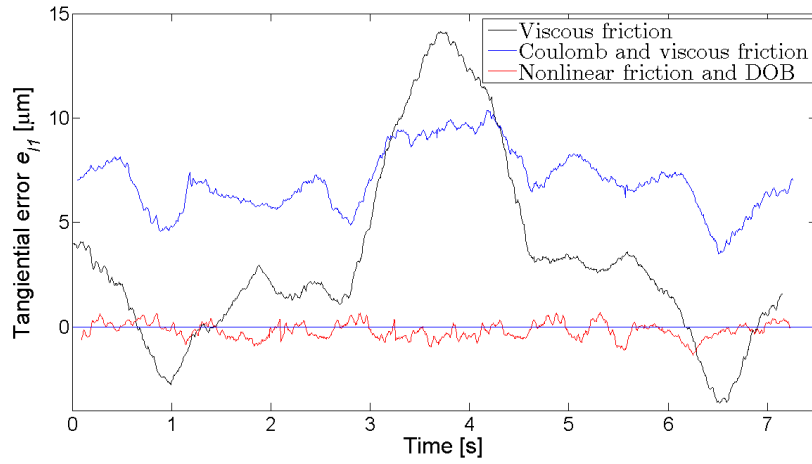


FIGURE 3.17: Tangential error profile

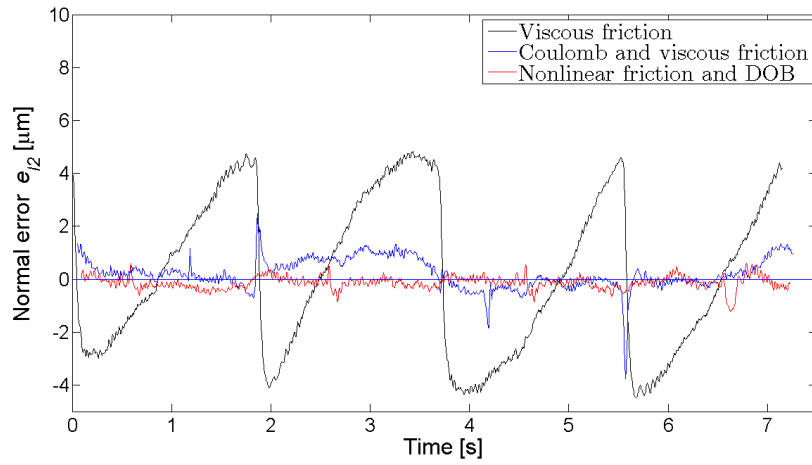


FIGURE 3.18: Normal error profile

From Figs. 3.20,3.21, our proposed friction model and DOB archived about $1 \mu\text{m}$ precise and a mean contour error of less than $0.5\mu\text{m}$. We increase the control gain to $\omega_{lt} = 60\text{rad/s}$, $\omega_{ln} = 70\text{rad/s}$ to verify the proposed method, and we obtain the following experimental results,

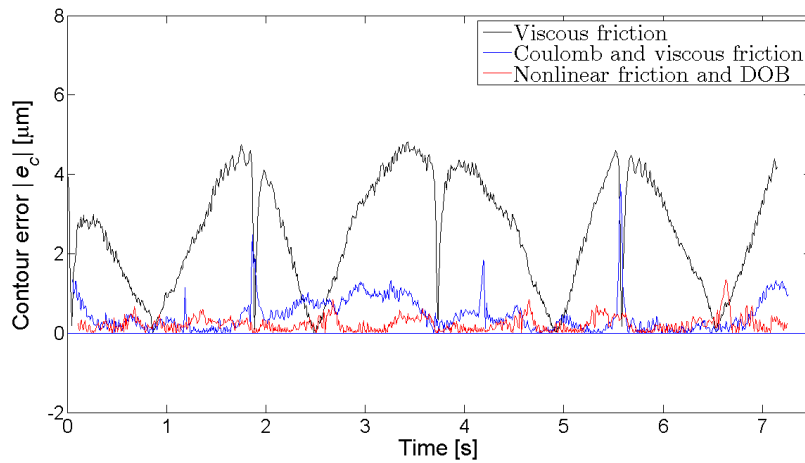


FIGURE 3.19: Contour error profile

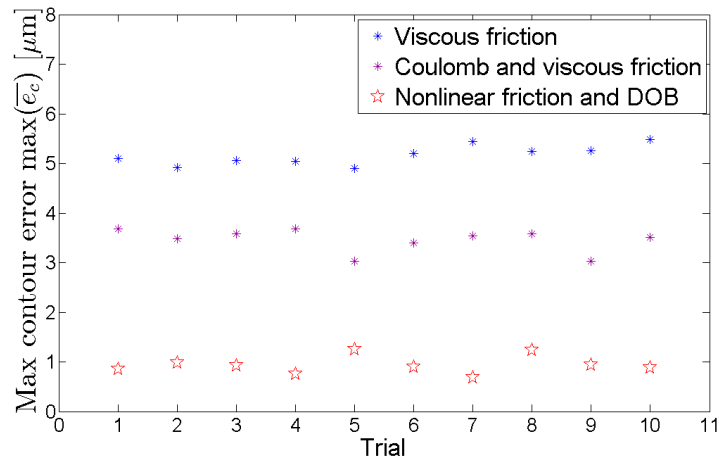


FIGURE 3.20: Maximum contour error

From Figs. 3.26,3.27, our proposed friction model obtains better control performance with high feed-back gain. Contouring control using our proposed method has a bigger range of feed-back gain and therefore obtains better control performance with high control gain. We conducted experiments with a non-circular curve to confirm the efficiency of our proposed method. First, we present experimental results for eight curve tracking.

Second is trifolium curve experimental results.

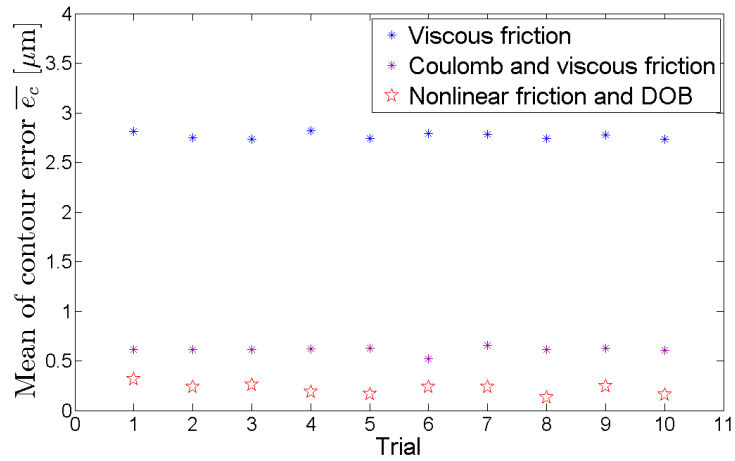


FIGURE 3.21: Mean of contour error in 10 times experiment

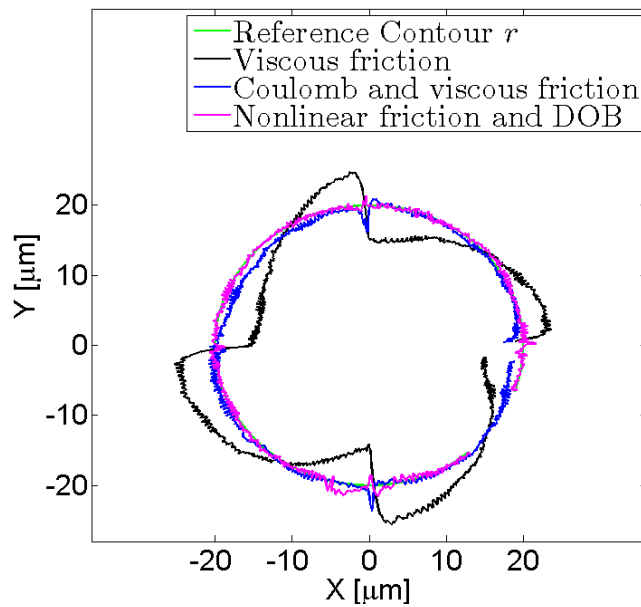


FIGURE 3.22: Reference and real circular contour

We conduct other experiment to compare the proposed method.

Table 3.1 summarizes the average contour error from 10 trials of each controller at a tangential tracking velocity of 3mm/s. We can see that the maximum contour error often occurs at a quadrant, and therefore its value equals the maximum quadrant glitch. However, for controller (c), the maximum contour error does not occur at a quadrant because of the modeling

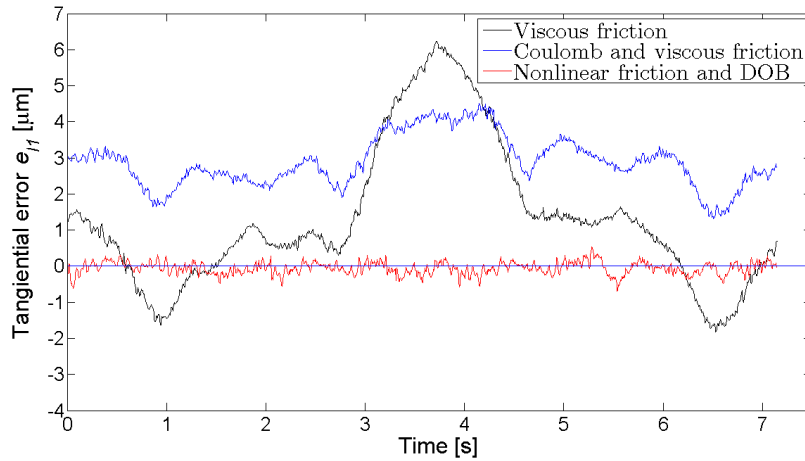


FIGURE 3.23: Tangential error profile

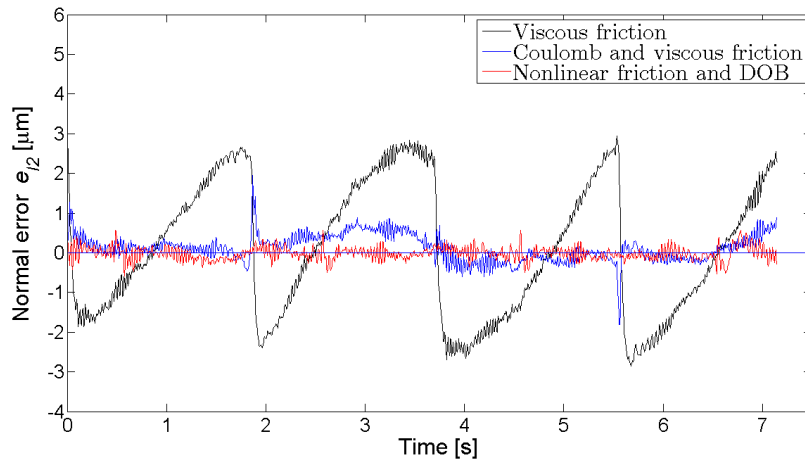


FIGURE 3.24: Normal error profile

error of the nonlinear friction. The DOB compensates for the modeling error of the friction model. The controller with the DOB and the conventional static friction model provides slightly better performance in that the maximum contour error is reduced to only $3.71\mu\text{m}$. However, by comparing the results in (b) and (c) for which only feed-forward compensation is applied, the nonlinear static friction model shows better performance. At the lower tracking speed region, although the maximum contour error and the quadrant glitch for (c) are the smallest, controller (f) that includes a DOB provides a better root mean square (RMS) error and standard deviation. We conclude that a controller that uses both feed-forward friction compensation and a DOB will reduce the contour error steadily.

The benefit of the proposed nonlinear friction model is evident in the high speed regime, as shown in Table 3.2, which summarizes the average results from 10 trials at a speed of 9.5mm/s . Figures 3.34 and 3.35 show the contouring-error results from applying controllers (a)–(f). In Table 3.2, we can see that the maximum contour error in (b) and (e) is greater than the maximum quadrant glitch because the nonlinear property of friction is

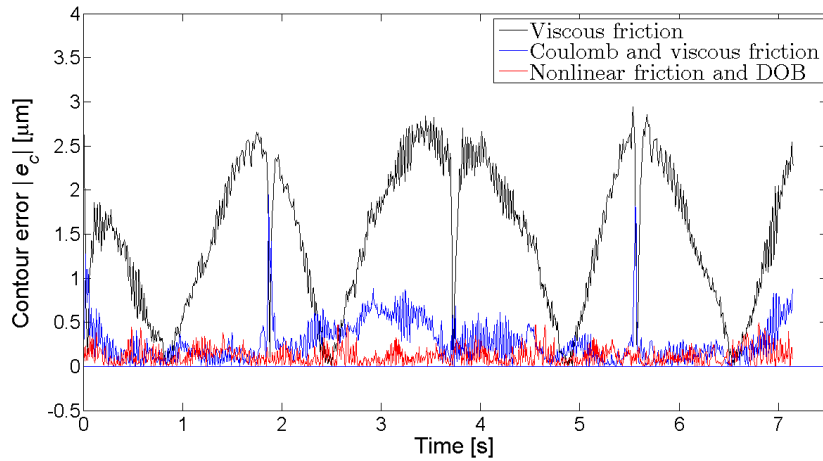


FIGURE 3.25: Contour error profile

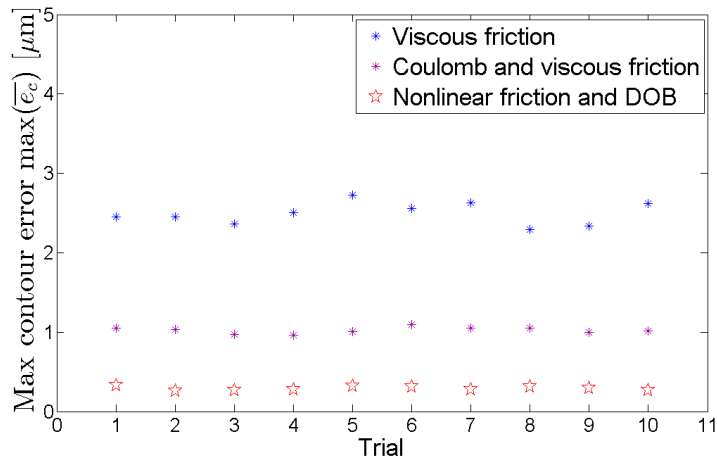


FIGURE 3.26: Maximum contour error

dominant in the high speed regime. Controller (f) clearly provides the best contour-error performance, where the maximum contour error is reduced to only $1.56\mu\text{m}$. The RMS of the contour error and its standard deviation are also improved to only $0.49\mu\text{m}$ and $0.94\mu\text{m}$, respectively.

3.2.4 Conclusions

The nonlinear friction properties in a mechanical feed drive system are analyzed. Because the contour error is important in machining applications, a contouring controller with Gaussian-augmented friction compensation is proposed to improve the contouring performance. Comparative experiments with several friction-compensations models in both the low-speed and high-speed regimes are conducted, and it is shown that the proposed controller is effective for high speed motion, the maximum contour error is reduced by 58% compared to that with a conventional static friction model.

The contouring performance would be improved further with a combination of the LuGre dynamic-friction model and the proposed Gaussian-augmented friction model. This extension is left for future research.

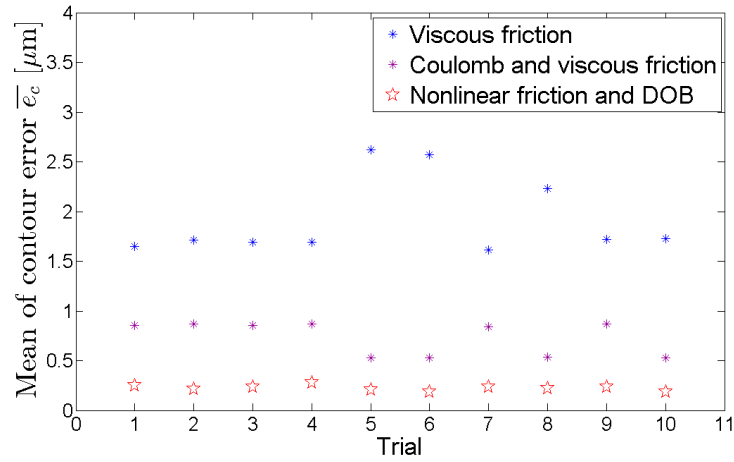


FIGURE 3.27: Mean of contour error in 10 times experiment

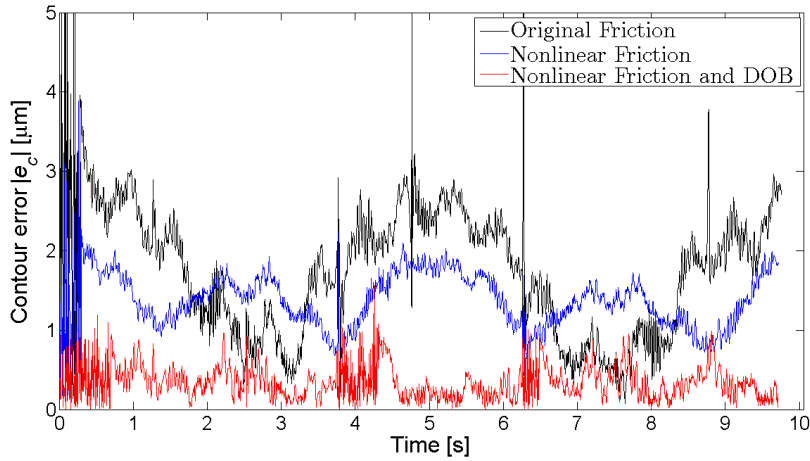


FIGURE 3.28: Contour error profile-Experiment results with eight curve

TABLE 3.1: Contour error in different friction compensation strategies at 3mm/s

Friction Compensation Techniques	Max Contour Error	Quadrant Glitch	Root Mean Square	Standard Deviation
(a). No Friction compensation	15.72 μm	15.72 μm	7.73 μm	11.21 μm
(b). Conventional friction compensation	7.36 μm	7.36 μm	1.14 μm	1.56 μm
(c). Proposed friction compensation	3.54 μm	3.32 μm	0.85 μm	1.34 μm
(d). Disturbance observer only	13.81 μm	13.81 μm	2.98 μm	3.04 μm
(e). Disturbance observer+ conventional friction model	3.71 μm	3.71 μm	0.43 μm	0.58 μm
(f). Disturbance observer+ Proposed friction model	5.43 μm	5.43 μm	0.55 μm	0.73 μm

TABLE 3.2: Contour error in different friction compensation strategies at 9.5mm/s

Friction Compensation Techniques	Max Contour Error	Quadrant Glitch	Root Mean Square	Standard Deviation
(a). No friction compensation	12.74 μm	12.74 μm	6.88 μm	9.73 μm
(b). Conventional friction compensation	5.38 μm	4.98 μm	2.23 μm	3.19 μm
(c). Proposed friction compensation	3.08 μm	2.99 μm	1.29 μm	1.81 μm
(d). Disturbance observer only	16.72 μm	16.72 μm	3.98 μm	3.38 μm
(e). Disturbance observer+ conventional friction model	3.82 μm	2.41 μm	1.01 μm	1.38 μm
(f). Disturbance observer+ Proposed friction model	1.56 μm	1.56 μm	0.49 μm	0.94 μm

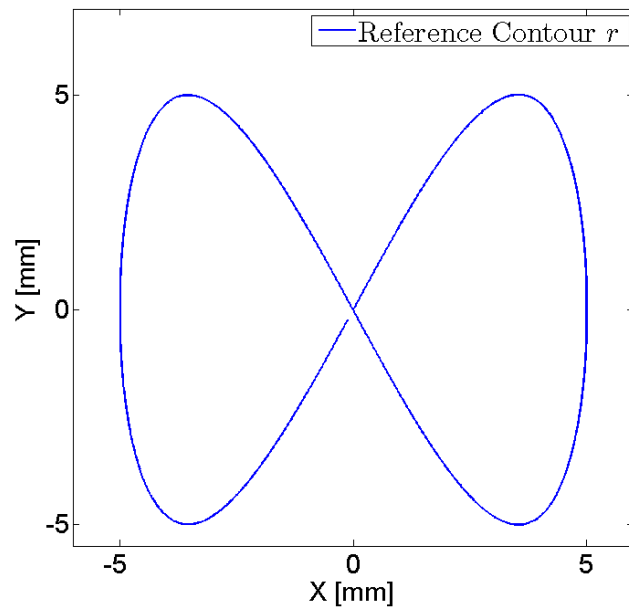


FIGURE 3.29: Reference contour -Experiment results with eight curve

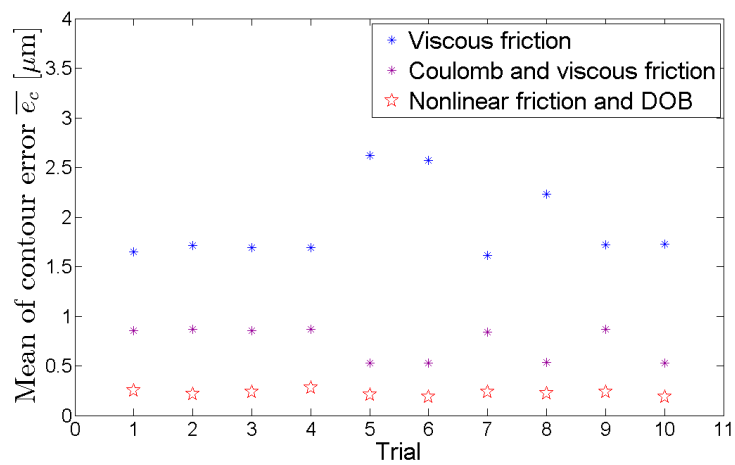


FIGURE 3.30: Max contour error in 10 times experiment -Experiment results with eight curve

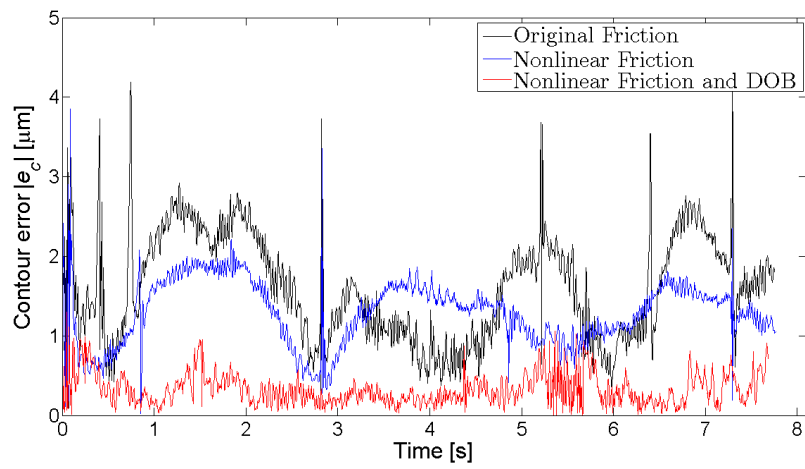


FIGURE 3.31: Contour error profile-Experiment results with trifolium curve

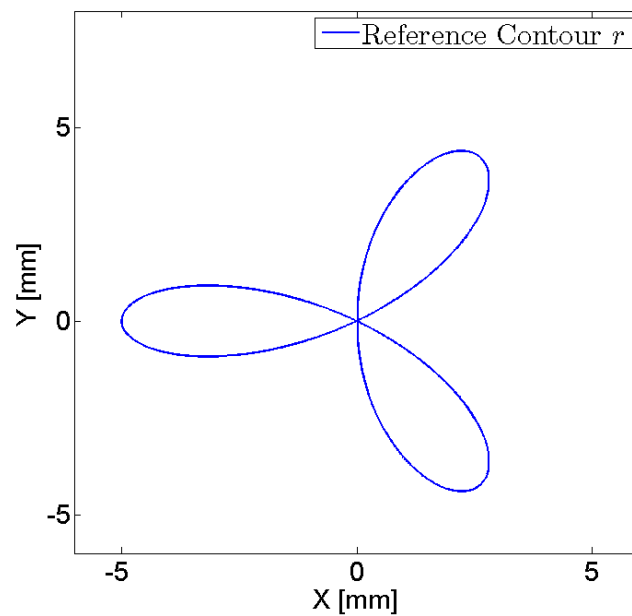


FIGURE 3.32: Reference contour -Experiment results with trifolium curve

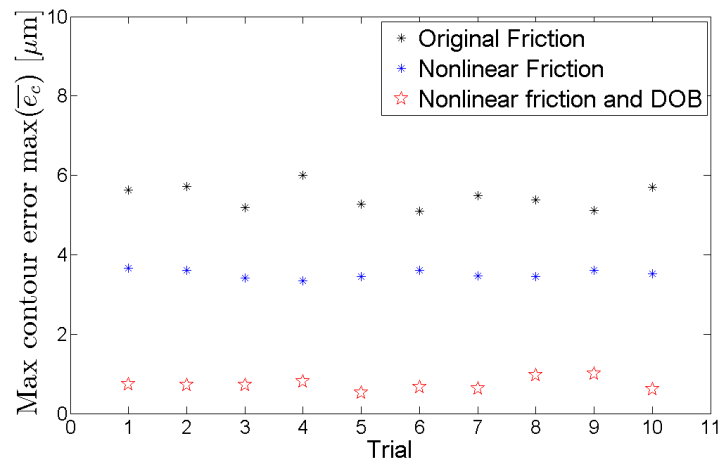


FIGURE 3.33: Max contour error in 10 times experiment -Experiment results with trifolium curve

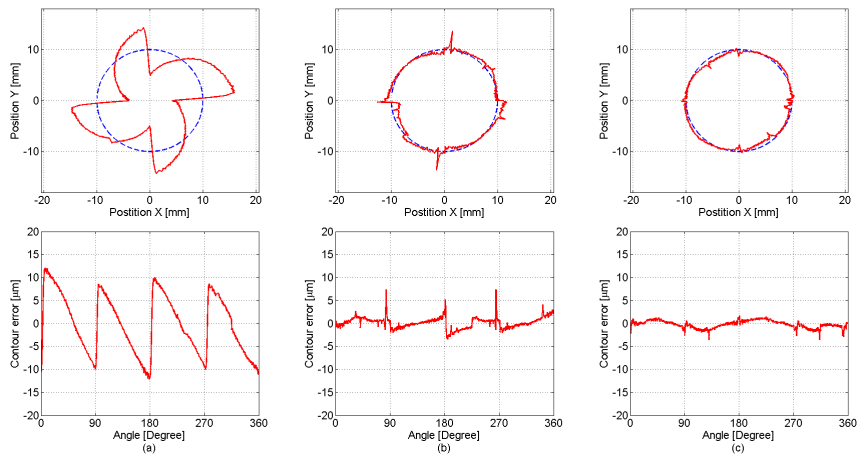


FIGURE 3.34: Measured position and contour error at 9.5mm/s for controller (a), (b), and (c)

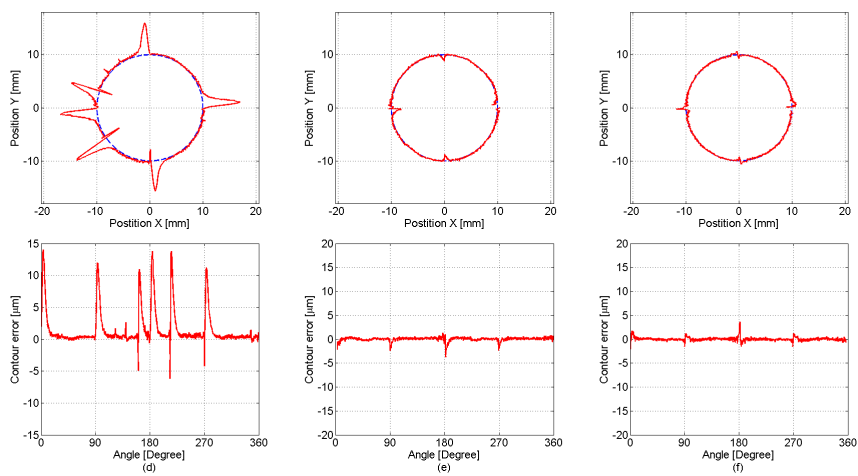


FIGURE 3.35: Measured position and contour error at 9.5mm/s for controllers (d), (e), and (f)

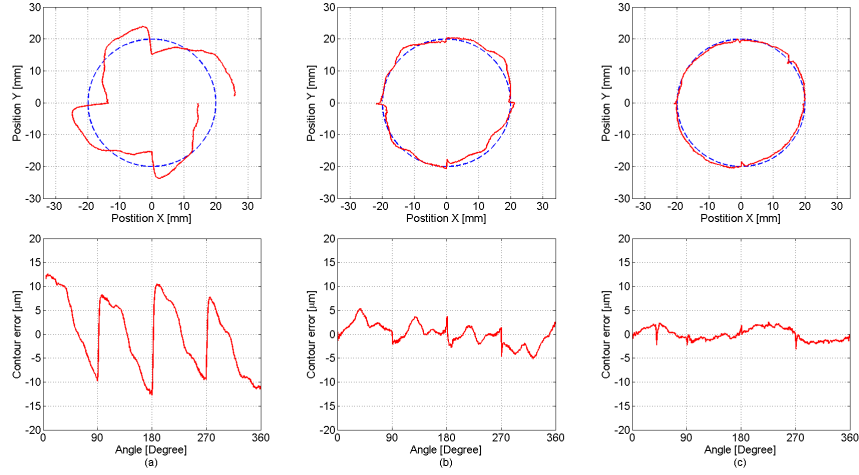


FIGURE 3.36: Measured position and contour error at 9.5mm/s for controller (a), (b), and (c)

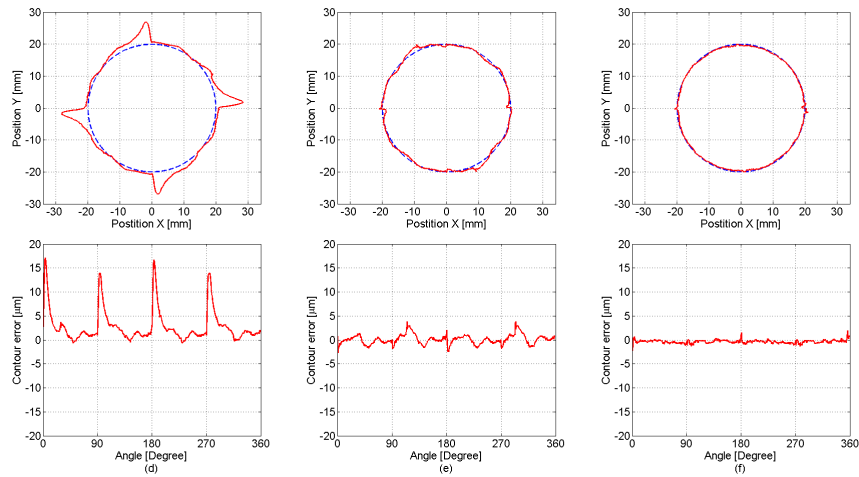


FIGURE 3.37: Measured position and contour error at 9.5mm/s for controllers (d), (e), and (f)

Chapter 4

Triaxial Machine Tool Control

4.1 Introduction

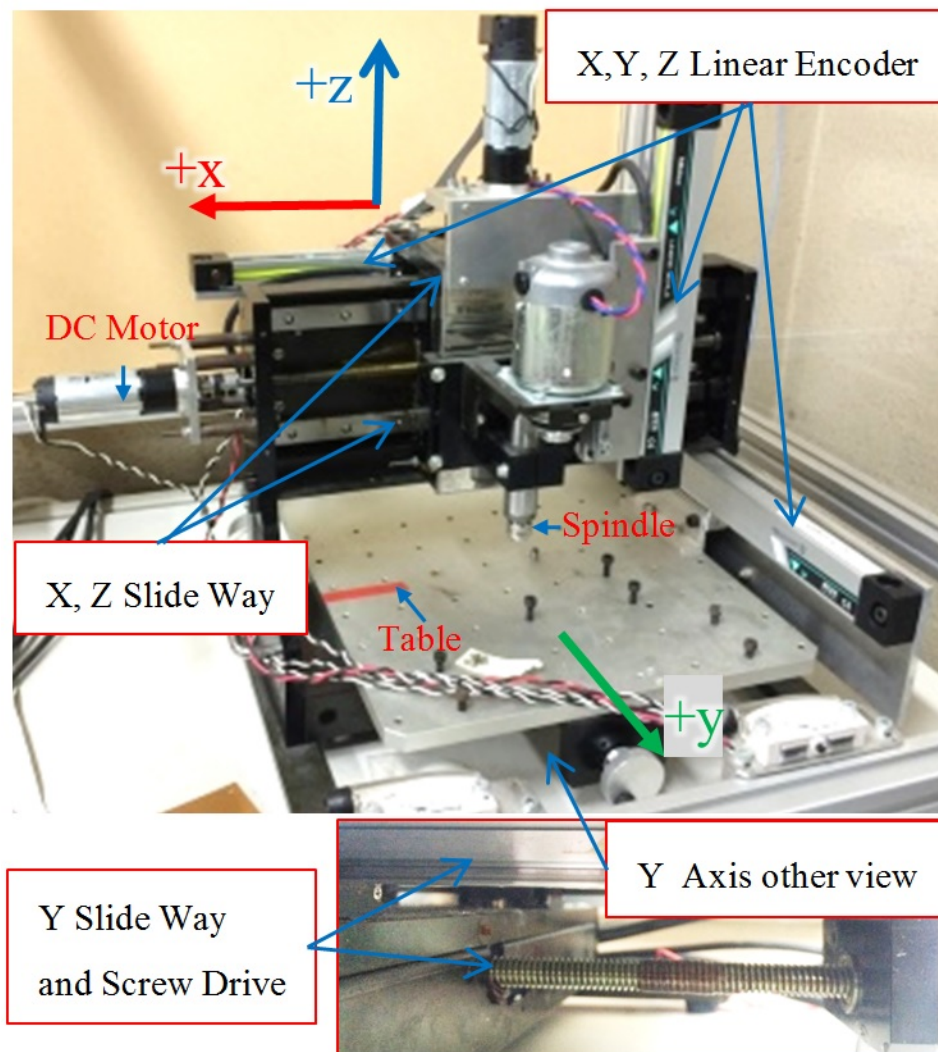


FIGURE 4.1: Triaxial machine tool

Friction is the dominant component that degrades machine-tool motion accuracy. There are many research methods for friction-compensation control

to improve the motion performance of machine tools [11], [26]. Variations on the structure of feed drives and the coupling between them result in highly nonlinear and time-invariant friction behavior [125], [126], and therefore implementation of friction-compensation control is challenging. Friction-compensation control methods can be categorized according which friction model they use [26]. Generally, friction-compensation techniques are divided into two categories: model-free methods and model-based methods. In model-free methods such as robust control and adaptive control, friction is considered as part of the disturbance [127], [128]. Yan et al. [129] proposed a combined two-degrees-of-freedom controller with a DOB to compensate for nonlinear friction, cogging effects, and external disturbances. Lin et al. [130] presented a robust controller that combines a variable-structure controller (VSC) with a DOB-based compensator, and compared the performance to that of a typical disturbance-compensation controller. Tung et al. applied a non model-based friction-compensation approach in the form of a repetitive controller, and demonstrated improved tracking performance and quadrant-glitch compensation [131]

On the other hand, model-based methods exactly cancel out the effect of the friction force on the feed drive by an additional driving force equivalent to the estimated friction [95], [132]. A friction model is incorporated into a feedback or feed-forward loop to estimate the friction. Armstrong have carried out a survey of friction models and compensation methods for the control of machines with friction [26]. Canudas and Lischinsky utilized the LuGre friction model for adaptive friction compensation [112]. Tjahjowidodo et al. have shown that a nonlinear gain-scheduled controller based on the Maxwell-slip- model yields a fast response and a low steady-state error for friction compensation in electro-mechanical systems [121]. Regarding application to real machine-tool control, Erkorkmaz et al. proposed an unbiased identification method and demonstrated the effectiveness of Coulomb-viscous-Stribeck friction compensation [27]. Jamaludin et al. used a dynamic friction model (GMS friction model) for friction compensation techniques and evaluated it experimentally on a linear-drive xy table [78], [122]. However, the GMS friction model or other dynamic friction models provide better performance than that of the conventional static friction model only at low speeds. Although the effect of friction can be suppressed effectively, model-based methods are difficult to apply to actual machine tools because the performance of the friction compensator is highly dependent on the accuracy of the friction model [133]–[135]. Therefore, a precise friction model of feed drives in machine tool is required, which considers not only linear guide friction but also friction behavior inside the lead-screw drive, for example. A Suitable friction model is necessary to improve the performance of the system. Ba and Uchiyama [119] have proposed a nonlinear friction model that includes a nominal Coulomb-viscous friction model and a number of nonlinear friction sources represented by Gaussian functions for describing precise nonlinear behavior. They also designed a contouring controller that consists of a feed-forward compensation term with the proposed friction model and a DOB. Experiments were conducted on a biaxial feed-drive system through which the performance was verified. However, they did not give a corresponding explanation about of the nonlinear part of the model, nor did they identify parameters that are complex in high-speed machine tools. There has been some other research on contouring control of multi-axis systems [136]–[141].

Contouring control with five axes is proposed in [11], [142]–[148]

. This paper is based on the assumption of Bui and Uchiyama that friction in the feed drive of a machine tool is from many friction sources with complicated and nonlinear properties. In particular, we focus on the properties of a lead-screw drive with insufficient lubrication. We show that this acts like a spring, and we propose a nonlinear friction model that includes the typical Coulomb-viscous friction and a nonlinear sinusoidal friction term for to describe the lead screw. In addition, this study presents a controller design with feed-forward friction compensation using the proposed friction model. Experiments are conducted to compare the control performance between the proposed and conventional static friction models. The proposed controller largely improves the control performance with a 26 % reduction in the mean contouring error.

The experimental system used in this study is a desktop triaxial machine tool as shown in Fig. 2.21. It consists of three axes driven by DC servo motors (15 W, 24 V dc) coupled to, and driving three lead screws. It has a spindle attach to z axis and a table attach to y axis. In addition, a linear encoder (resolution 0.1 μm) is attached to each feed-drive axis to measure the real position of the feed-drive system. Modeling of the feed drive on each axis shown in Fig. 2.21 includes a linear guide and a lead-screw/nut system to translate the rotation of the motor into linear motion of the feed drive.

4.2 Identification of Triaxial Machine Tool

The linear dynamics of the feed drive can be represented as shown in Fig. 4.2. Here, u (V) is the control signal applied to the input of the current amplifier, whose gain is k_a (A/V). The amplifier produces a current i (A) in the motor armature, resulting in a motor torque t_m , that is linearly proportional to i with the motor torque constant k_t (Nm/A). The motor torque generates a driving force f_u (N), that is linearly proportional to t_m with the lead screw gain r_g (rad/mm). In addition, the feed drive is also subjected to a disturbance force that contains the effect of friction in the linear guide ways f_{fli} , ball screw f_{fle} , as well as the cutting force f_c . The difference between f_u and $f_c + f_{fli} + f_{fle}$ is used to actuate the mechanical system consisting of the equivalent translational-axis mass m (kg) of the corresponding axis. The lead screw gain r_g is calculated as follows:

$$r_g = \frac{2\pi}{L}, \quad (4.1)$$

where L is the lead of the screw. This gain is used in a lead-screw system to translate rotation into linear motion and the motor torque into a driving force. The other parameter values of the machine are given in Table 4.1.

4.3 Tool Position Contour Error Estimation

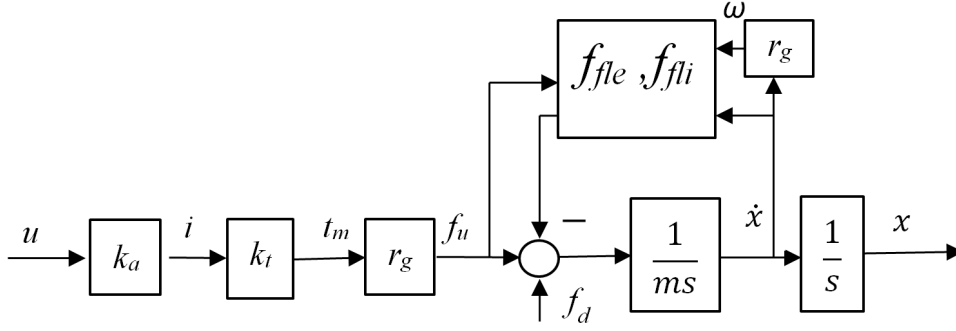


FIGURE 4.2: Linear dynamics of a feed drive

TABLE 4.1: Triaxial machine tool parameters

	x axis	y axis	z axis
m (Ns ² /mm)	1.0	0.8	0.8
L (mm)	2	2	2
k_a (A/V)	0.21	0.21	0.21
k_t (Nm/A)	38.2	38.2	38.2

In machining, the contour error is an important criterion for the quality of the machining surface. Figure 4.3 explains the relationship between the tracking and contour errors schematically. The coordinate frame Σ_w , whose x, y and z axes correspond to the feed drive axes, is a fixed frame. The blue contour represents the desired path of the feed drive of the triaxial machine tool. The symbol $q_d = [q_{dx}, q_{dy}, q_{dz}]^T$ denotes the desired position at time t , and is defined in Σ_w . The real position of the feed drive is assumed to be $q = [q_x, q_y, q_z]^T$, which is also defined in Σ_w . The contour error is defined as the shortest distance from q to the desired path and represented by symbol e_c . The contouring controller is concerned with reducing this error. The tracking error vector e_w , which consists of the tracking errors in the three feed-drive axes, is defined as follows:

$$e_w = [e_{wx}, e_{wy}, e_{wz}]^T = q - q_d. \quad (4.2)$$

The approximated contour error is defined in a local coordinate frame Σ_l . Its origin is at the desired position q_d and with the three axes t, n, b , as shown in the figure. The t axis is in the tangential direction of desired path at q_d , the direction of n axis is perpendicular to t at q_d and the b axis is the bi-normal component normal to t and n . For the parametric trajectory, the tangential, normal, and bi-normal vectors are denoted as t, n and b , respectively, and are calculated at a time t_s as follows:

$$n_{temp} = \left(\frac{\ddot{q}_d}{\|\ddot{q}_d\|}, \forall \ddot{q}_d \neq 0 \right) \text{Or} \left((1, 0, 0), \ddot{q}_d = 0, \forall t \neq (1, 0, 0) \right) \\ \text{Or} \left((0, 1, 0), \ddot{q}_d = 0, t = (1, 0, 0) \right), t = \frac{\dot{q}_d}{\|\dot{q}_d\|}, \quad (4.3) \\ b = t \times n_{temp}, n = b \times t,$$

where n_{temp} is the vector to find a plane that contains vectors t and n . The

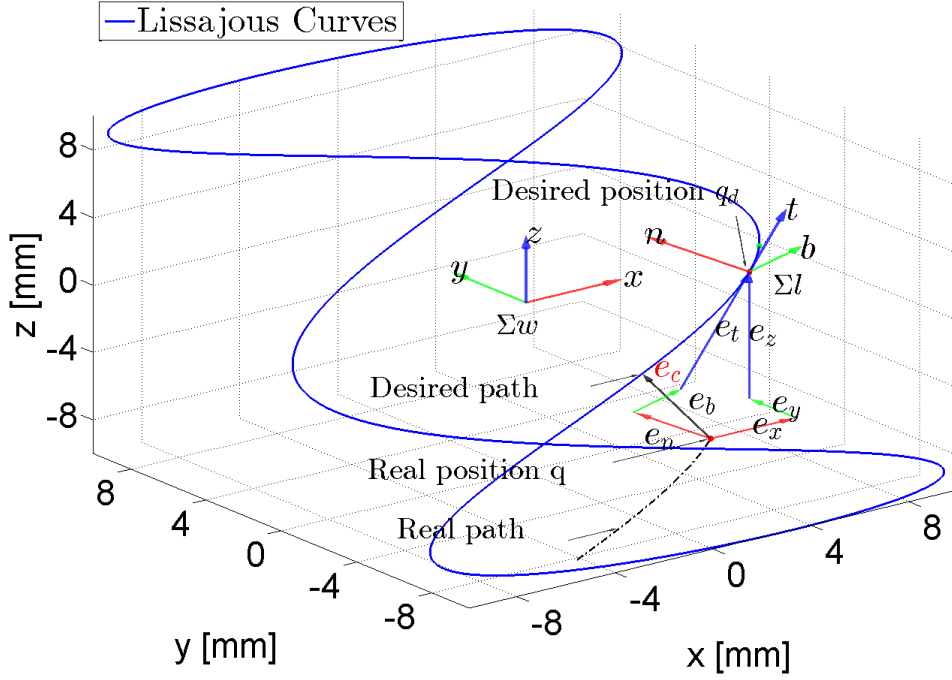


FIGURE 4.3: Definition of contour error

normal vector n is calculated from vectors b and t . The error between the real position and the desired position can be expressed with respect to Σ_l as follows:

$$\begin{aligned}
 e_l &= [e_{lt}, e_{ln}, e_{lb}]^T = R^T e_w, \\
 R &= [t, n, b], \\
 e_c &\approx \sqrt{e_{ln}^2 + e_{lb}^2},
 \end{aligned} \tag{4.4}$$

where $R^T R = I$ and I is the identity matrix. The contour error e_c is used in the design of the contouring controller.

4.4 Contouring Control Design with Eccentric Configuration Friction Model

4.4.1 Identification of Conventional Friction Model

When the feed drive in Fig. 4.1 is operated at constant velocity without machining, main disturbance is the friction force. Based on the estimation method in [119], a feed drive tracking controller with a disturbance observer is used to actuate the feed drive at constant velocities of 0.01, 0.04, 0.08, 0.15, 0.2, 0.4, 0.5, 1.0, 1.5, 2.5, 3.0, 3.5, 4.0, 4.5, 5.0, 5.5, 6.0, 6.5, 7.0, 7.5, 8.0, 8.5, 9.0, 10.0, 11.0, 12.0, 13.0, 14.0 and 15.0 mm/s. Fig. 4.4 shows the observed and the fitted friction force represented by Eq. (2.9). The Nelder-Mead downhill simplex method with the function "fminsearch" in MATLAB is used to identify friction model parameters. The obtained parameters are shown in Table. 4.2.

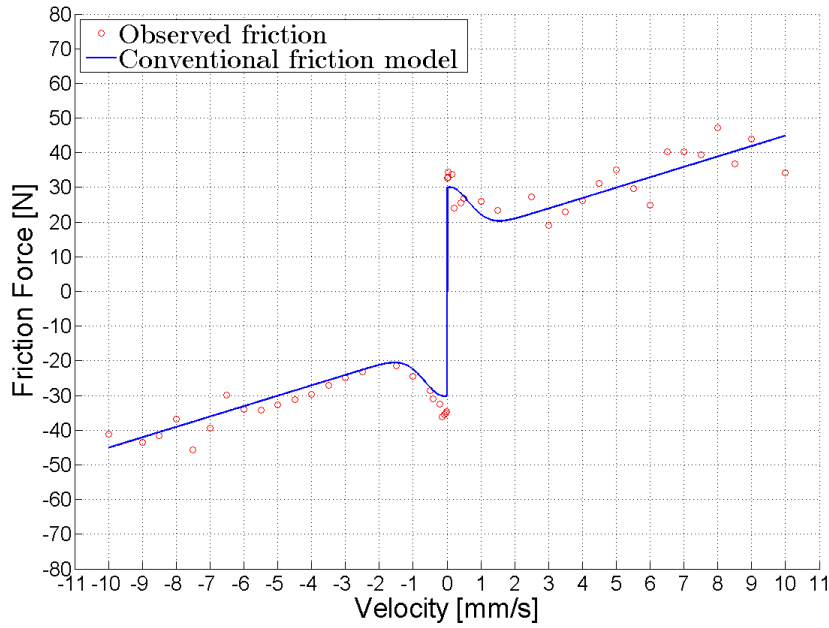


FIGURE 4.4: Observed friction and approximation by a conventional friction model

TABLE 4.2: Estimated conventional friction model parameters

	α_0 (N)	α_1 (N)	α_2 (Ns/mm)	ν_0	δ
x	20	35	5.0	0.6	2
y	15	30	3.0	0.9	2
z	25	40	5.0	0.4	2

4.4.2 Identification of Eccentric Configuration Friction Model

Similar as in single-axis feed drive systems and bi-axial table, observed time-friction map and identified conventional friction model show high deviation. But not like as in bi-axial table system, observed friction-velocity map in triaxial machine tool is more complex with repetitive sinusoidal properties. Therefore, the Gaussian augmented friction model is not suitable to model this friction behavior because it will increase the number of Gaussian function and friction model complexity. For this reason, other friction model should be used. Beside velocity-friction map, position-friction map is proposed to support to figure out the cause of repetitive friction component. Position-friction map confirm the appearance of eccentric friction as assumption in chapter 2. Therefore, eccentric consideration friction model in chapter 2 are chosen to model friction in triaxial machine tool.

Fig. 4.7 show that the proposed model is better describe friction behavior than the original one. Estimated eccentric configuration friction model parameters are shown in Table. 4.3

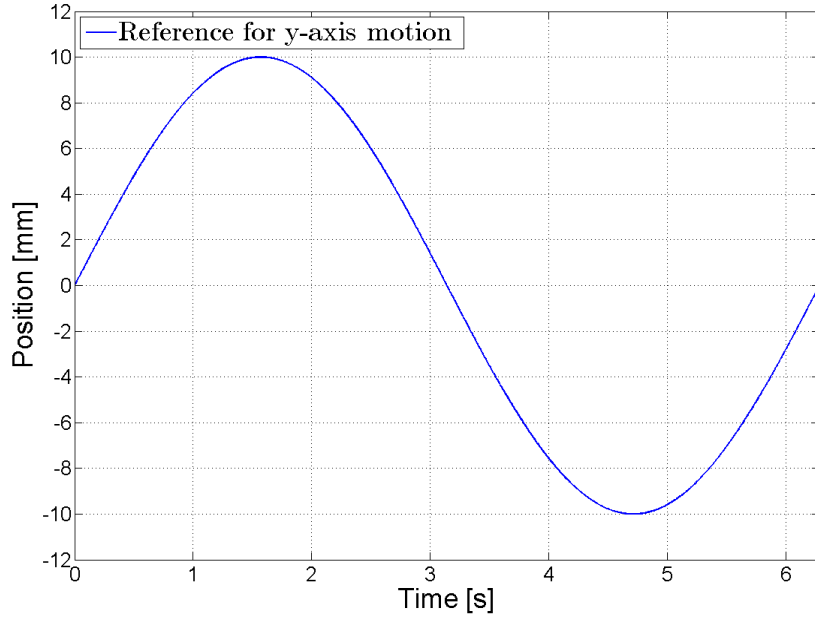


FIGURE 4.5: Reference for y-axis motion

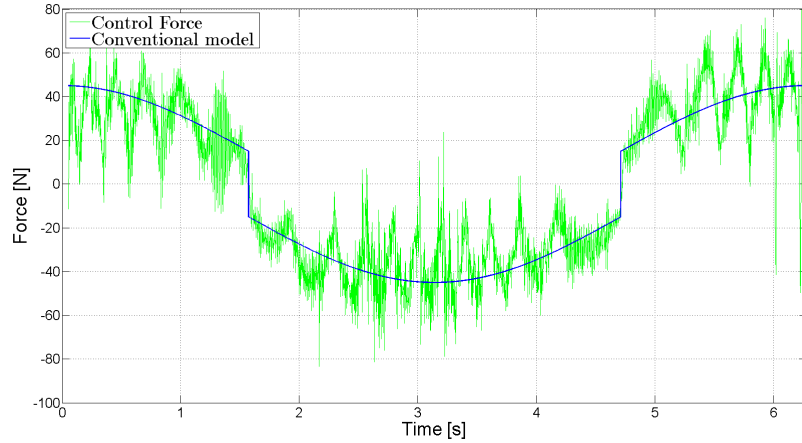


FIGURE 4.6: Conventional friction model and observed friction on y-axis

4.4.3 Contouring Controller Design

We have the following improved contouring controller in which a feed-forward friction compensation is included in the controller [123], [149]:

$$\begin{aligned}
 F_u &= M \left\{ \ddot{q}_d - R \left(K_{vl} \dot{e}_l + K_{pl} e_l + \ddot{R}^T e_w + 2\dot{R}^T \dot{e}_w \right) \right\} + F_r \\
 F_u &= [f_{ux}, f_{uy}, f_{uz}]^T, M = \text{diag}\{m_x, m_y, m_z\}, \\
 F_r &= [f_{rx}, f_{ry}, f_{rz}]^T, K_{vl} = \text{diag}\{k_{vlt}, k_{vln}, k_{vlb}\}, \\
 K_{pl} &= \text{diag}\{k_{plt}, k_{pln}, k_{plb}\},
 \end{aligned} \tag{4.5}$$

where F_u , M and \ddot{q}_d are the driving force vector, the table mass matrix and the reference acceleration vector of the desired contour, respectively. The symbols K_{vl} and K_{pl} are the velocity and position-feedback gain matrices,

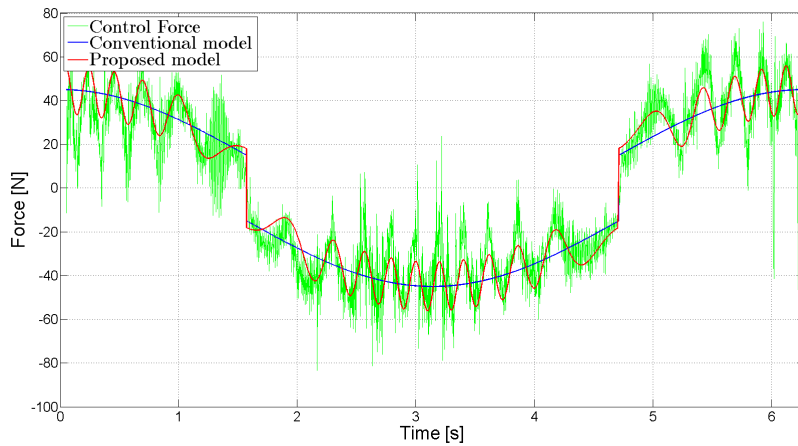


FIGURE 4.7: Eccentric configuration friction model and observed friction

TABLE 4.3: Estimated eccentric configuration friction model parameters

	η_0 (N)	η_1 (Ns/mm)	η_2 (N)	η_3 (rad)
x	18	4.5	4.2	0.28
y	15	3	11.2	-0.27
z	24	4	2.5	+0.31

respectively. They are assumed to be diagonal matrices with positive constant elements.

4.4.4 Experimental Results

The proposed nonlinear friction model is verified experimentally with the triaxial machine tool in Fig. 2.21. Here, the feed-drive motion is verified on its own without machining a workpiece. We used C++ to implement a controller program that connect to the experimental system through a 16 bit DA board and a 32 bit pulse counter board. Figure 4.8 shows the graphical user interface for the experiment. The friction-compensation performance is verified based on tracking control results with a circular and non-circular reference. The maximum and RMS contour errors are used to validate the friction compensation performance, which is compared for the following different controller configurations (All the controllers are based on the contouring controller in Eq. (3.8)):

- (a). Contouring controller without friction compensation
- (b). Contouring controller with conventional friction model compensation
- (c). Contouring controller with proposed friction model compensation

For comparison purpose, the same controller gains are used in all controllers as $K_{vl} = \text{diag}\{60\text{s}^{-1}, 60\text{s}^{-1}40\text{s}^{-1}\}$, $K_{pl} = \text{diag}\{3600\text{s}^{-2}, 3600\text{s}^{-2}, 1600\text{s}^{-2}\}$.



FIGURE 4.8: Graphical user interface for experiment

4.4.4.1 Experimental Results of Circular Contouring

Firstly, the following three dimensional desired circular contour is used in the experiment:

$$\begin{aligned}
 q_x &= 10 \cos\left(\frac{4\pi}{15}t\right) \text{ mm}, \\
 q_y &= 10 \sin\left(\frac{4\pi}{15}t\right) \text{ mm}, \\
 q_z &= 10 \sin\left(\frac{4\pi}{15}t\right) \text{ mm}, \\
 t &= [0.0, 15.0] \text{ s}
 \end{aligned} \tag{4.6}$$

Figures 4.9, 4.10, and 4.11 show the contouring controller results by applying the controllers (a), (b), and (c), respectively. Figures 4.12 compares the maximum contour error for 10 trials and Fig. 4.13 is for the mean contour error. In Figs. 4.12 and 4.13, the contouring controller without friction compensation exhibits larger contour errors than those of the contouring controllers that use friction compensation. The contouring controller that uses the proposed friction model results in a smaller maximum contour error than that with the conventional model. Furthermore, the average mean contouring error and the maximum contour error are reduced by about 26% and 9.3% in comparison with conventional ones, respectively.

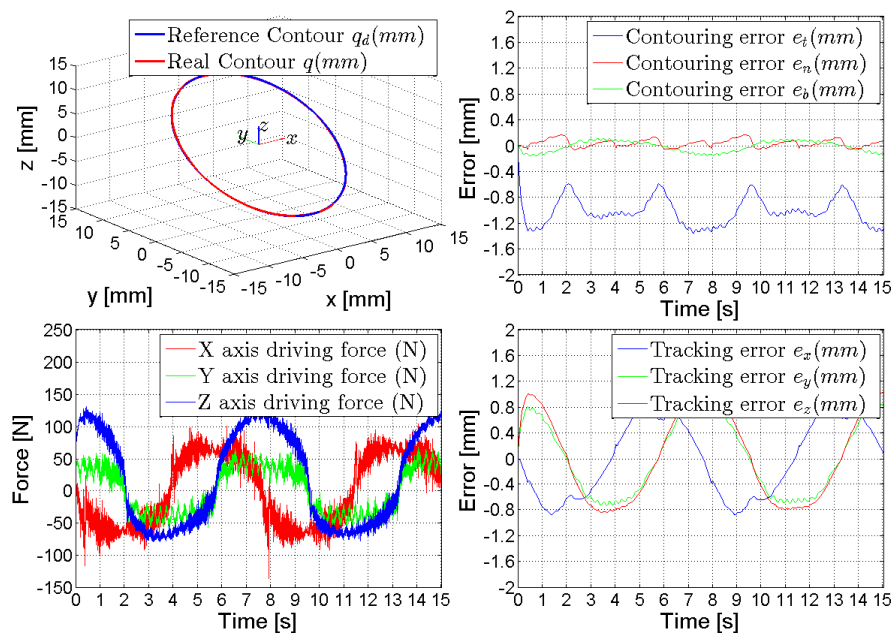


FIGURE 4.9: Circular contour tracking results for controller (a)

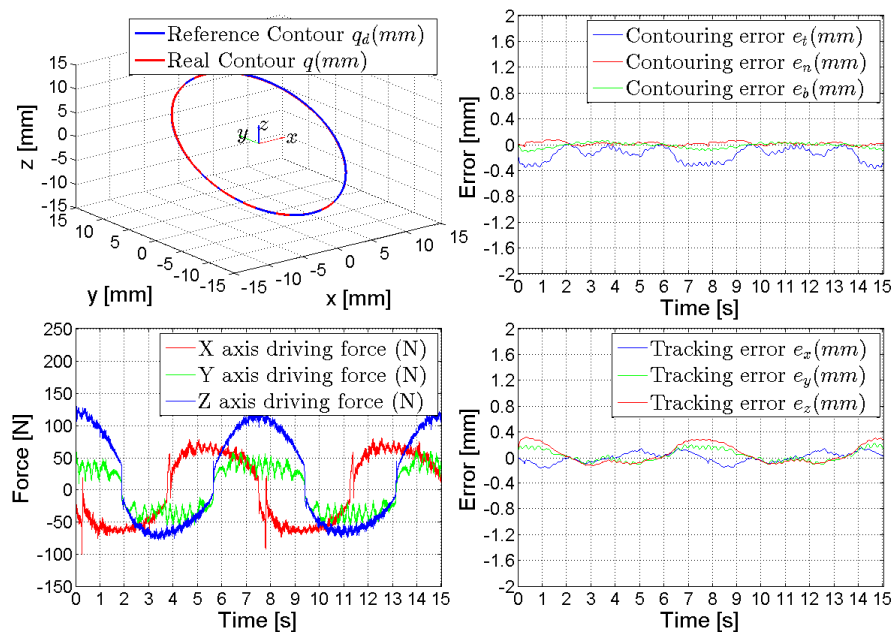


FIGURE 4.10: Circular contour tracking results for controller (b)

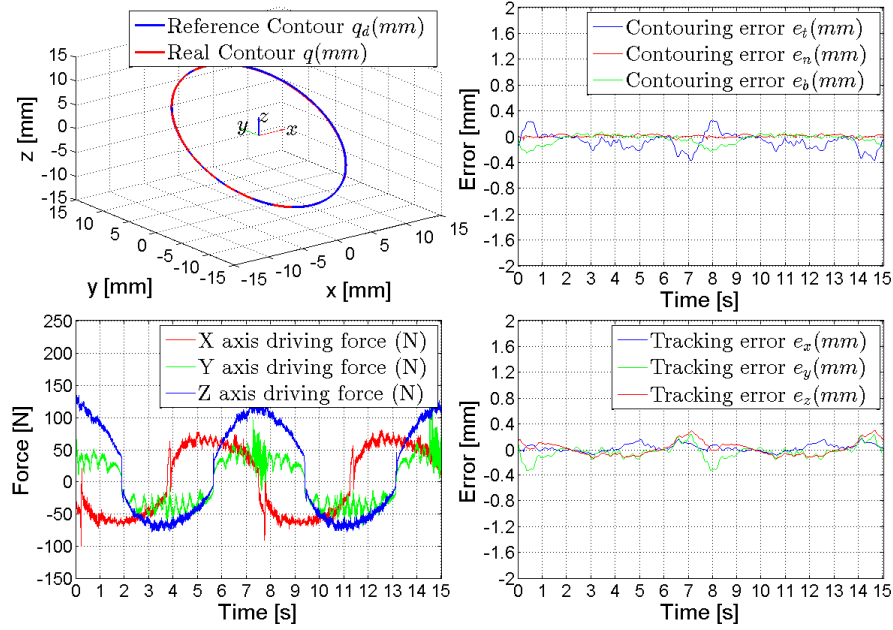


FIGURE 4.11: Circular contour tracking results for controller (c)

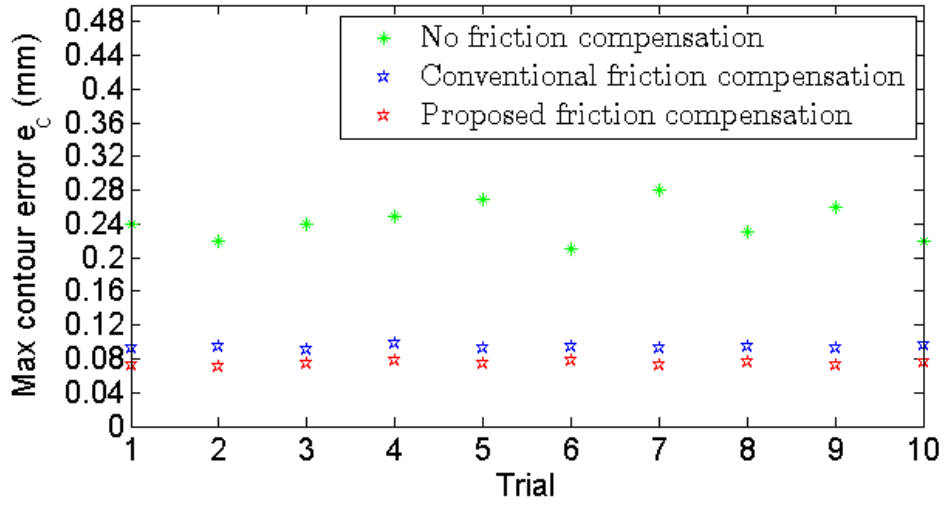


FIGURE 4.12: Maximum contour error results in circular reference

4.4.4.2 Experimental Results of Non-Circular Contouring

The following three-dimensional non-circular contour is used in the experiment:

$$\begin{aligned}
 q_x &= 10 \cos\left(\frac{\pi}{10}t\right)^2 \left(4 \sin\left(\frac{\pi}{10}t\right)^2 - 1\right) + 10 \text{ mm}, \\
 q_y &= 10 \cos\left(\frac{\pi}{10}t\right) \sin\left(\frac{\pi}{10}t\right) \left(4 \sin\left(\frac{\pi}{10}t\right)^2 - 1\right) \text{ mm}, \\
 q_z &= 10 \cos\left(\frac{\pi}{10}t\right)^2 \left(4 \sin\left(\frac{\pi}{10}t\right)^2 - 1\right) + 10 \text{ mm}, \\
 t &= [0.0, 10.0] \text{ s}.
 \end{aligned} \tag{4.7}$$

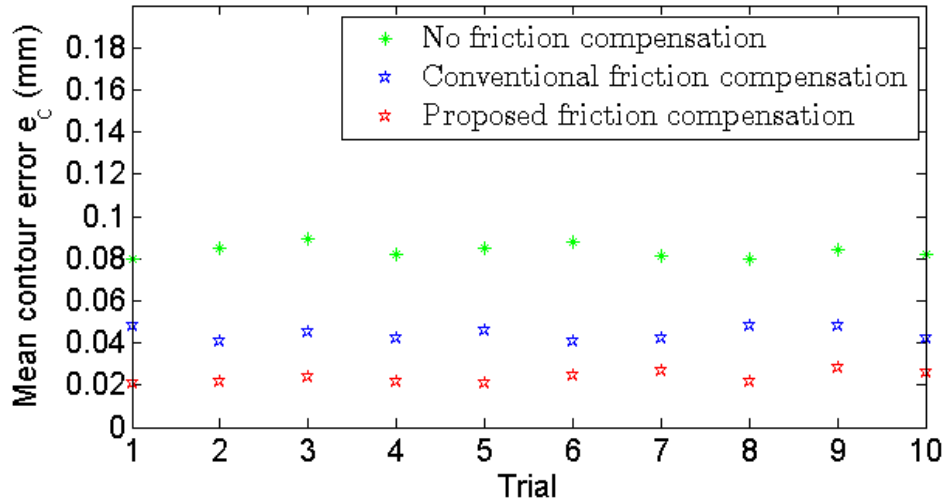


FIGURE 4.13: Mean contour error results in circular reference

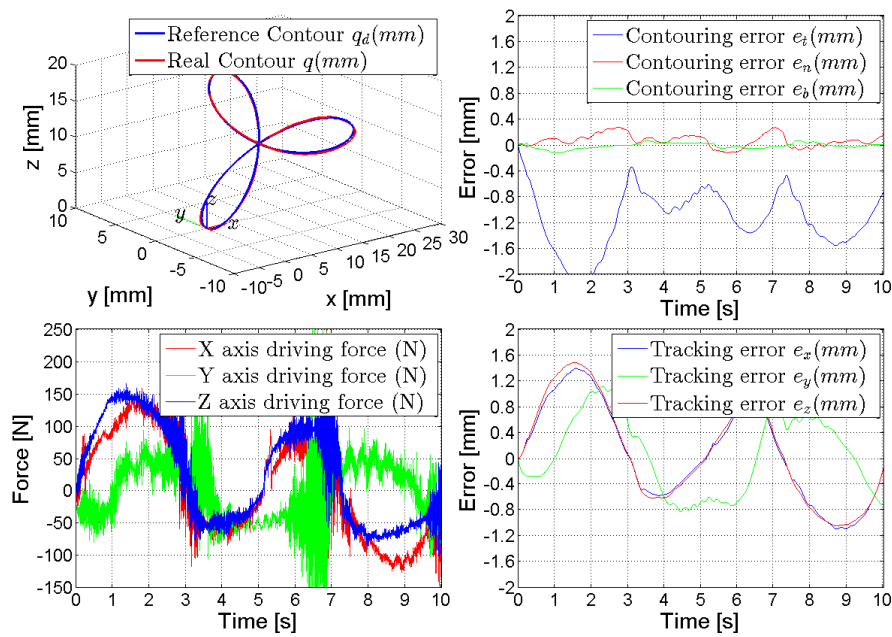


FIGURE 4.14: Non-circular contour tracking results for controller (a)

Figures 4.14, 4.15, and 4.16 show the contouring-controller results of applying controllers (a), (b), and (c). Fig. 4.17 compares the maximum contour

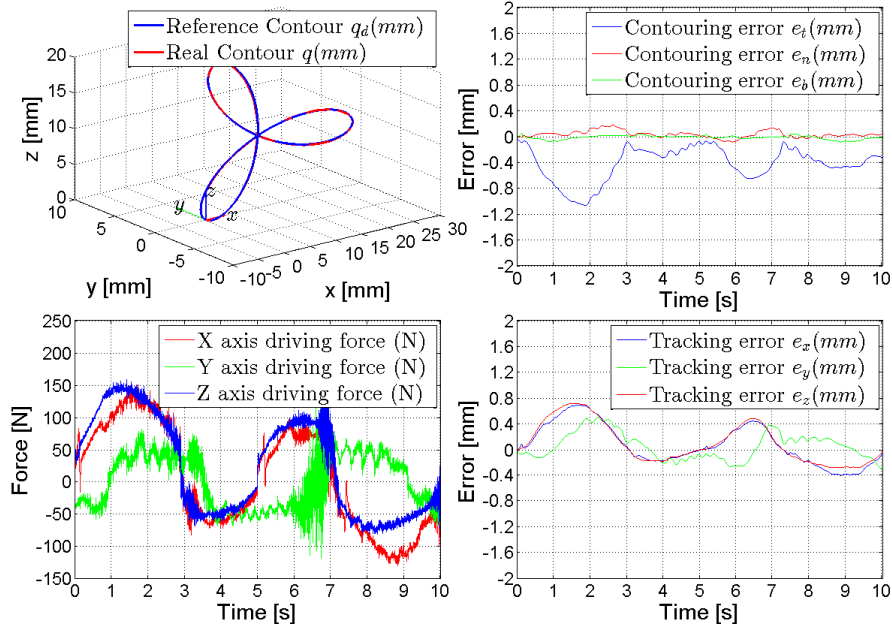


FIGURE 4.15: Non-circular contour tracking results for controller (b)

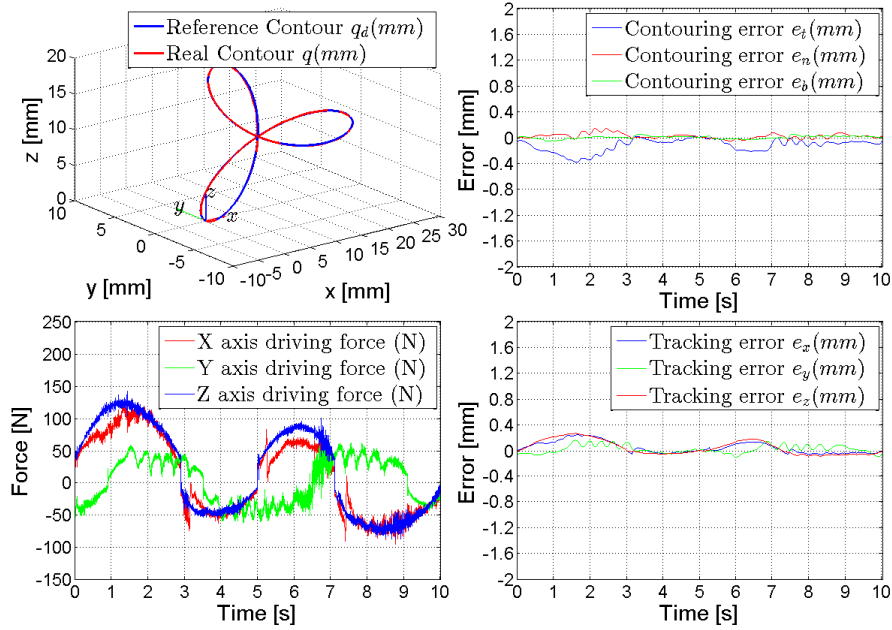


FIGURE 4.16: Non-circular contour tracking results for controller (c)

error for 10 times trial, and Figs. 4.18 is for the mean contour error. Similar results are obtained for the circular-contour cases. The mean contouring error and the maximum contour error have average reductions of 16% and 35.4%, respectively, in comparison with the conventional ones. Although the mean contour error reduction is lower than that in a circular case, the maximum contour error reduction is much better.

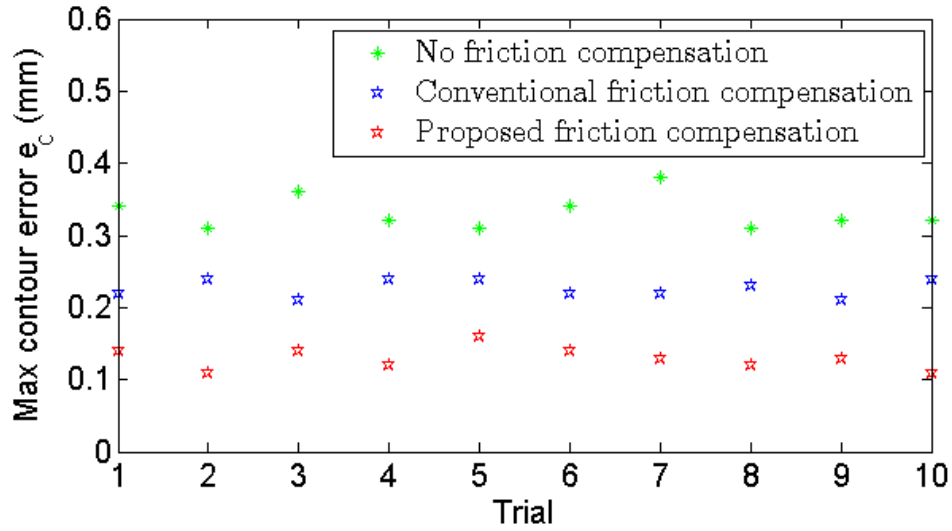


FIGURE 4.17: Maximum contour error results in non-circular reference

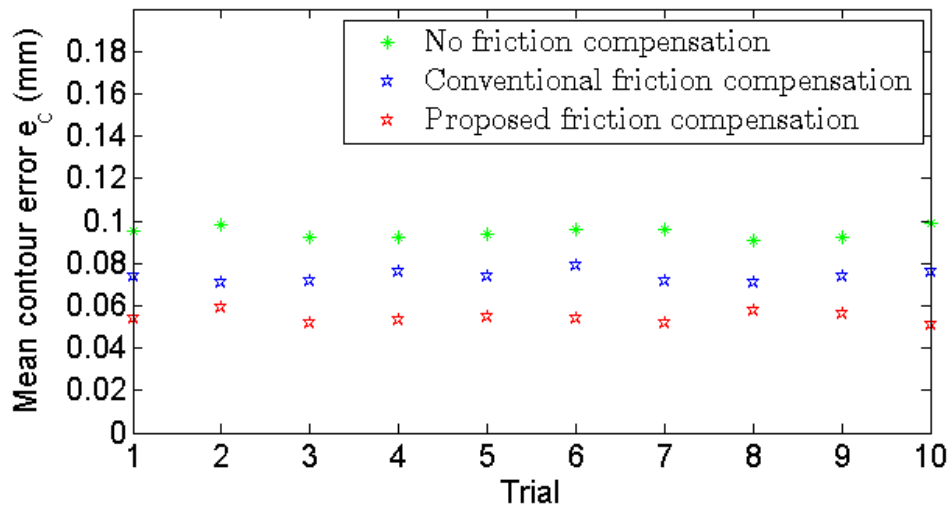


FIGURE 4.18: Mean contour error results in non-circular reference

4.5 Sliding Mode Contouring Controller Design with Adaptive Friction Compensation

4.5.1 Sliding Mode Contouring Controller Design

In general, triaxial machine-tool dynamics are represented by the following differential equation:

$$\begin{aligned}
 f_u &= M\ddot{q} + f_f + g, \\
 f_u &= [f_{ux}, f_{uy}, f_{uz}]^T = K_t u, \\
 K_t &= \text{diag}\{k_{ti}\}, u = [u_x, u_y, u_z]^T, \\
 M &= \text{diag}\{m_i\}, i = x, y, z, \\
 f_f &= [f_{fx}, f_{fy}, f_{fz}]^T, g = [g_x, g_y, g_z]^T,
 \end{aligned} \tag{4.8}$$

where $f_{ui}, k_{ti} (> 0)$, and u_i are the driving force, the force-control input coefficient, and the control input voltage in drive axis i , respectively. Furthermore, $m_i (> 0)$, f_{fi} , and g_i are the equivalent mass, the friction force and the gravitational force in the drive axis i , respectively. The symbol $\text{diag}\{\alpha_i\}$ denotes a diagonal matrix with the elements α_i at the i th diagonal position.

We design the sliding surface vector based on the transformed error e_l as follows:

$$\begin{aligned}
 s &= \dot{e}_l + \lambda e_l, \\
 s &= [s_t, s_n, s_b]^T,
 \end{aligned} \tag{4.9}$$

where $\lambda = \text{diag}\{\lambda_i\}$ ($i = t, n, b$) is a 3×3 matrix in which $\lambda_i (> 0)$ is a positive constant. From Eqs. (3.7) and (4.9), we have

$$\begin{aligned}
 \dot{e}_l &= \dot{R}^T e_w + R^T \dot{e}_w, \\
 \ddot{e}_l &= \ddot{R}^T e_w + 2\dot{R}^T \dot{e}_w + R^T \ddot{e}_w, \\
 \ddot{e}_w &= \ddot{q} - \ddot{q}_d, \\
 \dot{s} &= \dot{e}_l + \lambda \dot{e}_l, \\
 &= \ddot{R}^T e_w + 2\dot{R}^T \dot{e}_w + R^T (\ddot{q} - \ddot{q}_d) + \lambda \dot{R}^T e_w + \lambda R^T \dot{e}_w.
 \end{aligned} \tag{4.10}$$

From Eqs. (4.8) and (4.10) we have

$$\begin{aligned}
 \dot{s} &= \ddot{R}^T e_w + 2\dot{R}^T \dot{e}_w + R^T \{M^{-1}(f_u - f_f - g) - \ddot{q}_d\} \\
 &\quad + \lambda \dot{R}^T e_w + \lambda R^T \dot{e}_w.
 \end{aligned} \tag{4.11}$$

The best approximation driving force \hat{f}_u in a continuous control law that achieves $\dot{s} = 0$ is thus

$$\begin{aligned}
 \hat{f}_u &= \hat{M} \{\ddot{q}_d - R(\lambda \dot{R}^T e_w + \lambda R^T \dot{e}_w + \ddot{R}^T e_w + 2\dot{R}^T \dot{e}_w)\} \\
 &\quad + \hat{f}_f + \hat{g},
 \end{aligned} \tag{4.12}$$

where \hat{M} , \hat{f}_f , and \hat{g} denote the estimated values of real parameters in dynamics system in Eq. (4.8). There exists an error between estimated and real parameters, and therefore, in order to satisfy the sliding condition, we add discontinuous terms across the surface $s = 0$ and a continuous controller

term as follows:

$$f_u = \hat{f}_u - \hat{M}RAs - \hat{M}RLk, \quad (4.13)$$

where $k = [k_t, k_n, k_b]^T$ is a positive gain vector, $A = \text{diag}\{a_i\}$ ($i = t, n, b$) is a 3x3 matrix of positive diagonal elements, and $L = \text{diag}\{\text{sgn}(s_i)\}$ is a 3x3 matrix with the sign function defined as follows:

$$\text{sgn}(s_i) = \begin{cases} 1 & \text{if } s_i > 0, \\ 0 & \text{if } s_i = 0, \\ -1 & \text{otherwise.} \end{cases} \quad (4.14)$$

To prove the stability of the control system, we choose the following Lyapunov function candidate:

$$V = \frac{1}{2}s^T s. \quad (4.15)$$

From Eqs. (4.8), (4.12), and (4.13) we have

$$\begin{aligned} \ddot{q} &= M^{-1}[\hat{M}\{\ddot{q}_d - R(\lambda\dot{R}^T e_w + \lambda R^T \dot{e}_w + \ddot{R}^T e_w \\ &\quad + 2\dot{R}^T \dot{e}_w)\} + \tilde{f}_f + \tilde{g} - \hat{M}RAs - \hat{M}RLk] \\ &= \ddot{q}_d - R(\lambda\dot{R}^T e_w + \lambda R^T \dot{e}_w + \ddot{R}^T e_w + 2\dot{R}^T \dot{e}_w) \\ &\quad - RAs - RLk + M^{-1}[\tilde{M}\{\ddot{q}_d - R(\lambda\dot{R}^T e_w + \lambda R^T \dot{e}_w \\ &\quad + \ddot{R}^T e_w + 2\dot{R}^T \dot{e}_w)\} + \tilde{f}_f + \tilde{g} - \tilde{M}RAs - \tilde{M}RLk] \\ \tilde{M} &= \hat{M} - M, \tilde{f}_f = \hat{f}_f - f_f, \tilde{g} = \hat{g} - g, \end{aligned} \quad (4.16)$$

where \tilde{M} , \tilde{f}_f , and \tilde{g} denote the parameter estimation errors. From Eqs. (4.11), (4.15), and (4.16) we have

$$\begin{aligned} \dot{V} &= s^T \dot{s} \\ &= s^T [\ddot{R}^T e_w + 2\dot{R}^T \dot{e}_w + R^T \{-R(\lambda\dot{R}^T e_w + \lambda R^T \dot{e}_w \\ &\quad + \ddot{R}^T e_w + 2\dot{R}^T \dot{e}_w) - RAs - RLk + M^{-1}(\tilde{M}\{\ddot{q}_d \\ &\quad - R(\lambda\dot{R}^T e_w + \lambda R^T \dot{e}_w + \ddot{R}^T e_w + 2\dot{R}^T \dot{e}_w)\} + \tilde{f}_f + \tilde{g} \\ &\quad - \tilde{M}RAs - \tilde{M}RLk)\} + \lambda\dot{R}^T e_w + \lambda R^T \dot{e}_w] \\ &= -s^T As + s^T R^T M^{-1} \tilde{M}RAs \\ &\quad - s^T L[k - L^{-1}R^T \{M^{-1}(\tilde{M}\{\ddot{q}_d - R(\lambda\dot{R}^T e_w \\ &\quad + \lambda R^T \dot{e}_w + \ddot{R}^T e_w + 2\dot{R}^T \dot{e}_w)\} + \tilde{f}_f + \tilde{g})\}] \\ &\quad + s^T R^T M^{-1} \tilde{M}RLk. \end{aligned} \quad (4.17)$$

Estimation errors on parameter M , f_f , and g are assumed to be bounded, and the case $\text{sgn}(s_i) = 0$ is not considered. (i.e., $L = L^{-1}$). We have

$$\begin{aligned} &L^{-1}R^T (M^{-1}(\tilde{M}\{\ddot{q}_d - R(\lambda\dot{R}^T e_w \\ &\quad + \lambda R^T \dot{e}_w + \ddot{R}^T e_w + 2\dot{R}^T \dot{e}_w)\} + \tilde{f}_f + \tilde{g})) \\ &\leq |L^{-1}| |R^T| [\tilde{M}^{-1}(\tilde{M}\{\ddot{q}_d - R(\lambda\dot{R}^T e_w \\ &\quad + \lambda R^T \dot{e}_w + \ddot{R}^T e_w + 2\dot{R}^T \dot{e}_w)\} + \tilde{f}_f + \tilde{g})] \\ &= \bar{h}, \end{aligned} \quad (4.18)$$

where $|I|$ denotes the maximum element of the matrix I , $\bar{M}(> 0)$, $\bar{f}_f(> 0)$, and $\bar{g}(> 0)$ denote the upper bound of the maximum values of the estimated parameter error \tilde{M} , \tilde{f}_f , and \tilde{g} , respectively. \bar{M}^{-1} is a diagonal matrix whose diagonal elements are greater than those of M^{-1} . Letting

$$k = \gamma + \bar{h}, \quad (4.19)$$

where γ is a 3x1 positive gain vector, from Eqs. (4.14), (4.17) and (4.19), we have

$$\begin{aligned} \dot{V} = s^T \dot{s} \leq & -s^T A s + s^T R^T M^{-1} \tilde{M} R A s - s^T L \gamma \\ & + s^T R^T M^{-1} \tilde{M} R L k. \end{aligned} \quad (4.20)$$

Assuming that the estimated parameters $\hat{m}_i \in \hat{M}$ is not so far different from the actual parameter $m_i \in M$ (i.e. $\tilde{m}_i \in \tilde{M} \ll m_i \in M$), we have:

$$\begin{aligned} -s^T A s + s^T R^T M^{-1} \tilde{M} R A s & < 0 \\ -s^T L \gamma + s^T R^T M^{-1} \tilde{M} R L k & < 0, \end{aligned} \quad (4.21)$$

and hence $\dot{V} = s^T \dot{s} < 0$ is achieved.

Note that in this sliding-mode contouring controller, the switching gain k is not fixed, its value depends on the tracking error e_w as in Eq. (4.18). This nonlinear switching gain makes the controller robust to parameter uncertainties and non-linear friction properties. However, a higher switching gain leads to chattering in control input. To reduce the switching gain k , in the next section, we propose adaptive friction compensation to have better friction-compensation performance.

4.5.2 Friction Model Design for Adaptive Control

We propose an adaptive friction compensation design as follows:

$$\begin{aligned} f_f &= \Gamma \text{sgn}(\dot{q}) + \hat{\beta} + \Lambda \dot{q} \\ \Gamma &= \text{diag}\{\gamma_i\}, \\ \Lambda &= \text{diag}\{\lambda_i\}, i = (x, y, z), \end{aligned} \quad (4.22)$$

where $\hat{\beta}$ is an adaptive nonlinear friction term and estimated as follows:

$$\begin{aligned} \dot{\beta}_e &= K_c \{ \hat{M}^{-1} (f_u - \Gamma \text{sgn}(\dot{q}) - \Lambda \dot{q} - \hat{g}) - \beta_e + K_c \dot{q} \} \\ \dot{\hat{\beta}} &= \beta_e - K_c \dot{q}, \end{aligned} \quad (4.23)$$

where $K_c = \text{diag}\{k_{ci}\}$ is a 3x3 matrix of adaptive friction-compensation gains. The important point of the proposed method is that it compensates for the nonlinearity in the viscous friction force. In the conventional friction model, the viscous friction force is calculated based on the steady-state friction behavior that changes slowly. However, in a real system with parameter uncertainty and nonlinear friction, chattering in the velocity occurs and differences exist between the real velocity and the desired velocity. Therefore, adaptive friction compensation is regulated to compensate for the difference and reduce the error and the magnitude of sliding surface s . The parameter β_e is included in Eq. (4.23) for the boundedness of β_e , and therefore the

TABLE 4.4: Machine tool parameters

	x axis	y axis	z axis
m (Ns ² /mm)	1.0	0.8	0.8
g (N)	0.0	0.0	10.0
k_t (N/V)	25	25	25

TABLE 4.5: Controller gains

Controller parameters	(a)	(b)
$(\lambda_t, \lambda_n, \lambda_b)$	(20,40,40)	(20,40,40)
(a_t, a_n, a_b)	(10,20,20)	(10,20,20)
$(\tilde{m}_x, \tilde{m}_y, \tilde{m}_z)$	(0.1,0.1,0.1)	(0.1,0.1,0.1)
$(\gamma_t, \gamma_n, \gamma_b)$	(10,20,20)	(5,10,10)
(k_{cx}, k_{cy}, k_{cz})		(10,20,20)

bounded adaptive friction term $\hat{\beta}$ is achieved. The estimation of $\hat{\beta}$ converges when $\dot{\beta}_e = 0$, which leads to $\hat{\beta} = f_u - \hat{M}\ddot{q}_d - \Gamma \text{sgn}(\dot{q}) - \Lambda\dot{q} - \hat{g}$ that compensates for the difference between the model controller force and the actual required force f_u .

4.5.3 Experimental Results

The machine tool in Fig. 2.21 consists of three axes driven by DC servo motors coupled to, and driving three ball screws. In addition, a linear encoder whose resolution is $0.1 \mu\text{m}$ is attached to each feed-drive axis to measure the real position of the feed-drive system. The estimated parameter values of the machine are given in Table 4.4. The value of k_t is calculated from the motor data-sheet and the lead-screw coefficient. The nominal weight m is obtained from identified experiments under constant acceleration. The nominal gravitational force g is estimated from the difference between the forward and backward feed-drive force at constant speed. The proposed controller is verified by means of a circular contour and non-circular contour. The RMS contour error and power consumption are used to validate the proposed controller. The effectiveness is compared with the following two different controller configurations (both controllers use the same λ in designing the sliding surface):

- (a) Sliding-mode contouring controller with conventional friction compensation
- (b) Sliding-mode contouring controller with adaptive friction compensation

Controller gains are given in Table 4.5.

First, the following three-dimensional desired circular contour is used in the experiment:

$$\begin{aligned} q_x &= 15 \cos\left(\frac{\pi}{4}t\right) \text{ mm}, \\ q_y &= 15 \sin\left(\frac{\pi}{4}t\right) \text{ mm}, \\ q_z &= 15 \sin\left(\frac{\pi}{4}t\right) \text{ mm}. \end{aligned} \quad (4.24)$$

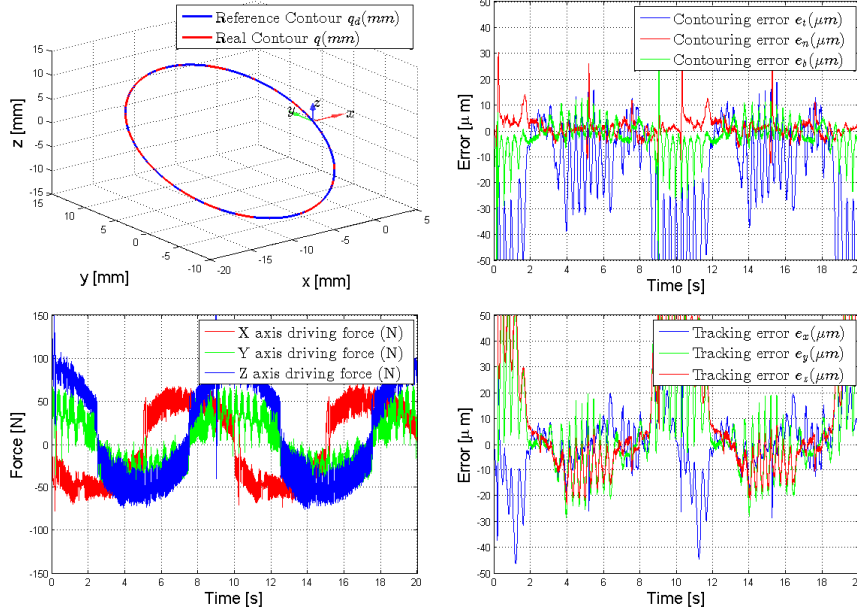


FIGURE 4.19: Circular contour tracking results for controller (a)

Figures 4.19 and 4.20 show the contouring-error results obtained by applying controllers (a) and (b). Figure 4.12 compares the mean contour errors for 10 trials, and Fig. 4.22 is for the power consumption. From Figs. 4.19 and 4.20, we can see that sliding-mode contouring controller with adaptive friction compensation gives better contour-error performance despite having a lower switching gain. Reduced chattering in the driving force results in lower power consumption. The mean contouring errors from 10 trials in Fig. 4.12 and the power consumption in Fig. 4.22 are reduced by about 28.6% and 7.1%, respectively in comparison with the conventional ones on the average.

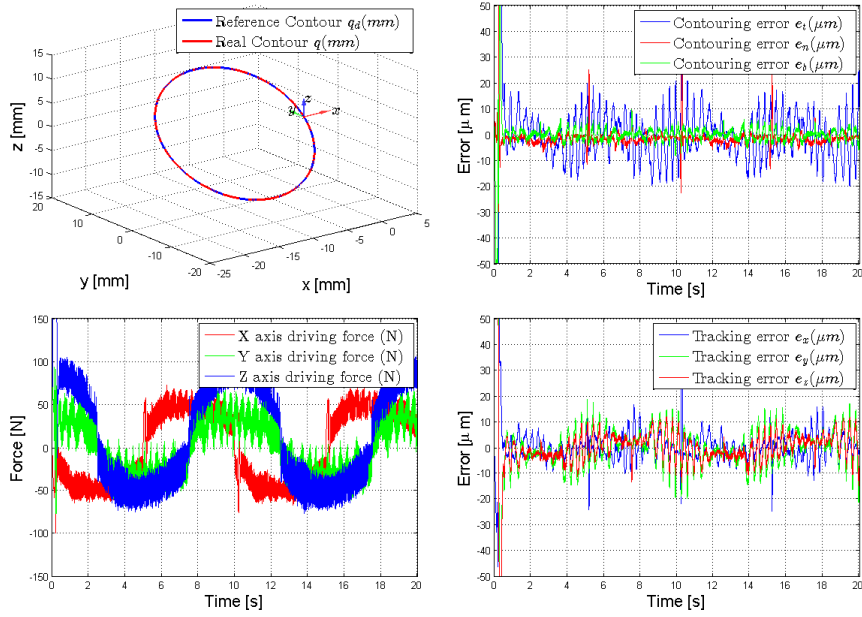


FIGURE 4.20: Circular contour tracking results for controller (b)

Next, the following three-dimensional non-circular contour is used in the experiment:

$$\begin{aligned}
 q_x &= 10 \sin\left(\frac{3\pi}{10}t + 1.256\right) \text{ mm}, \\
 q_y &= 15 \sin\left(\frac{\pi}{10}t\right) \text{ mm}, q_z = 15 \sin\left(\frac{\pi}{10}t\right) \text{ mm},
 \end{aligned} \tag{4.25}$$

Figure 4.23 and 4.24 show the contouring-error results obtained by applying controllers (a) and (b). Figure 4.25 compares the mean contour errors for 10 trials, and Figs. 4.26 is for the power consumption. Similar results are obtained with those from the circular-contour cases. The average contouring error and power consumption are reduced by about 34.2% and 2.5%, respectively, in comparison with the conventional ones.

The sliding-mode contouring controller (a) is implemented with the assumption of parameter uncertainty, and the switching gain is set to high values to keep the tracking and contouring errors low. In controller (b), adaptive friction compensation is used with a smaller switching gain, and better contouring performance is confirmed. The smaller switching gain provides smaller chattering in the control input, and therefore better energy-saving performance is achieved.

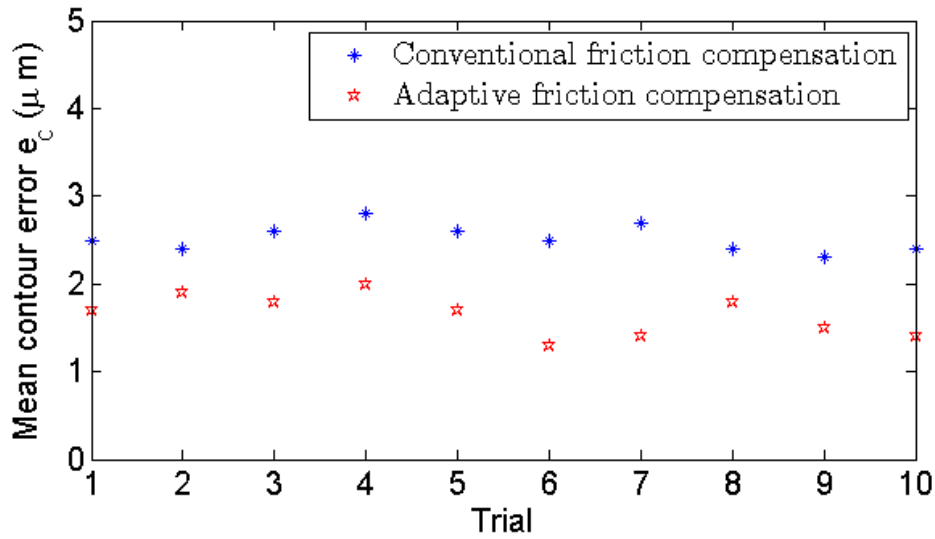


FIGURE 4.21: Mean contour error results

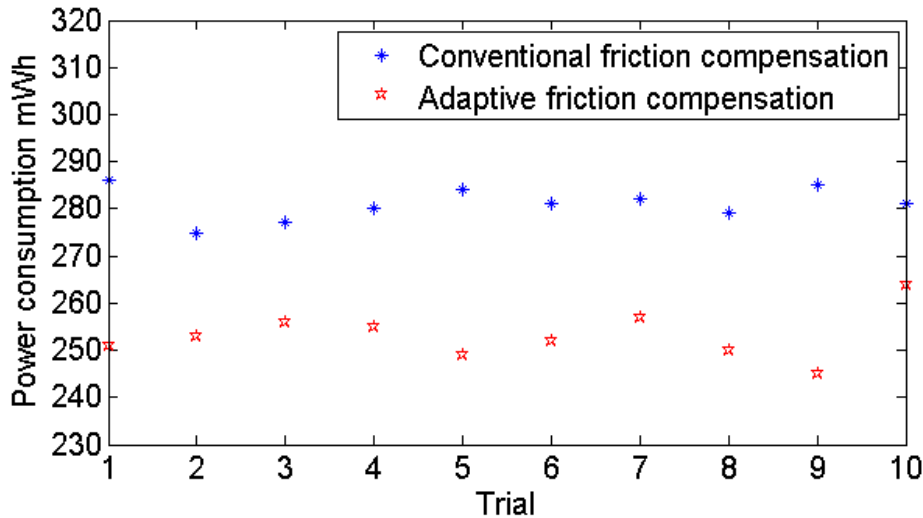


FIGURE 4.22: Power consumption results

4.6 Conclusions

The dynamics of the lead-screw feed drive in the triaxial machine tool are analyzed, and a nonlinear friction model is proposed that concerns the eccentricity between the lead-screw and the nut. Because the contour error is important in machining applications, a contouring controller with feed-forward friction compensation is designed. Experiments with out cutting were conducted based on a circular and a non-circular reference contour. Comparative experiments with different controller configurations show that the proposed method is more effective than both the contouring controller without friction compensation and that with conventional friction compensation. On average, the mean and maximum contour errors were reduced by about 26% and 9.3%, respectively, in the circular trajectories in comparison with the contouring controller that uses the conventional friction model.

This study shows how eccentricity between lead screw and nut lead to

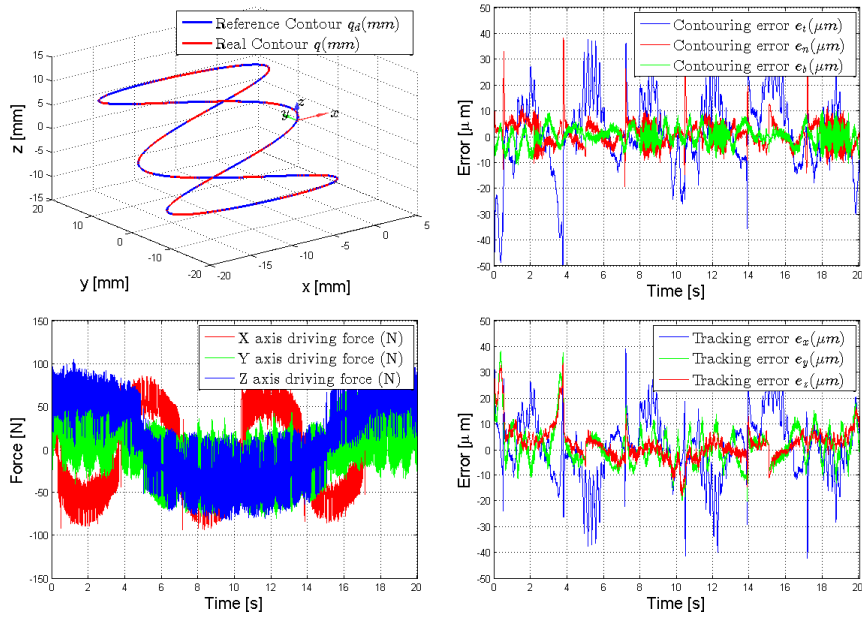


FIGURE 4.23: Non-circular contour tracking results for controller (a)

friction variations over one revolution of the screw. This effect may not be significant in brand-new machines manufactured by leading companies, which would have more stable and better lubrication condition. However, for machine tools that have been in operation for a long time, and are not well lubricated (i.e., where the effect of friction is dominant), the proposed method is effective. In addition, we can improve machining accuracy at low cost by simply updating the controller using the proposed nonlinear friction model.

The effectiveness of the proposed method is confirmed for non-cutting experiments. For cutting experiments, design of a cutting-force observer is required. In addition, the proposed method can be extended to other industrial machines such as a coordinate measurement machine (CMM). This extension is left for future research. In addition, a robust sliding-mode contouring controller with adaptive friction compensation is proposed with experimental verification. This chapter proposed a nonlinear switching gain and a stability proof for robust sliding-mode contouring control. In addition, an adaptive friction component was presented and its effectiveness was verified experimentally. It was shown that the proposed controller is effective in reducing contour error by about 28.6% and power consumption by about 7.1% in circular-contour tracking experiment.

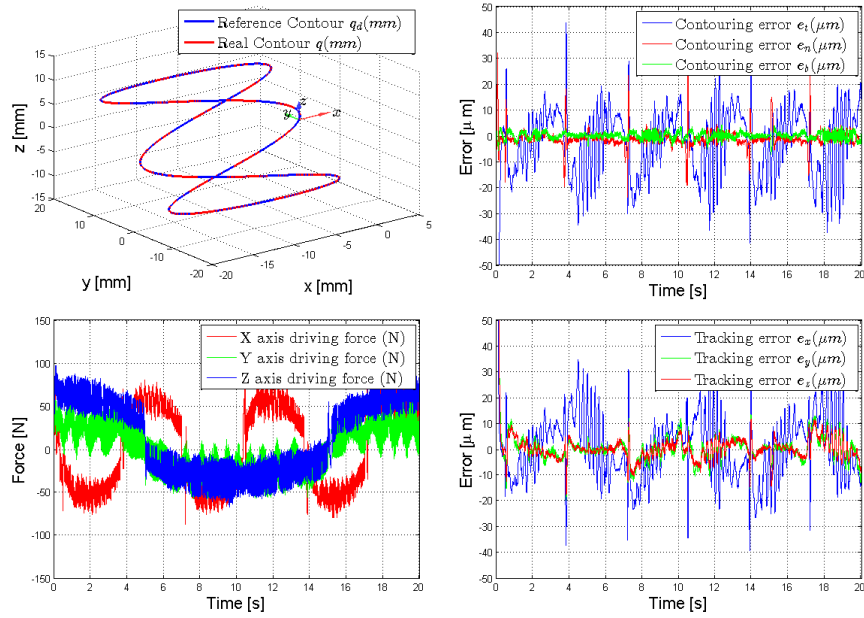


FIGURE 4.24: Non-circular contour tracking results for controller (b)

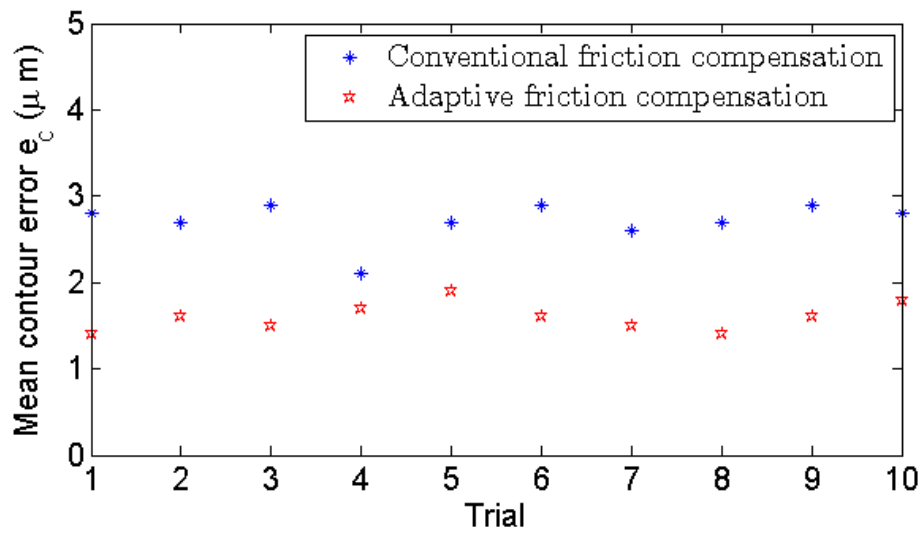


FIGURE 4.25: Mean contour error results

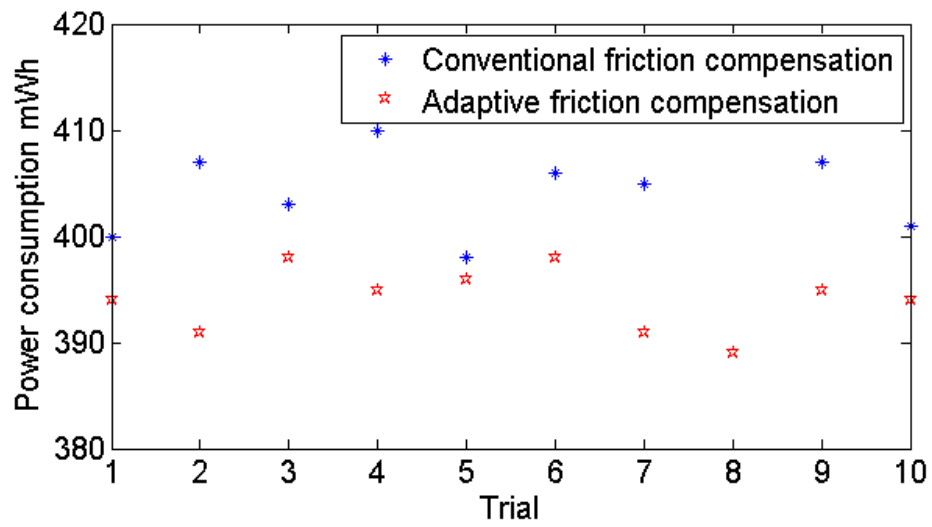


FIGURE 4.26: Power consumption results

Chapter 5

Conclusions and Future Research

5.1 Conclusions

This thesis considers nonlinear friction properties, identification, and compensation for feed-drive systems in machine tools. Design for tracking controllers and contouring controllers with the proposed nonlinear friction-compensation model were presented in order to reduce the tracking error in a uniaxial feed drive, the contour errors in a biaxial table and a triaxial machine tool. In addition, we proposed a robust sliding-mode contouring controller with adaptive friction compensation to further reduce the contour error and power consumption.

Compensation of friction forces acting on the feed-drive system is critical for high-speed, high-precision machine-tool control. The nonlinear friction properties in a feed-drive system were analyzed, and investigation of the experimental results showed that nonlinear friction phenomena appear at both low and high speeds. A nonlinear friction model that includes a conventional static friction model (Coulomb friction and viscous friction) and a number of nonlinear friction sources represented by Gaussian functions was proposed in order to model the nonlinear friction properties of high speed motion. In uniaxial feed-drive system control, a simple PD tracking controller design with feed-forward friction compensation and a DOB was proposed. Comparative experiments with several different friction-model configurations were conducted at both low and high speeds. It was shown that the proposed controller with nonlinear friction compensation is effective at reducing the tracking error in high speed experiments; the mean tracking error was reduced by 37% compared to that with a conventional static friction model.

In multi-axis feed-drive system, the combination of the tracking motion of each feed drive generates the contour motion. A biaxial table generates two-dimension motion of the work piece. In triaxial machine tool, the cutting tool is attached to the spindle on the z axis and three feed drives move the cutting tool in a three-dimensional contour motion for the cutting process. Therefore, besides the tracking error, there is a contour error that is defined as the component orthogonal to the desired contour curve; this is an important factor in the evaluation of surface machining.

We extended the proposed nonlinear friction-compensation model to consider the contour-following performance in biaxial table control. A contouring controller with feedforward friction compensation and a DOB was proposed. The friction compensation performances of the proposed methods

were compared based on the mean and maximum contour errors of circular and non-circular experimental results. The friction compensation based on the conventional static friction model and a number of nonlinear friction sources modeled by Gaussian functions. Comparative experiments with several different friction-compensation methods were conducted at both low and high speeds. It was shown that the proposed controller is effective in high speed control applications, for which the maximum contour error was reduced by 58% compared to that of a controller using the conventional static friction model. This can be explained by the ability of the nonlinear friction model to accurately describe the nonlinear friction properties of high speed motion.

For the triaxial machine tool, we found a repetitive nonlinear friction component from experiments on high-speed motion of the lead-screw feed-drive systems. This friction property appeared clearly in lead-screw feed drives that had been in operation for a long time or that were poorly lubricated. We presented a friction model that combines the conventional Coulomb-viscous friction model and a nonlinear sinusoidal component in order to fully describe the eccentric friction behavior of feed-drive systems. In addition, we presented a contouring-controller design with feed-forward compensation based on the proposed friction model to improve contour-error performance. Experiments with out cutting were conducted based on a circular and a non-circular reference contour. Comparative experiments with different controller configurations showed that the proposed method is more effective than the contouring controller without friction compensation or that with conventional friction compensation. In detail, the mean and maximum contour errors were reduced by about 26% and 9.3%, respectively, in circular trajectories in comparison with the contouring controller that used the conventional static friction model. The proposed eccentric friction model shows how eccentricity between lead screw and nut lead to friction variations over one revolution of the screw. This effect may not be significant in brand-new machines manufactured by leading companies, which are likely to be more stable and better lubricated. However, for machine tools that have been in operation for a long time, or that are poorly lubricated (i.e., for which friction is dominant), the proposed method is effective. Moreover, we can improve machining accuracy at low cost by simply updating the controller using the proposed nonlinear friction model.

For further improvement, we proposed a robust sliding-mode contouring controller with adaptive friction compensation to compensate for parameter uncertainty and friction-model inaccuracy and to reduce power consumption. A nonlinear switching gain and a stability proof for robust sliding-mode contouring control were presented along with an adaptive friction design. The effectiveness was verified experimentally. It was shown that the proposed controller is effective in reducing contour errors by about 28.6% and power consumption by about 7.1% in circular-contour tracking experiments.

5.2 Future Research

The nonlinear friction model, identification and compensation method developed in this thesis are directly applicable to current tracking and contouring controllers of single- and multi-axis feed-drive systems. Extension of the model to more complex systems such as industrial robots and five-axis machine tools is possible, and would realize the benefits of increased productivity, reduced energy consumption, and the maintenance of long operational lives.

The proposed nonlinear friction model can be combined with dynamical friction models such as the LuGre and GMS models to fully describe nonlinear friction behavior in the pre-sliding regime, and the low speed and high speed sliding regimes. We also expect to conduct experiments with advanced controllers for adaptive sliding-mode control and model predictive control (MPC) to increase the feed-drive limiting bandwidth and achieve better contouring performance.

The proposed methods for triaxial machine-tool control can be extended to other industrial machines such as a coordinate measurement machine (CMM) in order to improve measurement precision. Because the simulation and experimental results for the non-cutting process verified that employing a sliding-mode contouring controller with adaptive friction compensation reduces the control-input variation and hence reduces vibrations and increases stability, we would like to conduct actual cutting processes to confirm the effectiveness of proposed model in future work.

Bibliography

- [1] T. Moriwaki, “Trends in recent machine tool technologies”, *NTN Technical Review*, pp. 2–7, 2006. [Online]. Available: www.ntnglobal.com/en/products/review/pdf/NTN_TR74_en_P002.pdf.
- [2] Y. Altintas, A. Verl, C. Brecher, *et al.*, “Machine tool feed drives”, *CIRP Annals - Manufacturing Technology*, vol. 60, no. 2, pp. 779–796, 2011, ISSN: 0007-8506. DOI: 10.1016/j.cirp.2011.05.010. [Online]. Available: <http://www.sciencedirect.com/science/article/pii/S0007850611002125>.
- [3] B. D. Bui, “Contouring control with friction compensation and disturbance observer in industrial systems”, Master’s thesis, Toyohashi University of Technology, Japan, Mar. 2014.
- [4] Z. Jamaludin, “Disturbance compensation for machine tools with linear motor drives”, PhD thesis, Department of Werktuigkunde, Katholieke Universiteit Leuven, 2008.
- [5] K. Erkorkmaz, “Optimal trajectory generation and precision tracking control for multi-axis machines”, PhD thesis, University of British Columbia, 2004. DOI: 10.14288/1.0080705. [Online]. Available: <https://open.library.ubc.ca/cIRcle/collections/831/items/1.0080705>.
- [6] C. C. de Wit, H. Olsson, K. J. Astrom, *et al.*, “A new model for control of systems with friction”, *IEEE Transactions on Automatic Control*, vol. 40, no. 3, pp. 419–425, Mar. 1995, ISSN: 0018-9286. DOI: 10.1109/9.376053.
- [7] A. Kamalzadeh, “Precision control of high speed ball screw drives”, PhD thesis, 2009. [Online]. Available: <http://hdl.handle.net/10012/4189>.
- [8] Y. Koren and C. Lo, “Advanced controllers for feed drives”, *CIRP Annals - Manufacturing Technology*, vol. 41, no. 2, pp. 689–698, 1992, ISSN: 0007-8506. DOI: 10.1016/S0007-8506(07)63255-7. [Online]. Available: <http://www.sciencedirect.com/science/article/pii/S0007850607632557>.
- [9] A. Matsubara, K. Lee, S. Ibaraki, *et al.*, “Enhancement of feed drive dynamics of nc machine tools by actively controlled sliding guideway”, *JSME International Journal Series C*, vol. 74, no. 1, pp. 150–158, 2004. DOI: 10.1299/jsmec.47.150. [Online]. Available: <http://ci.nii.ac.jp/naid/110004820721>.
- [10] K. V. Kripa and A. N. Samir, “The dynamics of lead-screw drives: Low-order modeling and experiments”, *Journal of Dynamic Systems, Measurement, and Control*, vol. 126, no. 2, pp. 388–396, 2004, ISSN: 0022-0434. DOI: 10.1115/1.1771690. [Online]. Available: <http://dx.doi.org/10.1115/1.1771690>.

- [11] K. Zhang, A. Yuen, and Y. Altintas, "Pre-compensation of contour errors in five-axis cnc machine tools", *International Journal of Machine Tools and Manufacture*, vol. 74, pp. 1–11, 2013, ISSN: 0890-6955. DOI: 10.1016/j.ijmachtools.2013.07.003. [Online]. Available: <http://www.sciencedirect.com/science/article/pii/S0890695513001120>.
- [12] A. E.K.M. A. Mohammad, "Nonlinear control for high precision motion and energy saving in multi-axis industrial systems", PhD thesis, Toyohashi University of Technology, Japan, 2013.
- [13] C. Okwudire, "Finite element modeling of ballscrew feed drive systems for control purpose", Master's thesis, The University of British Columbia Department of Mechanical Engineering Vancouver Canada, 2005.
- [14] K. K. Varanasi and S. A. Nayfeh, "The dynamics of lead-screw drives: Low-order modeling and experiments", *Journal of Dynamic Systems, Measurement, and Control*, vol. 126, no. 2, pp. 388–396, 2004, ISSN: 0022-0434. DOI: 10.1115/1.1771690. [Online]. Available: <http://dx.doi.org/10.1115/1.1771690>.
- [15] M. F. Zaeh, T. Oertli, and J. Milberg, "Finite element modelling of ball screw feed drive systems", *CIRP Annals*, vol. 53, no. 1, pp. 289–293, 2004.
- [16] J. F. Cuttino, T. A. Dow, and B. F. Knight, "Analytical and experimental identification of nonlinearities in a single-nut, preloaded ball screw", *Journal of Mechanical Design*, vol. 119, no. 1, pp. 15–19, 1997, ISSN: 1050-0472. DOI: 10.1115/1.2828782. [Online]. Available: <http://dx.doi.org/10.1115/1.2828782>.
- [17] S. A.H., *Precision machine design*. Society of Manufacturing Engineers, Dearborn MI, 1992.
- [18] C. C. Wei and J. F. Lin, "Kinematic analysis of the ball screw mechanism considering variable contact angles and elastic deformations", *Journal of Mechanical Design*, vol. 125, no. 4, pp. 717–733, 2004. DOI: 10.1115/1.1623761. [Online]. Available: <http://dx.doi.org/10.1115/1.1623761>.
- [19] N. Matsui, T. Makino, and H. Satoh, "Autocompensation of torque ripple of direct drive motor by torque observer", *IEEE Transactions on Industry Applications*, vol. 29, no. 1, pp. 187–194, Jan. 1993, ISSN: 0093-9994. DOI: 10.1109/28.195906.
- [20] H. Nagase, T. Okuyama, J. Takahashi, *et al.*, "A method for suppressing torque ripple of an ac motor by current amplitude control", *IEEE Transactions on Industrial Electronics*, vol. 36, no. 4, pp. 504–510, Nov. 1989, ISSN: 0278-0046. DOI: 10.1109/41.43009.
- [21] F. Parasiliti, R. Petrella, and M. Tursini, "Torque ripple compensation in permanent magnet synchronous motors based on kalman filter", in *Industrial Electronics, 1999. ISIE '99. Proceedings of the IEEE International Symposium on*, vol. 3, 1999, 1333–1338 vol.3. DOI: 10.1109/ISIE.1999.796897.

- [22] D. A. Vicente, R. L. Hecker, F. J. Villegas, *et al.*, “Modeling and vibration mode analysis of a ball screw drive”, *The International Journal of Advanced Manufacturing Technology*, vol. 58, no. 1, pp. 257–265, 2012, ISSN: 1433-3015. DOI: 10.1007/s00170-011-3375-6. [Online]. Available: <http://dx.doi.org/10.1007/s00170-011-3375-6>.
- [23] H. Zhang, W. Zhao, J. Zhang, *et al.*, “Research on the modeling of dynamics for vertical axis ball screw feed system”, in *2013 IEEE International Symposium on Assembly and Manufacturing (ISAM)*, Jul. 2013, pp. 208–213. DOI: 10.1109/ISAM.2013.6643529.
- [24] P. Waszczuk, “Cnc feed drive module model simplification and estimation of its parameters”, in *2015 20th International Conference on Methods and Models in Automation and Robotics (MMAR)*, Aug. 2015, pp. 834–839. DOI: 10.1109/MMAR.2015.7283985.
- [25] B.-K. M. Wonkyun Lee Chan-Young Lee, “Improvement of machine tool friction compensation controller using detailed feed drive component models”, in *Proceedings of the International Conference of Manufacturing Technology Engineers (ICMTE) 2014*, 한국생산제조학회, 2014, pp. 17–17. [Online]. Available: <http://www.dbpia.co.kr/Article/NODE02486668>.
- [26] B. Armstrong-Hélouvry, P. Dupont, and C. C. D. Wit, “A survey of models, analysis tools and compensation methods for the control of machines with friction”, *Automatica*, vol. 30, no. 7, pp. 1083 – 1138, 1994, ISSN: 0005-1098. DOI: 10.1016/0005-1098(94)90209-7. [Online]. Available: <http://www.sciencedirect.com/science/article/pii/0005109894902097>.
- [27] K. Erkorkmaz and Y. Altintas, “High speed cnc system design. part ii: Modeling and identification of feed drives”, *International Journal of Machine Tools and Manufacture*, vol. 41, no. 10, pp. 1487–1509, 2001, ISSN: 0890-6955. DOI: 10.1016/S0890-6955(01)00003-7. [Online]. Available: <http://www.sciencedirect.com/science/article/pii/S0890695501000037>.
- [28] H. S. Lee and M. Tomizuka, “Robust motion controller design for high-accuracy positioning systems”, *IEEE Transactions on Industrial Electronics*, vol. 43, no. 1, pp. 48–55, Feb. 1996, ISSN: 0278-0046. DOI: 10.1109/41.481407.
- [29] A. Kamalzadeh and K. Erkorkmaz, “Compensation of axial vibrations in ball screw drives”, *CIRP Annals - Manufacturing Technology*, vol. 56, no. 1, pp. 373–378, 2007, ISSN: 0007-8506. DOI: <http://dx.doi.org/10.1016/j.cirp.2007.05.087>. [Online]. Available: <http://www.sciencedirect.com/science/article/pii/S0007850607000911>.
- [30] C. Okwudire, “Modeling and control of high speed machine tool feed drive”, PhD thesis, The University of British Columbia, 2009.
- [31] R. Kalman, “A new approach to linear filtering and prediction problem”, *Journal of Basic Engineering*, vol. 82, pp. 35–44, 1960.

- [32] A. M.A.E. K. Mohammad, N. Uchiyama, and S. Sano, “Energy saving in feed drive systems using sliding-mode-based contouring control with a nonlinear sliding surface”, *IEEE/ASME Transactions on Mechatronics*, vol. 20, no. 2, pp. 572–579, Apr. 2015, ISSN: 1083-4435. DOI: 10.1109/TMECH.2013.2296698.
- [33] Y. Koren, *Computer control of manufacturing system*, 1st ed. McGraw-Hill, New York, 1983.
- [34] G. Pritschow, “On the influence of the velocity gain factor on the path deviation”, *CIRP Annals - Manufacturing Technology*, vol. 45, no. 1, pp. 367–371, 1996, ISSN: 0007-8506. DOI: [http://dx.doi.org/10.1016/S0007-8506\(07\)63082-0](http://dx.doi.org/10.1016/S0007-8506(07)63082-0). [Online]. Available: <http://www.sciencedirect.com/science/article/pii/S0007850607630820>.
- [35] K. Erkorkmaz, “High speed contouring control for machine tool drives”, Master’s thesis, The University of British Columbia, Department of Mechanical Engineering, Vancouver, 1999.
- [36] Y. Koren and C.-C. Lo, “Advanced controllers for feed drives”, *Annals of CIRP*, vol. 41, no. 2, pp. 689–698, 1992.
- [37] S. J. Van Brussel H. Chen C.-H., “Accurate motion controller design based on an extended pole placement method and a disturbance observer”, *Annals of CIRP*, vol. 43, no. 1, pp. 367–372, 1994.
- [38] M. Tomizuka, “Zero Phase Error Tracking Algorithm for Digital Control”, *ASME Journal of Dynamic Systems, Measurements, and Control*, vol. 109, pp. 65–68, 1987.
- [39] G. Pritschow and W. Philipp, “Research on the efficiency of feed-forward controllers in m direct drives”, *Annals of CIRP*, vol. 41, no. 1, pp. 411–415, 1992.
- [40] T. M. Tsao Tsu-Chin, “Adaptive zero phase error tracking algorithm for digital control”, *Journal of Dynamic Systems, Measurement, and Control*, vol. 109, no. 4, pp. 349–354, 1987. DOI: <http://dx.doi.org/10.1115/1.3143866>. [Online]. Available: <http://dx.doi.org/10.1115/1.3143866>.
- [41] Y. Koren, “cross-coupled biaxial control for manufacturing systems”, *ASME Journal of Dynamic Systems, Measurement, and Control*, vol. 102, pp. 265–272, 1980. [Online]. Available: <https://ykoren.engin.umich.edu/wp-content/uploads/sites/122/2014/05/5-Cross-Coupled-Biaxial-Computer-Control-for-Mfg-Systems.pdf>.
- [42] H. Ho, Y. Jia-Yush, and S. Lu, “A decoupled path-following control algorithm based upon the decomposed trajectory error”, *International Journal of Machine Tools and Manufacture*, vol. 39, pp. 1619–1630, 1999.
- [43] M.-Y. Cheng, K.-H. Su, and S.-F. Wang, “Contour error reduction for free-form contour following tasks of biaxial motion control systems”, *Robotics and Computer-Integrated Manufacturing*, vol. 25, no. 2, pp. 323–333, 2009.
- [44] M. Cheng and C. Lee, “On real-time contour error estimation for contour following tasks”, in *Proc. IEEE/ASME International Conference of Advanced Intelligent Mechatronics*, 2005, pp. 1047–1052.

- [45] Y. S. Tarng, H. Y. Chuang, and W. T. Hsu, "Intelligent cross-coupled fuzzy feedrate controller design for cnc machine tools based on genetic algorithms", *International Journal of Machine Tools and Manufacture*, vol. 39, pp. 1673–1692, 1999.
- [46] J.-H. Chin, Y.-M. Cheng, and J.-H. Lin, "Improving contour accuracy by fuzzy-logic enhanced cross-coupled precompensation method", *Robotics and Computer-Integrated Manufacturing*, vol. 20, pp. 65–76, 2004.
- [47] S. Yeh and P. Hsu, "Adaptive-feedrate interpolation for parametric curves with a confined chord error", *Computer-Aided Design*, vol. 34, no. 3, pp. 229–237, 2002.
- [48] S. Jee and Y. Koren, "Adaptive fuzzy logic controller for feed drives of a cnc machine tool", *Journal of Mechatronics*, vol. 14, pp. 299–326, 2004.
- [49] P. K. Kulkarni and K. Srinivasan, "Optimal contouring control of multi-axial feed drive servomechanisms", *ASME Journal of Engineering for Industry*, vol. 111, no. 2, pp. 140–148, 1989. DOI: 10.1115/1.3188743. [Online]. Available: <http://manufacturingscience.asmedigitalcollection.asme.org/article.aspx?articleid=1447145>.
- [50] S. L. Chen and K. C. Wu, "Contouring control of smooth paths for multiaxis motion systems based on equivalent errors", *IEEE Transactions on Control Systems Technology*, vol. 15, no. 6, pp. 1151–1158, Nov. 2007, ISSN: 1063-6536. DOI: 10.1109/TCST.2007.899719.
- [51] L. Chih-Ching and C. Ching-Yei, "Tangential-contouring controller for biaxial motion control", *Journal of Dynamic Systems, Measurement, and Control*, vol. 121, no. 1, pp. 126–129, 1999, ISSN: 0022-0434. DOI: 10.1115/1.2802430. [Online]. Available: <http://dx.doi.org/10.1115/1.2802430>.
- [52] G. T. C. Chiu and M. Tomizuka, "Contouring control of machine tool feed drive systems: A task coordinate frame approach", *IEEE Transactions on Control Systems Technology*, vol. 9, no. 1, pp. 130–139, Jan. 2001, ISSN: 1063-6536. DOI: 10.1109/87.896754.
- [53] X. Ye, X. Chen, X. Li, *et al.*, "A cross-coupled path precompensation algorithm for rapid prototyping and manufacturing", *The International Journal of Advanced Manufacturing Technology*, vol. 20, no. 1, pp. 39–43, 2002, ISSN: 1433-3015. DOI: 10.1007/s001700200121. [Online]. Available: <http://dx.doi.org/10.1007/s001700200121>.
- [54] N. Uchiyama, T. Nakamura, and K. Yamazaki, "Reduction of consumed energy and control input variance in machine tool feed drives by contouring control", *International Journal of Automation Technology*, vol. 3, no. 4, 2009. DOI: 10.20965/ijat.2009.p0401. [Online]. Available: <http://dx.doi.org/10.20965/ijat.2009.p0401>.
- [55] B. Bandyopadhyay, F. Deepak, and K.-S. Kim, *Sliding mode control using novel sliding surfaces*, 1st ed. Berlin Heidelberg: Springer-Verlag, 2009, 15.
- [56] U. Itkis, *Control systems of variable structure*. New York: Wiley, 1976.
- [57] Utkin, "Variable structure systems with sliding mode", *IEEE Transactions on Automatic Control*, vol. 22, no. 2, 212–222, 1977.

- [58] J. Guldner and V. Utkin, "Tracking the gradient of artificial potential fields: Sliding mode control for mobile robots", *Modern Machinery Science Journal*, vol. 63, no. 3, pp. 417–432, 1996.
- [59] A. Zinober, O. El-Ghezawi, and S. Billings, "Multi variable structure adaptive model-following control systems", *Proceedings of IEE*, vol. 129, pp. 6–12, 1982.
- [60] J. Slotine, J. Hedrick, and E. Misawa, "On sliding observers for nonlinear systems", *Transactions of the ASME: Journal of Dynamic Systems Measurement and Control*, vol. 109, pp. 245–252, 1987.
- [61] S. Drakunov and V. Utkin, "Sliding mode observers. tutorial", in *Proceedings of the 34th Conference on Decision and Control, New-Orleans, LA., 1995*.
- [62] B. Drazenovic, "The invariance conditions in variable structure systems", *Automatica*, vol. 5, no. 3, pp. 287–295, 1969.
- [63] K. Furuta, "Sliding mode control of a discrete system", *Systems and Control Letters*, vol. 14, pp. 145–152, 1990.
- [64] H. Sira-Ramirez, "Differential geometric methods in variable-structure control", *International Journal of Control*, vol. 48, no. 4, pp. 1359–1390, 1988.
- [65] R. D. Carlo, S. Zak, and G. Matthews, "Variable structure control of nonlinear variable systems: A tutorial", *Proceedings of IEEE*, vol. 76, pp. 212–232, 1988.
- [66] C. Edwards and S. Spurgeon, *Sliding mode control: Theory and applications*. Taylor and Francis, 1998.
- [67] U. Itkis, *Control systems of variable structure*. New York: Wiley, 1976.
- [68] V. Utkin, *Sliding modes in control optimization, communication and control engineering series*. Springer-Verlag, 1992.
- [69] W. Perruquetti and J.-P. Barbot, *Sliding mode control in engineering*, 1st ed. Berlin Heidelberg: Springer-Verlag, 2009, 1 5.
- [70] N. Rafan, Z. Jamaluddin, L. Abdullah, *et al.*, "Review on friction compensation approach for machine tools application", in *IDECON 2012 - International Conference on Design and Concurrent Engineering*, 2012.
- [71] Y. Altintas, A. Verl, C. Brecher, *et al.*, "Machine tool feed drives", *CIRP Annals - Manufacturing Technology*, vol. 60(2), 2011.
- [72] V. Lampaert, J. Swevers, and F. Al-Bender, "Comparison of model and non-model based friction compensation techniques in the neighbourhood of pre-sliding friction", in *Proceedings of the 2004 American Control Conference*, vol. 2, Jun. 2004, 1121–1126 vol.2.
- [73] J. Swevers, F. A. Bender, C. Ganseman, *et al.*, "An integrated friction model structure with improved pre-sliding behaviour for accurate friction compensation", *IEEE Trans. on Automatic Control*, vol. 45(4), pp. 675–686, 2000.
- [74] R. H. A. Hensen, M. J. G. van de Molengraft, and M. Steinbuch, "Frequency domain identification of dynamic friction model parameters", *IEEE Transactions on Control Systems Technology*, vol. 10, no. 2, pp. 191–196, Mar. 2002, ISSN: 1063-6536. DOI: 10.1109/87.987064.

- [75] D. Hoshino, N. Kamamichi, and J. Ishikawa, "Friction compensation using time variant disturbance observer based on the lugre model", in *2012 12th IEEE International Workshop on Advanced Motion Control (AMC)*, Mar. 2012, pp. 1–6. DOI: 10.1109/AMC.2012.6197030.
- [76] V. Lampaert, F. Al-Bender, and J. Swevers, "A generalized maxwell-slip friction model appropriate for control purposes", in *2003 IEEE International Workshop on Workload Characterization (IEEE Cat. No.03EX775)*, vol. 4, Aug. 2003, 1170–1177 vol.4. DOI: 10.1109/PHYCON.2003.1237071.
- [77] Z. Jamaludin, H. V. Brussel, G. Pipeleers, *et al.*, "Accurate motion control of xy high-speed linear drives using friction model feedforward and cutting forces estimation", *CIRP Annals - Manufacturing Technology*, vol. 57, no. 1, pp. 403–406, 2008, ISSN: 0007-8506. DOI: <http://dx.doi.org/10.1016/j.cirp.2008.03.037>. [Online]. Available: <http://www.sciencedirect.com/science/article/pii/S0007850608000358>.
- [78] Z. Jamaludin, H. V. Brussel, and J. Swevers, "Friction compensation of an xy feed table using friction-model-based feedforward and an inverse-model-based disturbance observer", *IEEE Transactions on Industrial Electronics*, vol. 56, no. 10, pp. 3848–3853, Oct. 2009, ISSN: 0278-0046. DOI: 10.1109/TIE.2009.2017560.
- [79] J. J. Choi, J. S. Kim, and S. I. Han, "Pre-sliding friction control using the sliding mode controller with hysteresis friction compensator", *KSME International Journal*, vol. 18, no. 10, pp. 1755–1762, 2004, ISSN: 1738-494X. DOI: 10.1007/BF02984324. [Online]. Available: <http://dx.doi.org/10.1007/BF02984324>.
- [80] V. Lampaert, J. Swevers, and F. Al-Bender, "Modification of the leuven integrated friction model structure", *IEEE Transactions on Automatic Control*, vol. 47, no. 4, pp. 683–687, Apr. 2002, ISSN: 0018-9286. DOI: 10.1109/9.995050.
- [81] F. Al-Bender, V. Lampaert, and J. Swevers, "The generalized maxwell-slip model: A novel model for friction simulation and compensation", *IEEE Transactions on Automatic Control*, vol. 50, no. 11, pp. 1883–1887, Nov. 2005, ISSN: 0018-9286. DOI: 10.1109/TAC.2005.858676.
- [82] E. D. Tung, G. Anwar, and M. Tomizuka, "Low velocity friction compensation and feedforward solution based on repetitive control", *Journal of Dynamic Systems, Measurement, and Control*, vol. 115, pp. 279–284, 1993.
- [83] T. Takemura and H. Fujimoto, "Proposal of novel rolling friction compensation with data-based friction model for ball screw driven stage", in *IECON 2010 - 36th Annual Conference on IEEE Industrial Electronics Society*, Nov. 2010, pp. 1932–1937. DOI: 10.1109/IECON.2010.5675329.
- [84] H. Wang, C. Vasseur, and V. Koncar, "Friction compensation of an x-y robot using a recursive model free controller", in *2010 IEEE International Conference on Industrial Technology*, Mar. 2010, pp. 355–360. DOI: 10.1109/ICIT.2010.5472706.

- [85] T. H. Lee, K. K. Tan, and S. Huang, "Adaptive friction compensation with a dynamical friction model", *IEEE/ASME Transactions on Mechatronics*, vol. 16, no. 1, pp. 133–140, Feb. 2011, ISSN: 1083-4435. DOI: 10.1109/TMECH.2009.2036994.
- [86] W. Lee, C.-Y. Lee, Y. H. Jeong, *et al.*, "Friction compensation controller for load varying machine tool feed drive", *International Journal of Machine Tools and Manufacture*, vol. 96, pp. 47–54, 2015, ISSN: 0890-6955. DOI: <http://dx.doi.org/10.1016/j.ijmachtools.2015.06.001>. [Online]. Available: <http://www.sciencedirect.com/science/article/pii/S089069551530047X>.
- [87] R. Mahdi, K. Stephan, and B. Friedrich, "Experimental investigations on stick-slip phenomenon and friction characteristics of linear guides", *Procedia Engineering*, vol. 100, pp. 1023–1031, 2015, ISSN: 1877-7058. DOI: <http://dx.doi.org/10.1016/j.proeng.2015.01.462>. [Online]. Available: <http://www.sciencedirect.com/science/article/pii/S1877705815004890>.
- [88] M. Reuss, A. Dadalau, and A. Verl, "Friction variances of linear machine tool axes", *Procedia CIRP*, vol. 4, pp. 115–119, 2012, ISSN: 2212-8271. DOI: <http://dx.doi.org/10.1016/j.procir.2012.10.021>. [Online]. Available: <http://www.sciencedirect.com/science/article/pii/S2212827112003125>.
- [89] C. Rebelein, J. Vlacil, and M. F. Zaeh, "Modeling of the dynamic behavior of machine tools: Influences of damping, friction, control and motion", *Production Engineering*, pp. 1–14, 2016, ISSN: 1863-7353. DOI: 10.1007/s11740-016-0704-5. [Online]. Available: <http://dx.doi.org/10.1007/s11740-016-0704-5>.
- [90] W. Chen, K. Kong, and M. Tomizuka, "Dual-stage adaptive friction compensation for precise load side position tracking of indirect drive mechanisms", *IEEE Transactions on Control Systems Technology*, vol. 23, no. 1, pp. 164–175, Jan. 2015, ISSN: 1063-6536. DOI: 10.1109/TCST.2014.2317776.
- [91] J. Kabziński and M. Jastrzębski, "Practical implementation of adaptive friction compensation based on partially identified lugre model", in *2014 19th International Conference on Methods and Models in Automation and Robotics (MMAR)*, Sep. 2014, pp. 699–704. DOI: 10.1109/MMAR.2014.6957439.
- [92] W. Lee, C. Y. Lee, Y. H. Jeong, *et al.*, "Distributed component friction model for precision control of a feed drive system", *IEEE/ASME Transactions on Mechatronics*, vol. 20, no. 4, pp. 1966–1974, Aug. 2015, ISSN: 1083-4435. DOI: 10.1109/TMECH.2014.2365958.
- [93] M. Ruderman, "Tracking control of motor drives using feedforward friction observer", *IEEE Transactions on Industrial Electronics*, vol. 61, no. 7, pp. 3727–3735, Jul. 2014, ISSN: 0278-0046. DOI: 10.1109/TIE.2013.2264786.
- [94] M. C. Tsai, I. F. Chiu, and M. Y. Cheng, "Design and implementation of command and friction feedforward control for cnc motion controllers", *IEE Proceedings - Control Theory and Applications*, vol.

- 151, no. 1, pp. 13–20, Jan. 2004, ISSN: 1350-2379. DOI: 10.1049/ip-cta:20040100.
- [95] A. Elfizy, G. Bone, and M. Elbestawi, “Model-based controller design for machine tool direct feed drives”, *International Journal of Machine Tools and Manufacture*, vol. 44, no. 5, pp. 465–477, 2004, ISSN: 0890-6955. DOI: <http://dx.doi.org/10.1016/j.ijmachtools.2003.11.005>. [Online]. Available: [//www.sciencedirect.com/science/article/pii/S0890695503003110](http://www.sciencedirect.com/science/article/pii/S0890695503003110).
- [96] Y. Shih and A. Lee, “Survey on modeling and control for motion systems with friction”, *Journal of the Chinese Society of Mechanical Engineers, Transactions of the Chinese Institute of Engineers*, vol. 24, no. 4, pp. 337–352, 2003.
- [97] S.-S. Yeh, Z.-H. Tsai, and P.-L. Hsu, “Applications of integrated motion controllers for precise cnc machines”, *The International Journal of Advanced Manufacturing Technology*, vol. 44, no. 9, p. 906, 2009, ISSN: 1433-3015. DOI: 10.1007/s00170-008-1919-1. [Online]. Available: <http://dx.doi.org/10.1007/s00170-008-1919-1>.
- [98] Z.-q. Mei, Y.-c. Xue, and R.-q. Yang, “Nonlinear friction compensation in mechatronic servo systems”, *The International Journal of Advanced Manufacturing Technology*, vol. 30, no. 7, p. 693, 2005, ISSN: 1433-3015. DOI: 10.1007/s00170-005-0113-y. [Online]. Available: <http://dx.doi.org/10.1007/s00170-005-0113-y>.
- [99] J.-S. Chen, Y.-H. Kuo, and W.-Y. Hsu, “The influence of friction on contouring accuracy of a cartesian guided tripod machine tool”, *The International Journal of Advanced Manufacturing Technology*, vol. 30, no. 5, pp. 470–478, 2006, ISSN: 1433-3015. DOI: 10.1007/s00170-005-0088-8. [Online]. Available: <http://dx.doi.org/10.1007/s00170-005-0088-8>.
- [100] J. Awrejcewicz and P. Olejnik, “Analysis of dynamic systems with various friction laws”, *Applied Mechanics Reviews*, vol. 58, no. 6, pp. 389–411, 2005, ISSN: 0003-6900. DOI: 10.1115/1.2048687. [Online]. Available: <http://dx.doi.org/10.1115/1.2048687>.
- [101] C. Chen, M. Jang, and K. Lin, “Modeling and high-precision control of a ball-screw-driven stage”, *Precision Engineering*, vol. 28, no. 4, pp. 483–495, 2004, ISSN: 0141-6359. DOI: <http://dx.doi.org/10.1016/j.precisioneng.2004.03.001>. [Online]. Available: [//www.sciencedirect.com/science/article/pii/S0141635904000455](http://www.sciencedirect.com/science/article/pii/S0141635904000455).
- [102] R. Persianoff, P. Ray, and O. Vidal, “Comparison between an experimental study and a numerical model of the dynamic behaviour of machine-tool slideways”, *Proceedings of the Institution of Mechanical Engineers, Part B: Journal of Engineering Manufacture*, vol. 217, no. 8, pp. 1111–1115, 2003. DOI: 10.1177/095440540321700808. [Online]. Available: <http://dx.doi.org/10.1177/095440540321700808>.
- [103] C. Hsieh and Y.-C. Pan, “Dynamic behavior and modelling of the pre-sliding static friction”, *Wear*, vol. 242, no. 1-2, pp. 1–17, 2000, ISSN: 0043-1648. DOI: [http://dx.doi.org/10.1016/S0043-1648\(00\)00399-9](http://dx.doi.org/10.1016/S0043-1648(00)00399-9). [Online]. Available: [//www.sciencedirect.com/science/article/pii/S0043164800003999](http://www.sciencedirect.com/science/article/pii/S0043164800003999).

- [104] A. A. Polycarpou and A. Soom, “A two-component mixed friction model for a lubricated line contact”, *Journal of Tribology*, vol. 118, no. 1, pp. 183–189, 1996, ISSN: 0742-4787. DOI: 10.1115/1.2837076. [Online]. Available: <http://dx.doi.org/10.1115/1.2837076>.
- [105] S. Cetinkunt, W. Yu, J. Filliben, *et al.*, “Friction characterization experiments on a single point diamond turning machine tool”, *International Journal of Machine Tools and Manufacture*, vol. 34, no. 1, pp. 19–32, 1994, ISSN: 0890-6955. DOI: [http://dx.doi.org/10.1016/0890-6955\(94\)90037-X](http://dx.doi.org/10.1016/0890-6955(94)90037-X). [Online]. Available: <http://www.sciencedirect.com/science/article/pii/089069559490037X>.
- [106] E. Marui and H. Endo, “Significance of contact resistance in boundary lubrication”, *Wear*, vol. 156, no. 1, pp. 49–55, 1992, ISSN: 0043-1648. DOI: [http://dx.doi.org/10.1016/0043-1648\(92\)90143-V](http://dx.doi.org/10.1016/0043-1648(92)90143-V). [Online]. Available: <http://www.sciencedirect.com/science/article/pii/004316489290143V>.
- [107] B. Armstrong-Hélouvy, *Control of machines with friction*. Kluwer Academic Publishers, Massachusetts, 1991.
- [108] B. S. R. Armstrong and Q. Chen, “The z-properties chart”, *IEEE Control Systems*, vol. 28, no. 5, pp. 79–89, Oct. 2008, ISSN: 1066-033X. DOI: 10.1109/MCS.2008.928939.
- [109] J.-H. Kim, H.-K. Chae, J.-Y. Jeon, *et al.*, “Identification and control of systems with friction using accelerated evolutionary programming”, *IEEE Control Systems*, vol. 16, no. 4, pp. 38–47, Aug. 1996, ISSN: 1066-033X. DOI: 10.1109/37.526914.
- [110] C. C. Ka, H. Hongxing, and K. L. Nan, “Modeling and identification of a class of servomechanism systems with stick-slip friction”, *Journal of Dynamic Systems, Measurement, and Control*, vol. 110, no. 3, pp. 324–328, Oct. 1988, ISSN: 0022-0434. DOI: 10.1115/1.3152689. [Online]. Available: <http://dx.doi.org/10.1115/1.3152689>.
- [111] D. Karnopp, “Computer simulation of stick-slip friction in mechanical dynamic systems”, *Journal of Dynamic Systems, Measurement, and Control*, vol. 107, no. 1, pp. 100–103, 1985. DOI: 10.1115/1.3140698. [Online]. Available: <http://dx.doi.org/10.1115/1.3140698>.
- [112] C. C. de Wit and P. Lischinsky, “Adaptive friction compensation with partially known dynamic friction model”, *International Journal of Adaptive Control and Signal Processing*, vol. 11, no. 1, pp. 65–80, 1997, ISSN: 1099-1115. DOI: 10.1002/(SICI)1099-1115(199702)11:1<65::AID-ACS395>3.0.CO;2-3. [Online]. Available: [http://dx.doi.org/10.1002/\(SICI\)1099-1115\(199702\)11:1<65::AID-ACS395>3.0.CO;2-3](http://dx.doi.org/10.1002/(SICI)1099-1115(199702)11:1<65::AID-ACS395>3.0.CO;2-3).
- [113] M. R. Popovic and A. A. Goldenberg, “Modeling of friction using spectral analysis”, *IEEE Transactions on Robotics and Automation*, vol. 14, no. 1, pp. 114–122, Feb. 1998, ISSN: 1042-296X. DOI: 10.1109/70.660854.

- [114] S.-S. Yeh and H.-C. Su, “Development of friction identification methods for feed drives of cnc machine tools”, *The International Journal of Advanced Manufacturing Technology*, vol. 52, no. 1, pp. 263–278, 2011, ISSN: 1433-3015. DOI: 10.1007/s00170-010-2720-5. [Online]. Available: <http://dx.doi.org/10.1007/s00170-010-2720-5>.
- [115] K Ohnishi, “A new servo method in mechatronics”, *Transactions of the Japan Society for Electrical Engineering*, vol. 107, no. D, pp. 83–86, 1987.
- [116] L. Ljung, *System identification: Theory for the user, 2nd edition*. Prentice-Hall Of Canada Ltd, 1998.
- [117] Y. Li, Q. Zheng, and L. Yang, “Design of robust sliding mode control with disturbance observer for multi-axis coordinated traveling system”, *Computers & Mathematics with Applications*, vol. 64, no. 5, pp. 759–765, 2012, Advanced Technologies in Computer, Consumer and Control, ISSN: 0898-1221. DOI: <http://dx.doi.org/10.1016/j.camwa.2011.11.053>. [Online]. Available: <http://www.sciencedirect.com/science/article/pii/S0898122111010364>.
- [118] J. A. Nelder and R. Mead, “A simplex method for function minimization”, *The Computer Journal*, vol. 7(4), pp. 304–313, 1965. DOI: 10.1093/comjnl/7.4.308.
- [119] B. D. Bui, N. Uchiyama, and S. Sano, “Nonlinear friction modeling and compensation for precision control of a mechanical feed-drive system”, *Sensors and Materials*, vol. 27, no. 10, pp. 971–984, 2015. DOI: 10.18494/SAM.2015.1134.
- [120] P. Dahl, “Measurement of solid friction parameters of ball bearings”, in *Proc. of 6th Annual Symp. on Incremental Motion, Control System and Devices*, 1977.
- [121] T. Tjahjowidodo, F. Al-Bender, H. V. Brussel, *et al.*, “Friction characterization and compensation in electro-mechanical systems”, *Journal of Sound and Vibration*, vol. 308, no. 3-5, pp. 632–646, 2007, Vibro-Impact Systems, ISSN: 0022-460X. DOI: 10.1016/j.jsv.2007.03.075. [Online]. Available: <http://www.sciencedirect.com/science/article/pii/S0022460X07002593>.
- [122] Z. Jamaludin, H. Van Brussel, and J. Swevers, “Quadrant glitch compensation using friction model-based feedforward and an inverse-model-based disturbance observer”, in *Advanced Motion Control, 2008. AMC '08. 10th IEEE International Workshop on*, Mar. 2008, pp. 212–217. DOI: 10.1109/AMC.2008.4516068.
- [123] N. Uchiyama, T. Nakamura, and H. Yanagiuchi, “The effectiveness of contouring control and a design for three-dimensional machining”, *International Journal of Machine Tools and Manufacture*, vol. 49, no. 11, pp. 876–884, 2009, ISSN: 0890-6955. DOI: 10.1016/j.ijmachtools.2009.05.004. [Online]. Available: <http://www.sciencedirect.com/science/article/pii/S0890695509000807>.

- [124] N. Uchiyama, "Robust contouring control for biaxial feed drive systems", *International Journal of Machine Tools and Manufacture*, vol. 48, no. 11, pp. 1234–1241, 2008, ISSN: 0890-6955. DOI: 10.1016/j.ijmachtools.2008.03.010. [Online]. Available: <http://www.sciencedirect.com/science/article/pii/S0890695508000588>.
- [125] W. Lee, C.-Y. Lee, and B.-K. Min, "Simulation-based energy usage profiling of machine tool at the component level", *International Journal of Precision Engineering and Manufacturing-Green Technology*, vol. 1, no. 3, pp. 183–189, 2015, ISSN: 2198-0810. DOI: 10.1007/s40684-014-0023-2. [Online]. Available: <http://dx.doi.org/10.1007/s40684-014-0023-2>.
- [126] P. Dahl, "A solid friction model", *Technical Report TOR-158*, 3107–3118, 1968.
- [127] C.-J. Lin and C.-Y. Lee, "Observer-based robust controller design and realization of a gantry stage", *Mechatronics*, vol. 21, no. 1, pp. 185–203, 2011, ISSN: 0957-4158. DOI: 10.1016/j.mechatronics.2010.10.005. [Online]. Available: <http://www.sciencedirect.com/science/article/pii/S0957415810001856>.
- [128] C. Kempf and S. Kobayashi, "Disturbance observer and feedforward design for a high-speed direct-drive positioning table", *Control Systems Technology, IEEE Transactions on*, vol. 7, no. 5, pp. 513–526, Sep. 1999, ISSN: 1063-6536. DOI: 10.1109/87.784416.
- [129] M.-T. Yan and Y.-J. Shiu, "Theory and application of a combined feedback-feedforward control and disturbance observer in linear motor drive wire-edm machines", *International Journal of Machine Tools and Manufacture*, vol. 48, no. 3-4, pp. 388–401, 2008, ISSN: 0890-6955. DOI: 10.1016/j.ijmachtools.2007.09.006. [Online]. Available: <http://www.sciencedirect.com/science/article/pii/S0890695507001976>.
- [130] C.-J. Lin, H.-T. Yau, and Y.-C. Tian, "Identification and compensation of nonlinear friction characteristics and precision control for a linear motor stage", *Mechatronics, IEEE/ASME Transactions on*, vol. 18, no. 4, pp. 1385–1396, Aug. 2013, ISSN: 1083-4435. DOI: 10.1109/TMECH.2012.2202679.
- [131] E. Tung, G. Anwar, and M. Tomizuka, "Low velocity friction compensation and feedforward solution based on repetitive control", in *American Control Conference, 1991*, Jun. 1991, pp. 2615–2620.
- [132] A. Kamalzadeh, D. J. Gordon, and K. Erkorkmaz, "Robust compensation of elastic deformations in ball screw drives", *International Journal of Machine Tools and Manufacture*, vol. 50, no. 6, pp. 559–574, 2010, ISSN: 0890-6955. DOI: 10.1016/j.ijmachtools.2010.03.001. [Online]. Available: <http://www.sciencedirect.com/science/article/pii/S0890695510000337>.
- [133] L. Freidovich, A. Robertsson, A. Shiriaev, *et al.*, "Lugre-model-based friction compensation", *Control Systems Technology, IEEE Transactions on*, vol. 18, no. 1, pp. 194–200, Jan. 2010, ISSN: 1063-6536. DOI: 10.1109/TCST.2008.2010501.

- [134] T. H. Lee, K. K. Tan, and S. Huang, "Adaptive friction compensation with a dynamical friction model", *Mechatronics, IEEE/ASME Transactions on*, vol. 16, no. 1, pp. 133–140, Feb. 2011, ISSN: 1083-4435. DOI: 10.1109/TMECH.2009.2036994.
- [135] J.-S. Chen, K.-C. Chen, Z.-C. Lai, *et al.*, "Friction characterization and compensation of a linear-motor rolling-guide stage", *International Journal of Machine Tools and Manufacture*, vol. 43, no. 9, pp. 905–915, 2003, ISSN: 0890-6955. DOI: 10.1016/S0890-6955(03)00084-1. [Online]. Available: <http://www.sciencedirect.com/science/article/pii/S0890695503000841>.
- [136] D. Lam, C. Manzie, and M. C. Good, "Multi-axis model predictive contouring control", *International Journal of Control*, vol. 86, no. 8, pp. 1410–1424, 2013. DOI: 10.1080/00207179.2013.770170. [Online]. Available: <http://dx.doi.org/10.1080/00207179.2013.770170>.
- [137] J. Ling, Z. Feng, D. Yao, *et al.*, "A position domain iteration learning control for contour tracking with application to a multi-axis motion testbed", in *2016 American Control Conference (ACC)*, Jul. 2016, pp. 1247–1252. DOI: 10.1109/ACC.2016.7525088.
- [138] L.-B. Zhang, Y.-P. You, and X.-F. Yang, "A control strategy with motion smoothness and machining precision for multi-axis coordinated motion cnc machine tools", *The International Journal of Advanced Manufacturing Technology*, vol. 64, no. 1, pp. 335–348, 2013, ISSN: 1433-3015. DOI: 10.1007/s00170-012-4019-1. [Online]. Available: <http://dx.doi.org/10.1007/s00170-012-4019-1>.
- [139] L. Zhang, T. Wu, and F. Huang, "A coupling motional control method based on parametric predictive and variable universe fuzzy control for multi-axis cnc machine tools", *The International Journal of Advanced Manufacturing Technology*, vol. 74, no. 5, pp. 1097–1114, 2014, ISSN: 1433-3015. DOI: 10.1007/s00170-014-6011-4. [Online]. Available: <http://dx.doi.org/10.1007/s00170-014-6011-4>.
- [140] D. Lam, C. Manzie, and M. C. Good, "Model predictive contouring control for biaxial systems", *IEEE Transactions on Control Systems Technology*, vol. 21, no. 2, pp. 552–559, Mar. 2013, ISSN: 1063-6536. DOI: 10.1109/TCST.2012.2186299.
- [141] J. Yang, Z. Liu, X. Bi, *et al.*, "The research and design of high precision contour machining for multi-axis motion control", in *2015 Chinese Automation Congress (CAC)*, Nov. 2015, pp. 1594–1599. DOI: 10.1109/CAC.2015.7382756.
- [142] F. Huo and A.-N. Poo, "Precision contouring control of machine tools", *The International Journal of Advanced Manufacturing Technology*, vol. 64, no. 1, pp. 319–333, 2013, ISSN: 1433-3015. DOI: 10.1007/s00170-012-4015-5. [Online]. Available: <http://dx.doi.org/10.1007/s00170-012-4015-5>.
- [143] J. Yang and Y. Altintas, "A generalized on-line estimation and control of five-axis contouring errors of cnc machine tools", *International Journal of Machine Tools and Manufacture*, vol. 88, pp. 9–23, 2015, ISSN: 0890-6955. DOI: 10.1016/j.ijmachtools.2014.08.004.

- [Online]. Available: <http://www.sciencedirect.com/science/article/pii/S0890695514001229>.
- [144] N. Uchiyama, Y. Ogawa, A. E.K. M. Mohammad, *et al.*, “Energy saving in five-axis machine tools using synchronous and contouring control and verification by machining experiment”, *IEEE Transactions on Industrial Electronics*, vol. 62, no. 9, pp. 5608–5618, Sep. 2015, ISSN: 0278-0046. DOI: 10.1109/TIE.2015.2437354.
- [145] Y. Altintas and M. Khoshdarregi, “Contour error control of cnc machine tools with vibration avoidance”, *CIRP Annals - Manufacturing Technology*, vol. 61, no. 1, pp. 335–338, 2012, ISSN: 0007-8506. DOI: 10.1016/j.cirp.2012.03.132. [Online]. Available: <http://www.sciencedirect.com/science/article/pii/S0007850612001345>.
- [146] M. R. Khoshdarregi, S. Tappe, and Y. Altintas, “Integrated five-axis trajectory shaping and contour error compensation for high-speed cnc machine tools”, *IEEE/ASME Transactions on Mechatronics*, vol. 19, no. 6, pp. 1859–1871, Dec. 2014, ISSN: 1083-4435. DOI: 10.1109/TMECH.2014.2307473.
- [147] J. Yang, H.-T. Zhang, and H. Ding, “Contouring error control of the tool center point function for five-axis machine tools based on model predictive control”, *The International Journal of Advanced Manufacturing Technology*, pp. 1–11, 2016, ISSN: 1433-3015. DOI: 10.1007/s00170-016-8979-4. [Online]. Available: <http://dx.doi.org/10.1007/s00170-016-8979-4>.
- [148] S. Tulsyan and Y. Altintas, “Local toolpath smoothing for five-axis machine tools”, *International Journal of Machine Tools and Manufacture*, vol. 96, pp. 15–26, 2015, ISSN: 0890-6955. DOI: 10.1016/j.ijmactools.2015.04.014. [Online]. Available: <http://www.sciencedirect.com/science/article/pii/S0890695515300377>.
- [149] A. E. Khalick and N. Uchiyama, “Contouring controller design based on iterative contour error estimation for three-dimensional machining”, *Robotics and Computer-Integrated Manufacturing*, vol. 27, no. 4, pp. 802–807, 2011, Conference papers of Flexible Automation and Intelligent Manufacturing Intelligent manufacturing and services, ISSN: 0736-5845. DOI: 10.1016/j.rcim.2011.01.001. [Online]. Available: <http://www.sciencedirect.com/science/article/pii/S0736584511000159>.

Appendix A

Publications

The contents of this thesis are the results of original research and have not been submitted for a higher degree to any other university or institution.

Much of the work presented in this thesis has been published as journal or conference papers. Following is a list of these papers.

International Journal Papers

- (1) Ba Dinh Bui, Naoki Uchiyama, Shigenori Sano, “Nonlinear friction modeling and compensation for precision control of a mechanical feed-drive system”, *Sensors and Materials*, Vol 27, No. 10, pp.971-984, 2015. (*Impact Factor: 0.489*)
- (2) Ba Dinh Bui, Naoki Uchiyama, Kenneth Renny Simba, “Contouring control for three-axis machine tools based on nonlinear friction compensation for lead screws”, *International Journal of Machine Tools and Manufacture*, Vol 108, pp. 95-105, September 2016. (*Impact Factor: 3.315*)

International Conferences Papers

- (1) Ba Dinh Bui, Naoki Uchiyama and Shigenori Sano, “Friction compensation in contouring control for biaxial feed drive systems and experimental verification”. The 7th International Conference on Leading Edge Manufacturing in 21st Century, Matsushima, JSME, Miyagi, Japan, 6 pages, November 2013.
- (2) Ba Dinh Bui, Naoki Uchiyama and Shigenori Sano, “Nonlinear friction modeling and compensation for precision control of a mechanical feed drive system”. The 2nd International Conference of Global Network for Inovative Technology, TUT-USM Technology, Collaboration Centre, Penang, Malaysia, 6 pages, December 2014.
- (3) Ba Dinh Bui, Naoki Uchiyama, “Sliding mode contouring controller design with adaptive friction compensation for three-axis machine tool”. The 2016 American Control Conference, Boston, MA, USA, 6 pages, 6-8 July 2016.